Study of Composition and Thermal Treatments of Quaternary Compounds for Monograin Layer Solar Cells

KATRI MUSKA

TUT
PRESS

TALLINN UNIVERSITY OF TECHNOLOGY
Faculty of Chemistry and Materials Technology
Department of Materials Science
Chair of Semiconductor Materials Technology

This dissertation was accepted for the defence of the degree of Doctor of Philosophy in Natural and Exact Sciences on October 1st, 2012.

Supervisor: Senior Research Scientist Marit Kauk-Kuusik,
Department of Materials Science,
Tallinn University of Technology, Estonia

Opponents: Dr. António Ferreira da Cunha, Physics Department,
University of Aveiro, Portugal

Professor Enn Lust, Institute of Physical Chemistry,
University of Tartu, Estonia

Defence of the thesis: November 15th, 2012, at 11.00
Lecture hall: X-209
Tallinn University of Technology, Ehitajate tee 5, Tallinn

Declaration:
Hereby I declare that this doctoral thesis, my original investigation and achievement, submitted for the doctoral degree at Tallinn University of Technology has not been submitted for any academic degree.

/Katri Muska/

Päikesepatareides kasutatavate monoterapulbriliste nelikühendite koostise ja termotöötluste uurimine

KATRI MUSKA

Table of Contents

INTRODUCTION

Presently, the world's energy consumption is around 10 terawatts (TW) per year, and by 2050 it is assumed to be about 30 TW. The world will need about 20 TW of non-CO_2 energy to stabilize CO_2 in the atmosphere by mid-century. The simplest scenario to stabilize CO_2 by that time is to use photovoltaics (PV) and other renewables for electricity and transportation. The PV effect was discovered already in 1839 by Aléxandre Edmund Becquerel, but the first practical solar cell was made at Bell Laboratories in the 1950s. PV solar cells convert sunlight directly into electricity. All PV solar cells are based on semiconductors, where solar radiation produces electron-hole pairs, which are then separated by the *p-n* junction [1, 2].

During one year, the amount of solar radiation reaching the earth is 178 000 TW, so at the moment, the world's energy consumption forms only 0.007% of it. The PV industry holds only around 0.1% of the entire world's electrical consumption. The main obstacle for solar energy use is the price of the solar cells. Therefore, ongoing investigations aim at decreasing the cost of the solar cells to lower the price of the energy generated. One of alternatives could be the so-called kesterite based solar cells: $Cu_2ZnSn(S_{1-x}Se_x)$ $(0 \leq x \leq 1)$ [3]. Interest towards kesterites has been continuously increasing. If in 2005 the number of annual publications on kesterites was under 25, then by 2011 the number had increased almost 30 times [4]. One of the methods for producing kesterite absorber materials for solar cells is monograin powder growth, where $Cu_2ZnSn(S_{1-x}Se_x)$ $(0 \leq x \leq 1)$ solid solutions in the monograin powder form are used as absorber material in monograin layer (MGL) solar cells [3]. The main advantages of MGL solar cell technology are relatively low production costs and the potential of covering unlimited areas [5].

The objective of this thesis was to determine conditions for growing single-phase Cu_2ZnSnS_4 (CZTS), $Cu_2ZnSnSe_4$ (CZTSe), and $Cu_2ZnSn(S_{1-x}Se_x)_4$ $(0 < x < 1,$ CZTSSe) monograin powders and to find suitable thermal treatment of the absorber material to optimize MGL solar cell characteristics.

This thesis consists of three chapters. The first chapter reviews the relevant literature. The second chapter covers the growth and post-treatment of the monograins and also the analytical tools used to characterize the materials. The third chapter is divided into two parts: the first part gives an overview of the properties of synthesized as-grown monograin powders, with focus on the composition, structural, morphological and electrical properties; the second part concentrates on the influence of post-treatments in different atmospheres on as-grown monograin powders and MGL solar cells. The final part of the thesis summarizes the main results.

This thesis is based on the experimental work carried out in the Laboratory of Semiconductor Materials Technology at the Department of Materials Science, Tallinn University of Technology. The thesis is based on three published articles and on two accepted papers.

Acknowledgements

Tallinn, 2012
Katri Muska

List of publications

The thesis is based on the following papers, referred to in the text by Roman numerals **I-V**:

I   **K. Muska**, M. Kauk, M. Altosaar, M. Pilvet, M. Grossberg, O. Volobujeva. Synthesis of Cu_2ZnSnS_4 monograin powders with different compositions. Energy Procedia 10 (2011) 203 - 207.

II **K. Muska**, M. Kauk, M. Grossberg, J. Raudoja, O. Volobujeva. Influence of compositional deviations on the properties of $Cu_2ZnSnSe_4$ monograin powders. Energy Procedia 10 (2011) 323 - 327.

III **K. Muska**, M. Kauk, M. Grossberg, M. Altosaar, M. Pilvet, T. Varema, K. Timmo, O. Volobujeva, A. Mere. Impact of $Cu_2ZnSn(Se_xS_{1-x})_4$ (x = 0.3) compositional ratios on the monograin powder properties and solar cells. Thin Solid Films (provisionally accepted).

IV M. Kauk, **K. Muska**, M. Altosaar, J. Raudoja, M. Pilvet, T. Varema, K.Timmo, O. Volobujeva. Effects of sulphur and tin disulphide vapour treatments of $Cu_2ZnSnS(Se)_4$ absorber materials for monograin solar cells. Energy Procedia 10 (2011) 197 - 202.

V   M. Kauk, M. Altosaar, **K. Muska**, M. Pilvet, J. Raudoja, K. Timmo, T. Varema, M. Grossberg, E. Mellikov, O.Volobujeva. Post-growth annealing effect on the performance of $Cu_2ZnSnSe_4$ monograin layer solar cells. Thin Solid Films (provisionally accepted).

In Appendix A, copies of the following papers are included.

Author's own contribution

The contribution by the author to the papers included in the thesis is as follows:

I   Major part of experimental work (preparation of precursors and CZTS monograin powders), part of characterization (electrical measurements), analysis of the results and major part of writing.

II   Major part of experimental work (preparation of some precursors and CZTSe monograin powders), part of characterization (electrical measurements), analysis of the results and major part of writing.

III Major part of experimental work (preparation of some precursors and CZTSSe monograin powders, etching and thermal treatments of the monograins, CBD-CdS deposition), part of characterization (electrical measurements), analysis of the results and major part of writing.

IV   Part of experimental work (preparation of some precursors and monograin powders), part of characterization (electrical measurements) and minor part of writing.

V   Part of experimental work (preparation of some precursors and CZTSe monograin powder), part of characterization (electrical measurements).

SEM, EDX, XRD and Raman spectroscopic measurements were done by co-workers.

List of abbreviations and symbols

CBD   chemical bath deposition
CIG(S,Se)   CuInGa(S,Se)$_2$
CZTS   Cu$_2$ZnSnS$_4$
CZTSe   Cu$_2$ZnSnSe$_4$
CZTSSe   Cu$_2$ZnSn(S$_{1-x}$Se$_x$), $0 < x < 1$
DI-H$_2$O   deionized water
DT/TGA   thermogravimetrical analysis
E_g optical band gap
EDX   energy dispersive X-ray spectroscopy
FCC   face-centered cubic
FF fill factor
ICDD   International Centre for Diffraction Data
j_{sc} short circuit current density
KS   kesterite crystal structure
LT-ZnS   low temperature ZnS
MGL   monograin layer
PMCA   primitive mixed Cu-Au crystal structure
PV   photovoltaic
QE   quantum efficiency
RT   room temperature
SEM   scanning electron microscopy
ST   stannite crystal structure
TW   terawatt
V_{oc} open circuit voltage
XRD   x-ray diffraction
η efficiency of solar cell

1   Literature review and aim of the study
1.1   Kesterite based solar cells

Solar cells are based on semiconductors and they convert light into electricity by the photoelectric effect which was first noticed by French physicist Aléxandre Edmund Bequerel in 1839. The photons of light generate electron-hole pairs in the contact area of *p*- and *n*-type semiconductors called a *p-n* junction. These carriers with opposite charge are then separated by an electric field formed in the *p-n* junction. When the solar cell is connected to the load, electric current is generated. Solar cells consist of different layers: front contact, window layer, buffer layer, absorber layer, back contact and substrate. The *p-n* junction is formed between the buffer layer (*n*-type semiconductor) and the absorber layer (*p*-type semiconductor) [6]. Absorber layer works as a light absorber and one group of the materials that can be used as absorbers are kesterite type materials: $Cu_2ZnSn(S_{1-x}Se_x)$ ($0 \leq x \leq 1$).

Cu_2ZnSnS_4 (CZTS), $Cu_2ZnSnSe_4$ (CZTSe) and solid solutions of $Cu_2ZnSn(S_{1-x}Se_x)_4$ ($0 < x < 1$) (CZTSSe) are *p*-type semiconductors with direct band gap and high optical absorption coefficient of 10^4 cm^{-1} [7, 8]. The band gap energy of CZTS is around 1.5 eV, CZTSe has a band gap of 1.04 eV [9] and the band gap of CZTSSe lies somewhere in-between, depending on the sulfur to selenium ratio in the material [10, 11].

Kesterites are derived from the CIG(S,Se) structure by replacing In and Ga atoms (group III) in the chalcopyrite structure by Zn (group II) and Sn (group IV), thus maintaining the octet rule [9, 12]. The main advantage of this is that the standard solar cell device structure remains the same and therefore emphasis can be placed on the study of the properties of kesterites [13]. All the elements in quaternary semiconductor compound $Cu_2ZnSn(S_{1-x}Se_x)_4$ ($x = 0 - 1$) except selenium are earth abundant and environment benign [14]. It has been found that the abundance of Zn and Sn in the earth's crust is 1500 and 45 times higher than of In, respectively, and the price of In is almost two magnitudes higher than that of Zn and Sn. The photovoltaic effect in the Cu_2ZnSnS_4 material was first reported by Ito and Nakazawa in 1988 [8].

The techniques for the synthesis of kesterite thin films can mainly be classified into two main categories: vacuum and non-vacuum based methods. In vacuum based methods the constitute atoms of kesterites are sputtered or evaporated (co-evaporated) on the substrate. The technologies usually allow the composition to be easily controllable and it has good reproducibility, but the vacuum technologies are relatively expensive. Non-vacuum based methods are more cost-efficient as they use smaller amounts of energy. The non-vacuum technologies include spray pyrolysis, electrochemical deposition, spin coating, the hot injection method, the hydrothermal method, and wet ball milling combined with screen printing and monograin powder growth [15].

The best solar energy conversion efficiency achieved so far with the Cu_2ZnSnS_4 absorber material is 8.4% [16] and with the $Cu_2ZnSnSe_4$ absorber material 10.1% [17, 18]. The absorber layers in these solar cells were produced by vacuum-

deposition and vacuum co-evaporation, respectively. So far the best $Cu_2ZnSn(S_{1-x}Se_x)_4$ (0 < x < 1) based solar cell was produced by hydrazine-based solution processing at an efficiency of 11.1% [19].

1.2 Crystal structure of kesterite type materials

The unit cell of $Cu_2ZnSn(S_{1-x}Se_x)_4$ (x = 0 - 1) is shown in Figure 1.1. The mineral kesterite belongs to the $A^I_2B^{II}C^{IV}X^{VI}_4$ compound family with A = Cu, B = Zn, Fe (in the case of natural kesterites), C = Sn and X = S, Se [20]. There are two main tetragonal structure types for kesterites known from literature: kesterite-type (KS) with the space group $I\overline{4}$ (Figure 1.1a) and stannite-type (ST) with the space group $I\overline{4}2m$ (Figure 1.1b). The structures are closely related, differing only by the distributions of the Cu and Zn atoms [15]. It is also possible to have partially disordered form of a kesterite (PMCA), where the Cu and Zn atoms can be randomly arranged on their shared lattice plane (Figure 1.1c) [21]. However, as the kesterite phase is thermodynamically slightly more stable than the stannite-type, both Cu_2ZnSnS_4 (CZTS) and $Cu_2ZnSnSe_4$ (CZTSe) have the kesterite structure as a ground state, whereas the stannite and PMCA structures have higher total energies. The values of calculated lattice constant a of the KS CZTS and CZTSe are slightly larger than those of ST or PMCA structures [22]. For KS CZTS, the calculated lattice constants a and c are 5.443 Å and 10.786 Å, respectively. For KS CZTSe, the calculated lattice constants a and c are 5.717 Å and 11.378 Å, respectively [21]. Calculations show that the band gaps of the KS, ST and PMCA structures can differ by as much as 0.15 eV [21, 23] and it is suggested that estimated band gaps are: for KS CZTS = 1.56 - 1.64 eV, ST CZTS = 1.33 - 1.42 eV: KS CZTSe = 1.02 - 1.05 eV, and ST CZTSe = 0.86 - 0.89 eV [23, 24].

(a) Kesterite   **(b) Stannite**   **(c) PMCA**

Cu   Zn   Sn   S / Se
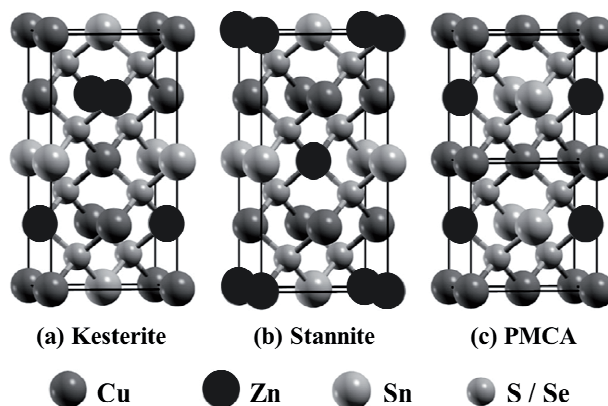
Figure 1.1 Unit cell of a) kesterite, b) stannite and c) PMCA structure for $Cu_2ZnSn(S_{1-x}Se_x)_4$ (x = 0 or 1). $Cu_2ZnSn(S_{1-x}Se_x)_4$ (0 < x < 1) structures are obtained by replacing some of the S with Se atoms [21]

In addition to kesterite type materials, ZnS or ZnSe and Cu_3SnS_4 or Cu_3SnSe_4 have a similar crystalline structure, differing only by metal cations. Thus, in all these structures, the sulfur (or selenium) face-centered cubic (FCC) sublattice determines the unit cell dimensions. But as XRD is not sensitive to the metal cation arrangement, it is a challenge to differentiate between KS, ST and PMCA structures or also between CZTS(Se), ZnS(Se) and CTS(Se) using XRD. One of the techniques which can do this is neutron scattering, but this is not an easily accessible tool. Another method can be Raman spectroscopy, where it is possible to compare active vibrational modes, which are different for these three structural types [21].

1.3 Phase diagrams

Quaternary phase diagrams of Cu_2ZnSnS_4 (CZTS) and $Cu_2ZnSnSe_4$ (CZTSe) are quite complicated and so far they have been discussed only in few papers.

I.D.Olekseyuk *et al.* investigated the phase equilibria of the quasi-ternary system of $Cu_2S-ZnS-SnS_2$ [25], $Cu_2Se-ZnSe-Cu_2SnSe_3$ [26], and $Cu_2SnSe_3-SnSe_2 - ZnSe$ [27] using differential thermal, X-ray phase and microstructure analysis methods. For the studies, both CZTS and CZTSe were synthesized through solid state chemical reaction between ZnS or ZnSe, Cu_2S or Cu_2Se and SnS_2 or $SnSe_2$.

In Figure 1.2a, vertical section Cu_2S-CZTS-$(ZnS+SnS_2)$ is presented and in Figure 1.2b, the same section for CZTSe (Cu_2Se-CZTSe-$(ZnSe+SnSe_2)$) is shown. In these phase diagrams the $ZnS+SnS_2$ consist of 50 mol% of ZnS and 50 mol% of SnS_2 and the $ZnSe+SnSe_2$ consists of 50 mol% of ZnSe and 50 mol% of $SnSe_2$. The CZTSe phase diagram presented in Figure 1.2b was constructed from two separate phase diagrams from [26, 27].

In the case of CZTS: α, β', γ, δ are solid solution regions of Cu_2S, LT-ZnS, SnS_2, and Cu_2ZnSnS_4, respectively. ZnS crystallizes in two structural types: sphalerite (LT-ZnS) and wurtzite, the temperature of polymorphic transformation is 1020°C [25]. In the case of CZTSe: α, β, γ, δ' are solid solution regions of Cu_2Se, ZnSe, $SnSe_2$, and $Cu_2ZnSnSe_4$, respectively. δ' is low temperature modification of $Cu_2ZnSnSe_4$.

Monograin powder is usually synthesized at 740°C, which is marked as a horizontal line (X) in Figure 1.2. The gray area on the graphs represents the single phase area for CZTS (Figure 1.2a, area 11) and CZTSe (Figure 1.2b, areas 7 and 9). The solid phase of $Cu_2ZnSnSe_4$ (Figure 1.2b) has a large homogeneity range and undergoes a polymorphous transformation (*9 ↔ 7*) in the temperature interval around 583-680°C (area 8) [27].
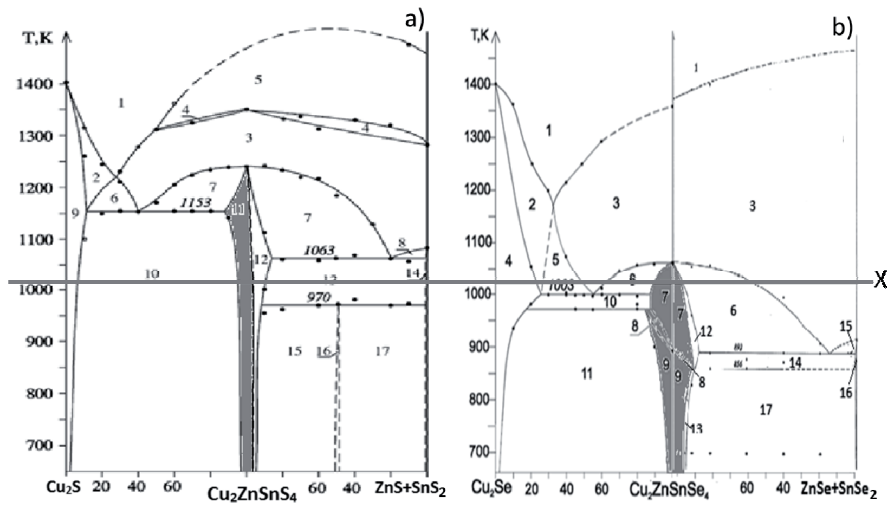
Figure 1.2 a) Phase diagram of the Cu_2S-(Cu_2ZnSnS_4)-$(ZnS+SnS)$ section, where (1) L, (2) L+α, (3) L+β′, (4) L+β+β′, (5) L+β, (6) L+α+β′, (7) L+β′+δ, (8) L+β′+γ, (9) α, (10) α+δ, (11) δ, (12) β′+δ, (13) β′+γ+δ, (14) β′+γ, (15) β′+δ+$Cu_2ZnSn_3S_8$, (16) β′+$Cu_2ZnSn_3S_8$, (17) β′+γ+$Cu_2ZnSn_3S_8$ [25] and b) phase diagram of the Cu_2Se-$(Cu_2ZnSnSe_4)$-$(ZnSe+SnSe)$ section, where (1) L, (2) L+α, (3) L+β, (4) α, (5) L+α+β, (6) L+δ+β, (7) δ, (8) δ+δ', (9) δ', (10) α+β, (11) α+δ', (12) β+δ, (13) β+δ', (14) β+γ+δ, (15) L+β+γ, (16) β+γ, (17) β+γ+δ' [26, 27]. The horizontal line (marked as X) represents the temperature (740ºC) of the monograin powder synthesis

It can be seen in Figure 1.2 that at around 400°C, the single phase area for CZTS (Figure 1.2a) is about ±2 mol% (2 mol% towards Cu_2S and 2 mol% towards ZnS+SnS$_2$) and the single phase area of CZTSe (Figure 1.2b) is around 7 mol% (2 mol% towards Cu_2Se and 5 mol% towards ZnSe+SnSe$_2$). So even a slight change in stoichiometry towards Cu_2S or Cu_2Se leads to the formation of Cu_2S (area 10) and Cu_2Se (area 11) secondary phases additionally to CZTS or CZTSe (Figure 1.2a and b, respectively). The single phase region of CZTS (area 9) is limited by the three-phase region of CZTS(liquid)+LT-ZnS+CZTS, and the line between them is the two-phase LT-ZnS+CZTS. The homogeneity region of the Cu_2S solid solution contains approximately 1 mol% of ZnS + SnS$_2$ at the annealing temperature and tends to increase with increasing temperatures reaching a maximum at the ternary peritectic temperature (Figure 1.2a). When kesterite composition is more Zn or Sn rich, then in addition to the main CZTS phase, ZnS (Figure 1.2a, area 12) or ZnSe (Figure 1.2b, area 12 and 13) can occur. When the composition is very Sn rich, also SnS$_2$ (area 13) and $Cu_2ZnSn_3S_8$ (formed at 697°C) secondary phases (area 15 and 16) can occur together with the CZTS phase (Figure 1.2a). The same conditions in CZTSe lead to the formation of ZnSe and SnSe$_2$ secondary phases (Figure 1.2b, area 14 and 17). In the case of CZTSe, the formation of other quaternary compounds has not been detected in this section.

14

The investigations on the phase diagrams of the systems by I. D. Olekseyuk *et al.* [25, 27, 26] show that the homogeneity range of the single phase $Cu_2ZnSnSe_4$ and Cu_2ZnSnS_4, are present only within a rather narrow range of compositions. The homogeneity region for both Cu_2ZnSnS_4 and $Cu_2ZnSnSe_4$ has a tendency to increase slightly with temperature. Theoretically, even a 2 - 3% compositional variation could lead to phase separation. Secondary phases, including ternary and quaternary compounds, are easier to form than kesterites due to the lower enthalpy of formation [28]. Walsh *et al*. [29] calculated the chemical-potential stability of CZTS and found that the stable region of CZTS is very small, and therefore secondary phases, especially ZnS and Cu_2SnS_3, are easily formed. Most of the growing methods of kesterites result in material consisting of secondary phases [29]. Therefore it is very challenging to find conditions for the formation of single-phase CZTS and CZTSe materials.

1.4   Formation and growth

Kesterites can be synthesized from either pure elements, binary compounds or from intermetallic compounds. Although investigations about the formation of kesterites are abundant, commonly it is assumed that the kesterite compound is formed through binary and ternary compounds.

R. Schurr *et al*. [30] found that during Cu_2ZnSnS_4 (CZTS) formation from electrochemically deposited Cu-Zn-Sn films via sulfurization, the Cu-Zn-Sn film is firstly decomposed to binary compounds and only then the formation of CZTS starts.

S. Schorr *et al.* [31] conducted in-situ high temperature XRD investigations and found that if kesterites are synthesized from binary sulfides, the formation of CZTS already starts around 300°C. Raman and XRD investigations of sulfurization of Cu/ZnSn/Cu precursors [32] revealed that the formation of CZTS started with a decrease in the CuS and SnS phase. At 270°C, only Cu_2S, SnS_2 and S peaks were observed in XRD. At 370°C, the sample consisted of metallic phases of Cu_6Sn_5 and Cu_3Sn in addition to binary sulfides. At 470°C CZTS peaks had emerged, but also ZnS, CuS and $Cu_{2-x}S$ were present. At 530°C the CZTS peak became the dominant peak, but a weak peak of Cu_2S remained in spectra. At 580°C the CZTS peak was sharp and well defined. Raman analysis indicated the presence of ternary phases such as Cu_2SnS_3, Cu_4SnS_4 and Cu_4SnS_6 and XRD investigations showed also the presence of Cu_2S, SnS and ZnSe. The authors suggested that the formation of Cu_2ZnSnS_4 probably goes through intermediate ternary phases, not straight from binaries to CZTS [32].

The main reaction baths for Cu_2ZnSnS_4 formation are presented below as Eqs. 1.1-1.3.

350-400°C: $Cu_2S + SnS_2 \rightarrow Cu_2SnS_3$ (1.1)

350-700°C: $Cu_2S + SnS_2 + ZnS \rightarrow \mathbf{Cu_2ZnSnS_4}$ (1.2)

350-700°C: $Cu_2SnS_3 + ZnS \rightarrow$ **Cu_2ZnSnS_4**   (1.3)

R. A. Wibowo *et al.* synthesized $Cu_2ZnSnSe_4$ (CZTSe) from elemental Cu, Zn, Sn and Se powders through a solid state reaction [33, 34]. XRD investigations and thermogravimetrical analysis (DT/TGA) were conducted and it was found that at 100°C hexagonal α-CuSe forms which then reacts with Se and forms an orthorhombic $CuSe_2$ phase. By 250°C, all elemental Cu is reacted to form Cu selenides. At 275°C elemental Zn is consumed to form an intermetallic Cu_5Zn_8 phase. The hexagonal γ-CuSe starts to form at around 300°C, after decomposing of $CuSe_2$ (Eq. 1.4). The reaction is completed by 320°C. At 320°C the cubic ZnSe phase was detected, which had probably formed through the reaction between Cu_5Zn_8 and liquid Se. Thus, by 320°C all the elements had formed binary compounds. At around 380°C the phase decomposition of γ-CuSe to β-Cu_2Se takes place (Eq. 1.5), which then reacts with liquid Se and SnSe, forming a ternary cubic Cu_2SnSe_3 phase (Eq. 1.6). As the ZnSe phase has disappeared by 350°C and Cu_2SnSe_3 phase by 400°C, it is most probable that at around 400-700°C $Cu_2ZnSnSe_4$ is already the dominant phase and the CZTSe formation reaction goes according to Eq. 1.7 [33].

The main reaction baths for $Cu_2ZnSnSe_4$ formation are presented below as Eqs. 1.4-1.7.

300-320°C: $CuSe_2 \rightarrow$ γ-CuSe + Se (liq.)   (1.4)
380°C: 2γ-CuSe $\rightarrow$ β-Cu_2Se + Se (liq.)   (1.5)
380°C: β-Cu_2Se + Se (liq.) + SnSe $\rightarrow Cu_2SnS_3$ (1.6)
400-700°C: $Cu_2SnSe_3 + ZnSe \rightarrow$ **$Cu_2ZnSnSe_4$**   (1.7)
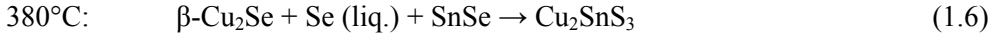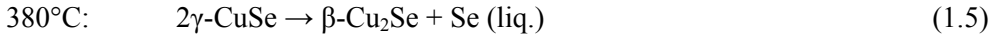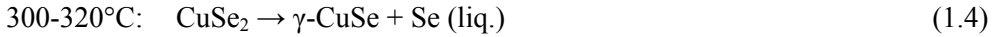
In the current work, the monograins were synthesized from ternary Cu-Zn-Sn-metal alloy and elemental sulfur and/or selenium while binary compounds were used to modify the composition, so the kesterite reaction bath in our case is more complex, but it is believed that the Cu-Zn-Sn-metal alloy decomposes to binary compounds and the formation reaction follows the above-mentioned routes.

1.5   Defect composition

Defects play an important role in determining the electrical properties of semiconductor materials. In kesterites the formation energies of dominating acceptor defects, which give the *p*-type conductivity to the materials, are lower than those of donor defects [29].

Chen *et al.* [35] performed theoretical electronic structure calculations to study the defect structure of the Cu_2ZnSnS_4 (CZTS) material. They found that in CZTS there are dominating self-compensated defect pair complexes such as [Cu_{Zn}^- + Zn_{Cu}^+] for Cu-rich/Zn-poor growth conditions and [V_{Cu}^- + Zn_{Cu}^+] for Cu-poor/Zn-rich condition. These electrically neutral defect complexes can remarkably

passivate the deep levels in the band gap, reducing the recombination in the PV device [15]. A similar result has also been reported by Nagoya *et al.* and Maeda *et al.* [36, 37]. They claimed that ZnS should be the main competing phase under the prevalent Cu-poor and Zn-rich growth conditions, and Cu at Zn sites (Cu_{Zn}) is the most stable defect in the entire stability range of CZTS [35]. This also suggests that *n*-type doping in CZTS compound will be difficult [38]. However, this is slightly different in the case of $Cu_2ZnSnSe_4$ (CZTSe). There are three basic bonds in the CZTSe structure: Cu-Se, Zn-Se and Sn-Se, the latter is more ionic than the first two, thus the Sn-Se bond is the strongest and so the formation energy of Sn vacancy is much larger than those of Cu and Zn vacancies [28]. For a ternary compound $CuInSe_2$, the dominant *p*-type acceptor defect is the Cu vacancy (V_{Cu}). However, in CZTSe, the formation energy of V_{Cu} is much larger than Cu_{Zn}, so in equilibrium growth conditions, the latter will dominate over V_{Cu}. But under Zn-rich conditions, where Zn-content in the bulk or even only near the surface is higher, it can lead to the easy formation of V_{Cu} at the surface, so both Cu_{Zn} and V_{Cu} could be candidates for the dominant acceptor defect [30, 39]. So, material growth under the Cu-poor/Zn-rich conditions is favorable to Cu-vacancy formation, although Cu-vacancies in CZTSe are more easily formed under these conditions than in CZTS.

1.6   Surface modification by thermal treatments

To achieve high-quality materials for photovoltaic devices, most kesterite preparation techniques use some kind of heat treatment step which is also common for chalcopyrites. Heating step provides energy needed for atoms to diffuse to their respective equilibrium positions, which might mean extensive reorganization of starting materials. For kesterite materials the reaction pathways and also the product material is not well understood and annealing often results in low quality, heterogeneous materials not suitable for solar cell devices. If a multinary compound is on a substrate and it is exposed to vacuum at elevated temperatures, the processes that might occur are interface reactions (at back contact/absorber material interface), reactions in the bulk of the absorber material and surface reactions. When monograins are involved, heat treatments are carried out in closed quartz ampoules, so the interface reactions can be neglected. The most important interaction is at the surface, where the multinary compound might decompose and release volatile material into the gas phase. A generic surface decomposition reaction could be written as Eq. 1.8 [40]:

Multinary (s) ↔ solid binaries (s) + volatile binary (g) + volatile element (g)   (1.8)

The reaction above is in principle reversible. When the material heated in a closed system, then at a given temperature, the volatile material evaporates and forms a certain partial vapor pressure in the atmosphere above the partially decomposed multinary compound, forming an equilibrium between the solid and gas phase. But

if a supply of gaseous products in suitable concentrations is intentionally provided, the decomposition process can be reversed or avoided completely.

The cation of the multinary compound that has the highest oxidation state is most likely to be the source of instabilities as it is the least stable element. In the case of Cu_2ZnSnS_4 (CZTS) and $Cu_2ZnSnSe_4$ (CZTSe), the problematic element is Sn^{IV} (not Cu^I or Zn^{II}) [40]. The vapor pressure of liquid Sn is far too low to see direct evaporation of the element from the compound, but tin sulfides are volatile and decompose according to Eq. 1.9 [41]. This means that in CZTS and CZTSe, SnS(Se) and S(Se) evaporate most likely and Cu_2S(Se) and ZnS(Se) remain in the solid material.

$$2SnS_2 \text{ (s)} \rightarrow Sn_2S_3 \text{ (s)} + \tfrac{1}{2}S_2 \text{ (g)} \rightarrow 2SnS \text{ (g)} + \tfrac{1}{2}S_2 \text{ (g)} \tag{1.9}$$
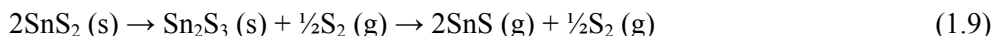
In some of the studies, dealing with the heat treatment of Cu-Zn-Sn-S layers under N_2+H_2S atmosphere, the Sn-loss was not observed. The evaporation of tin sulfides in the N_2+H_2S atmosphere is much lower than in vacuum, hence it is highly likely that the Sn loss first starts at top layers of the material [42].

Sn loss at lower temperatures is mostly linked to vacuum-based synthesis methods, where Sn loss is believed to happen because of decomposition of the Cu_2SnS_3 ternary phase [42]. At higher temperatures and also during thermal treatments of monograin powders, where all the ternary phases are most probably reacted to form a quaternary compound, the Sn loss is believed to happen due to the decomposition of quaternary compound (Eq. 1.10) noticeable around 515°C – 550°C [41, 42, 43, 44].

$$Cu_2ZnSnS_4 \text{ (s)} \rightarrow Cu_2S \text{ (s)} + ZnS \text{ (s)} + SnS \text{ (g)} + \tfrac{1}{2}S_2 \text{ (g)} \tag{1.10}$$

The decomposition rate, however, depends drastically on the experimental conditions such as temperature, total pressure inside the annealing container and partial pressures of the all involved volatile species. To some extent, the Sn loss from CZTS is reversible, as Cu_2S and ZnS could be converted to CZTS in the presence of sulfur and SnS vapors. But, when the decomposition products are transported away from the material surface, these reverse reactions cannot take place and therefore, the decomposition of CZTS has to be prevented. To avoid the Sn loss, additional inert gas atmosphere should be used to suppress material loss. Scragg *et al.* [43] showed by two different kinetic models that the ambient vapor phase with both of the components - chalcogen and tin-chalcogenide compound - is a prerequisite for stability of Cu_2ZnSnS_4 surface. Both of the proposed models predicted that if the product of the sulfur and SnS vapor pressures exceeds a certain value, the CZTS surface would be completely stabilized. Therefore it is important to determine this critical value, in order to produce CZTS with good surface quality that is vital for solar cell performance [41]. Scragg *et al.* [40] supposed that to stabilize the kesterite compound during thermal treatments a minimum 10% of the

equilibrium pressure predicted by the binary decomposition or evaporation reactions at the temperature of interest should be applied. So, to prevent the decomposition of CZTS at 550°C, the sulfur partial pressure should be greater than $2.3 \cdot 10^{-4}$ mbar and the product of partial pressures $p_{SnS} (p_{S_2})^{1/2}$ should be greater than $3.8 \cdot 10^{-5}$ mbar. As similar reaction paths occur also when dealing with CZTSe, it is believed that at 550°C, 0.1 mbar of Se and 10^{-4} mbar of SnSe should be supplied to prevent the decomposition of CZTSe [40].

1.7   Monograin powder technology

The formation of monograin powders takes place during the annealing process of precursors in the presence of the liquid phase of a suitable flux material.

The synthesized monograins are subsequently used in the monograin layer (MGL) solar cells as a single layer of grains to act as an absorber in solar cells. The idea of monograin layers for the construction of optoelectronic devices was proposed more than 30 years ago by the studies of the Philips Company [45, 46]. In the TUT Laboratory of Semiconductor Materials, the research with growing II-VI monograin powders in Na_2S_x and $CdCl_2$ started in the 1960s and growing I-III-VI monograin powders for use as absorber materials in solar cells began in 1994. In the first investigations Se, and CuSe as flux materials were used to grow $CuInSe_2$ [47, 48, 5] and Te and $CdCl_2$ to grow CdTe monograin powders [49]. Although using CuSe-Se as a flux resulted in monograins with nearly stoichiometric $CuInSe_2$ composition, the removal of the flux from the monograins after the synthesis was technologically difficult, so CuSe-Se was replaced by water soluble potassium iodide (KI) [50]. Starting from 2005, the group started investigations on I-II-IV-VI monograin powders [51]. In parallel, investigations to find alternative flux materials were also carried out. The flux materials should have low melting temperature and high solubility in water, allowing for an easy separation of the crystals from the flux [52]. Suitable candidates for fluxes are NaI and CdI_2 [52, 53, 54], but also ZnI_2 could be used. A.S. Ionkin *et al.* used even CsCl and different mixtures of CsCl and CsBr, KCl or KCl/NaCl as flux materials to prepare kesterite materials [55].

Growth of single-crystalline powder grains takes place at temperatures above the melting point of the used flux material, but at lower temperatures than the melting point of the semiconductor itself. The amount of the used flux material has to exceed a certain amount sufficient to fill all the empty space between initial precursor particles. This avoids particle sintering by repelling the precursor particles and the formed single crystalline monograins from each other [56]. Therefore, the volumes of the solid phase and molten phase are usually taken as equal ($V_S = V_L$) [48]. After the formation of the primary powder particles the recrystallization starts. This thermodynamically-driven spontaneous process occurs because crystals of different size have different surface energy, thus larger particles are energetically more favored than smaller particles. The process is called Ostwald ripening [57]. When the monograins have achieved a desired size, the synthesis process is stopped by

quenching and the flux is removed by washing with deionized water, releasing monograins.

The formation of $Cu_2ZnSnSe_4$ monograin powders from binary chalcogenides in KI flux has been studied in [53, 54]. It was found that the reaction bath is in correlation with literature (see section 1.4). Cu_2SnSe_3 and CZTSe, indicated by their Raman peaks, were present already at 400ºC, although the KI melting point is 685ºC. At around 680ºC some part of ZnSe, with a high melting point of 1526ºC, or SnSe (melting point 861ºC) are still unreacted. The chemical interactions are induced by the formation of the liquid phase [53].

At high temperatures, some part of chalcogenides and also kesterite material are dissolved in the flux. The solubility of ZnSe, CuSe and $Cu_2ZnSnSe_4$ in KI is below 0.6 mol% and the solubility of SnSe in KI is 3.6 mol% [53]. During the cooling of the batch of the material, part of the dissolved chalcogenides and/or dissolved kesterite precipitates on the surfaces of the monograins. These precipitates change the surface composition of monograins, which could lead to the change in p-n junction properties. Therefore, additional chemical and thermal treatments are needed to remove them.

Timmo *et al.* [58, 59] synthesized $Cu_2ZnSn(S_{1-x}Se_x)_4$ monograin powders with different S to Se ratios ($0 \leq x \leq 0.85$) in molten KI. It was found that higher sulfur content in monograin powders improves the values of open circuit voltages of MGL solar cells and shifts the absorption edge of normalized quantum efficiency (QE) spectra to shorter wavelengths. This indicates that the band gap energy value of the materials increases with increasing sulfur content. Solar cells based on $Cu_2ZnSn(S_{0.85}Se_{0.15})_4$ monograin powders had the highest values of open circuit voltage of 660 mV. The best solar cell characteristics were achieved with materials containing 75 mole% of sulfur and 25 mole% of selenium.

Although the monograin powder technology is relatively simple and cost-efficient and enables single crystal growth with a uniform structure, which can be used also for flexible devices, the technology has not yet found wide use in the industrial production of photoelectronic devices and solar cells. This could be explained by some unsolved technical and scientific problems, such as: finding the growth conditions of single phase kesterite powders, the reasons of large deviations from normal Gaussian size distribution of monograins, the optimal crystal growth and thermal and chemical post-treatments parameters are not yet defined for using kesterite monograin powders as absorbers in MGL solar cells.

1.8 Summary of the literature overview and the aim of the study

The studies on kesterite absorber materials can be summarized as follows:
- Previous reports have shown that monograin powder technology is relatively simple and cost-efficient and enables us to grow powders with single crystals that have uniform composition and structure. It was found that solid solutions of $Cu_2ZnSn(S_{1-x}Se_x)_4$ (x = 0 - 1) as solar cell absorber materials in a monograin powder form can be grown in KI. Resulting from the studies of the influence of

S/Se concentration ratio in solid solutions of CZTSSe on the properties of MGL solar cells based on these absorber materials, it was found that open circuit voltage values of solar cells can be changed in a large range of 300 - 700 mV. No systematic studies on the influences of the [Cu]/([Zn]+[Sn]) and [Zn]/[Sn] concentration ratios on the properties of kesterite monograin powders have been reported.

- The investigations on the phase diagrams of the systems have shown that the homogeneity range of single phase $Cu_2ZnSnSe_4$ and Cu_2ZnSnS_4 exists only within a rather narrow range of compositions. Theoretically even a 2 - 3% compositional variation could lead to phase separation and to the formation of secondary phases including binary and ternary compounds. Therefore it is very challenging to synthesize single phase $Cu_2ZnSnSe_4$ and Cu_2ZnSnS_4 monograin powders.

- From theoretical and experimental studies it can be summarized that Cu-poor and Zn-rich composition of absorber material can improve the efficiency of $Cu_2ZnSnSe_4$ solar cells. Cu vacancies in Cu-poor conditions form shallow acceptor levels in $Cu_2ZnSnSe_4$, which lead to *p*-doping. Zn-rich conditions also prevent the substitution of Cu on Zn sites, which would give rise to relatively deep acceptor levels. Therefore, a precise control of the composition and the phase structure of kesterite monograin powders are important to achieve high efficiency MGL solar cells.

- It was found that kesterite materials produced by vacuum technologies often suffer from decreased tin content. To avoid Sn loss by the decomposition of quaternary compounds during annealing processes, it is crucial to keep the sulfur (selenium) pressure high using tin dichalcogenides or elemental sulfur or selenium containing atmospheres. Controlling the tin losses in the annealing environment can improve the solar cell efficiency significantly and reproducibly. Comparative studies on the influence of annealing in well determined conditions and atmosphere on the elemental composition, structural and electrical properties of kesterite materials have not been reported in the literature.

On the basis of literature data summarized above, the objectives of the present doctoral thesis are:

- To study the influence of the initial composition of precursors on the composition and properties of synthesized Cu_2ZnSnS_4, $Cu_2ZnSnSe_4$ and $Cu_2ZnSn(S_{0.7}Se_{0.3})_4$ monograin powders to determine the single phase composition range for these materials. The elemental composition, phase composition, and electrical and morphological properties of synthesized materials are studied depending on the initial precursor composition.

- To investigate the impact of post-growth annealing in various gas atmospheres on the bulk composition of crystals and structural properties of the $Cu_2ZnSn(S_{1-x}Se_x)_4$ ($x = 0, 0.3, 1$) monograin powders.

- To prepare monograin layer solar cells and to study their properties depending on technological variables, such as absorber composition and post-growth annealing regimes.

2   Experimental

Divided into four parts, this section gives an overview of the main experimental processes and variables. The first three subsections describe the techniques and experimental conditions of monograin powder growth, thermal treatments, and monograin layer solar cell preparation. The last subsection covers the characterization methods used in the studies.

2.1   Preparation of monograins

The powder materials were synthesized from Cu-Zn-Sn metal alloy powder with $Cu_{1.67}Zn_{1.03}Sn_{1.0}$ composition and elemental sulfur (selenium) in evacuated quartz ampoules in the liquid phase of potassium iodide (KI) as flux. The composition of the monograin materials was modified by the addition of high-purity (99.999%) Cu_2S or CuSe, SnS or SnSe and ZnS or ZnSe binary powders. The process was similar to the one used to grow CIS monograin powders [50].
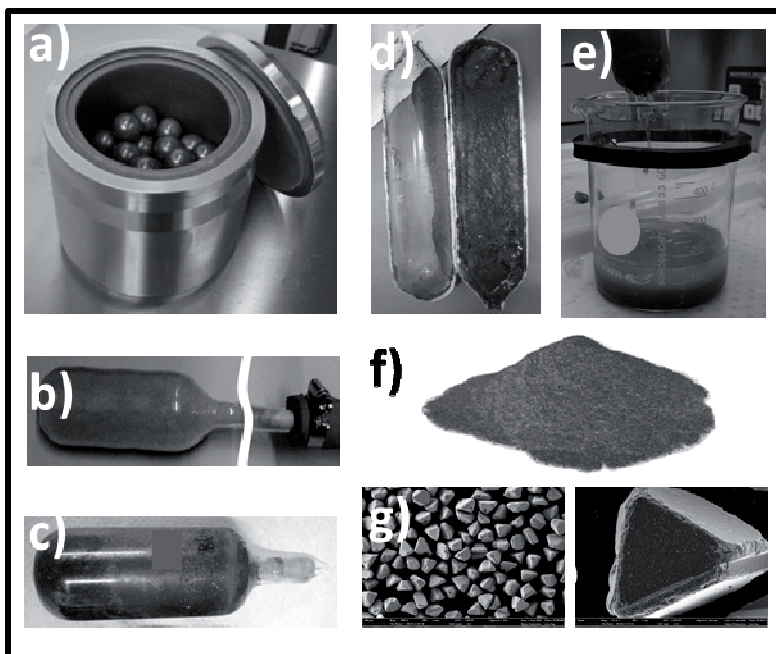
Figure 2.1 Technological steps of the monograin powder preparation process: a) mixing of precursors in a ball mill, b) degassing the mixture, c) quartz ampoule with monograin powder and KI after synthesis, d) opening of the ampoule, e) leaching process with DI water, f) powder after drying and g) powder grains after sieving

From the precursors used, $Cu_{1.67}Zn_{1.03}Sn_{1.0}$, ZnS, ZnSe, S, and Se, were commercial products purchased from different companies. Binary compounds, CuSe and SnSe, were self-synthesized from high purity (99.999%) elements in evacuated quartz ampoules at temperatures 500°C. Cu_2S and SnS binary compounds were self-synthesized at 740°C. All self-synthesized precursors were ground in an agate mortar before use in the powder growth process. KI was heated under dynamic vacuum (continuous vacuum pumping) at temperatures up to 270°C for dehydration. The precursors were mixed and ground in a ball mill (Figure 2.1a) in intended quantities and ratios. The initial compositions of precursor mixtures for Cu_2ZnSnS_4 (CZTS), $Cu_2ZnSnSe_4$ (CZTSe) and $Cu_2ZnSn(S_{0.7}Se_{0.3})_4$ (CZTSSe) monograin powder synthesis are presented in Table 2.1, Table 2.2 and Table 2.3, respectively.

After mixing and milling the precursors, the mixture was poured into a quartz ampoule, degassed under dynamic vacuum (Figure 2.1b), sealed, and annealed isothermally at 740°C for 90 hours.

The formation of kesterite monograin powders takes place during the heating process in the liquid phase of the KI flux. The latter must be used in an amount exceeding the limit for sintering of the initial precursor particles. The amount of the components for the kesterite synthesis and the amount of the flux were taken nearly equal to provide enough volume of the liquid phase for filling the free volume between the solid particles, which is one prerequisite for monograin growth. The formation of primary kesterite particles begins after the melting of the flux material. After the formation of the primary seed particles the recrystallization starts. This thermodynamically-driven spontaneous process occurs because larger particles are energetically more favored than smaller ones.

After the synthesis, ampoules were quenched to room temperature and opened (Figure 2.1c and d). The flux material was removed by leaching with deionized water (DI-H_2O) and solid particles were washed by decantation (Figure 2.1e). The released monograin powder was dried in a hot-air thermostat and sieved to narrow granulometrical fractions between 20 μm to 112 μm (Figure 2.1f and g).

Monograin powder growth and the materials used are described in papers [I-V].

Table 2.1 The initial composition of Cu_2ZnSnS_4 monograin powders

Sample	Compositions and element concentration ratios of input precursors							
	Cu at%	Zn at%	Sn at%	S at%	Se at%	Cu/ (Zn+Sn)	Zn/Sn	Cu/Sn
CZTS-1	22.57	13.92	13.51	50.00	-	0.82	1.03	1.67
CZTS-2	23.15	13.62	13.23	50.00	-	0.86	1.03	1.75
CZTS-3	23.70	13.34	12.95	50.00	-	0.90	1.03	1.83
CZTS-4	24.37	13.01	12.63	50.00	-	0.95	1.03	1.93
CZTS-5	25.06	12.65	12.29	50.00	-	1.00	1.03	2.04
CZTS-6	26.23	12.06	11.71	50.00	-	1.10	1.03	2.24
CZTS-7	24.53	12.09	13.38	50.00	-	0.96	0.90	1.83
CZTS-8	24.21	12.59	13.20	50.00	-	0.94	0.95	1.83
CZTS-9	23.28	13.99	12.72	50.00	-	0.87	1.10	1.83
CZTS-10	22.70	14.89	12.41	50.00	-	0.83	1.20	1.83

Table 2.2 The initial composition of $Cu_2ZnSnSe_4$ monograin powders

Sample	Compositions and element concentration ratios of input precursors							
	Cu at%	Zn at%	Sn at%	S at%	Se at%	Cu/ (Zn+Sn)	Zn/Sn	Cu/Sn
CZTSe-1	22.57	13.92	13.51	-	50.00	0.82	1.03	1.67
CZTSe-2	23.70	13.34	12.95	-	50.00	0.90	1.03	1.83
CZTSe-3	25.00	12.68	12.32	-	50.00	1.00	1.03	2.03
CZTSe-4	26.17	12.09	11.74	-	50.00	1.10	1.03	2.23
CZTSe-5	24.17	11.89	13.21	-	50.00	0.96	0.90	1.83
CZTSe-6	24.20	12.57	13.23	-	50.00	0.94	0.95	1.83
CZTSe-7	23.28	13.99	12.72	-	50.00	0.87	1.10	1.83
CZTSe-8	22.71	14.89	12.40	-	50.00	0.83	1.20	1.83
CZTSe-9	21.63	16.55	11.82	-	50.00	0.76	1.40	1.83

Table 2.3 The initial composition of $Cu_2ZnSn(S_{0.7}Se_{0.3})_4$ monograin powders

Sample	Compositions and element concentration ratios of input precursors								
	Cu at%	Zn at%	Sn at%	S at%	Se at%	Cu/(Zn+Sn)	Zn/Sn	Cu/Sn	S/(S+Se)
CZTSSe-1	22.57	13.92	13.51	35.00	15.00	0.82	1.03	1.67	0.70
CZTSSe-2	23.15	13.62	13.23	35.00	15.00	0.86	1.03	1.75	0.70
CZTSSe-3	23.70	13.34	12.95	35.00	15.00	0.90	1.03	1.83	0.70
CZTSSe-4	24.37	13.01	12.63	35.00	15.00	0.95	1.03	1.93	0.70
CZTSSe-5	25.00	12.68	12.32	35.00	15.00	1.00	1.03	2.03	0.70
CZTSSe-6	24.53	12.09	13.38	35.30	14.70	0.96	0.90	1.83	0.71
CZTSSe-7	24.21	12.59	13.20	35.30	14.70	0.94	0.95	1.83	0.71
CZTSSe-8	23.28	13.99	12.72	35.30	14.70	0.87	1.10	1.83	0.71
CZTSSe-9	22.70	14.89	12.41	35.30	14.70	0.83	1.20	1.83	0.71
CZTSSe-10	21.63	16.55	11.82	35.30	14.70	0.76	1.40	1.83	0.71

2.2 Post-treatment of as-grown monograins

During the cooling down period in the synthesis process, some precipitates from the material dissolved in the molten flux remain on the surfaces of the monograins (see section 1.7). In order to remove these precipitates, all the monograin powders were sequentially etched with 1% bromine in methanol (Br_2-MeOH), followed by etching with 10% aqueous solution of KCN at room temperature. After etching, the crystals were washed in DI-H_2O. The used etching process was developed by our group earlier, thus the details of the etching procedures are published elsewhere [60].

After chemical treatments, monograins were heat-treated in various atmospheres. The heat treatments were carried out in closed quartz ampoules using either isothermal or two-temperature zone arrangement. Isothermal treatments were carried out either in small, around 5 cm long, ampoules with no additional vapor source (Figure 2.2a) or with an additional vapor source (Figure 2.2b). The temperature along the whole ampoule length was kept constant. In the two-temperature zone setup, the ampoules used were around 30 cm long and the temperatures of both of the zones were regulated and controlled independently (Figure 2.2c). Elemental Se, S or $SnSe_2$, SnS_2 pellets were placed into the lower temperature zone of the ampoules. Monograin powder was heated in the higher temperature zone. The lowest temperature in the ampoule determines the vapor pressure of the components. After annealing, the ampoules were taken out of the furnace and cooled down to a ceramic plate at room temperature. Description of the thermal treatment procedure is given in papers [III, IV and V].
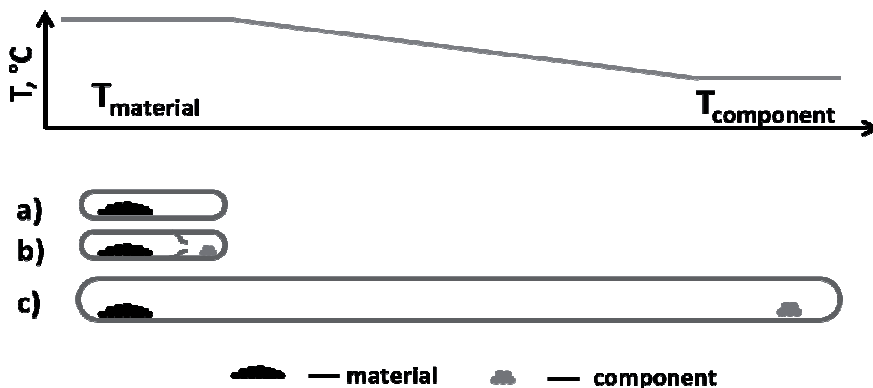
Figure 2.2 Temperature profile in the heat-treatment furnace along the ampoules in a) isothermal, b) isothermal with additional vapor source and b) two-temperature zone setup

Table 2.4 Conditions of thermal treatments

Material	Source of component	S	Se	SnS_2	$SnSe_2$	Ref.
CZTS	$T_{material}$, °C	550-740		740		[IV]
	$T_{component}$, °C	280-465		330-740		
	t, minutes	10-30		10-30		
CZTSe	$T_{material}$, °C		550-740		550-740	[IV, VI]
	$T_{component}$, °C		600		650	
	t, minutes		10-960		10-960	
CZTSSe	$T_{material}$, °C	740	650	740		[III, VI]
	$T_{component}$, °C	465	650	740		
	t, minutes	30	30	30		

Technological parameters of the applied thermal treatments are summarized in Table 2.4. The correlation between vapor pressures and temperature of different atmospheres is shown in Figure 2.3.
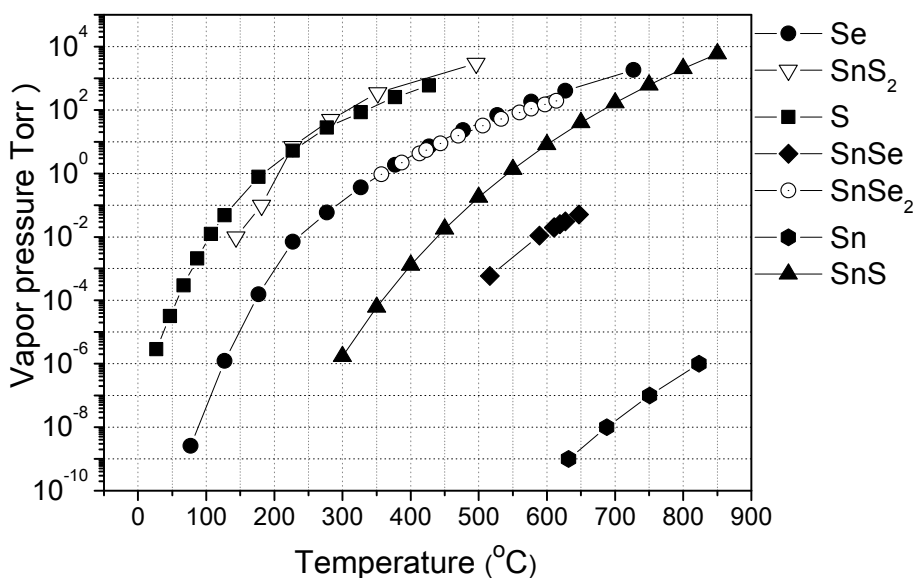
Figure 2.3 Equilibrium vapor pressure of different elements and compounds: Se, SnSe, SnSe$_2$ [61], S and Sn [62], SnS [63], and SnS$_2$ [64]

2.3   Preparation of monograin layer solar cells

All the post-treated monograin powders were used as absorber materials in MGL solar cells. The MGL solar cell has a superstrate structure: graphite/CZTS, CZTSe or CZTSSe/CdS /ZnO/ glass, where the MGL consists of a monolayer of powder grains embedded into a layer of epoxy. The cross section of the MGL solar cell is presented in Figure 2.4.
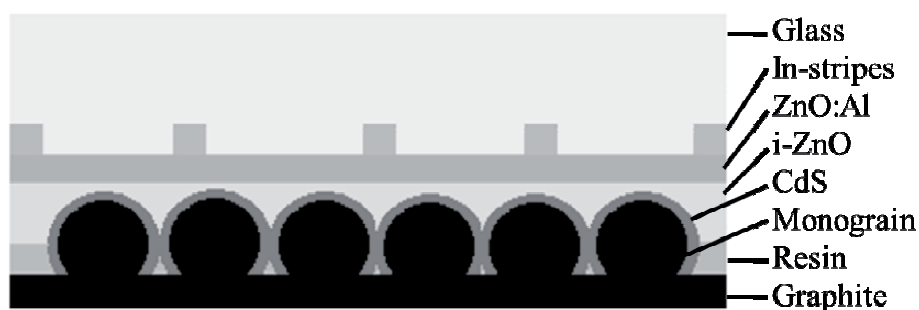
Figure 2.4 Cross section illustration of the monograin layer (MGL) solar cell

To make MGL solar cells, monograins from one specified fraction are used. The difference between monograin diameters within one fraction is around 10 - 20%. Monograins are covered with chemically deposited (CBD) CdS buffer layer. After the CdS deposition, the grains are embedded into the epoxy layer so that the top of the grains remains uncovered. After the hardening of epoxy, first the intrinsic ZnO (i-ZnO) and then aluminum doped ZnO (ZnO:Al) are sputtered on the top of CdS layer by radio frequency (RF) sputtering. After the deposition of the window layer, 1 - 2 μm thick indium grid contacts are evaporated on top and finally, the front of the structure is sealed by gluing the whole structure on a glass plate. For applying back contact, the epoxy from the back contact side of MGL is removed partly by etching with concentrated H_2SO_4, which enables access to each grain. The uncovered monograins are then mechanically polished with sandpaper and graphite contacts are applied on them. The active area of the MGL solar cells (on the front contact side of MGL) is around 75% of the total area. The other 25% of the total area, comprising epoxy between the absorber crystals, is passive.

2.4 Characterization of monograins and solar cells

The characterization methods used to analyze monograin powders and solar cells are summarized in Table 2.5. More detailed information about the instrumentation can be found in the experimental sections of References I-V.

Table 2.5 Characterization techniques and apparatus used in the study

Properties	Analytical method	Apparatus	Ref.
Elemental composition	Energy dispersive x-ray spectroscopy (EDX)	ZEISS HR SEM ULTRA 55 with Röntec EDX XFlash 3001 detector	[I-V]
Morphology	High resolution scanning electron microscope (SEM)	ZEISS HR SEM ULTRA 55	[I-V]
Phase composition	Room temperature (RT) Micro Raman spectroscopy (Raman)	Horiba's LabRam HR spectrometer	[I-V]
Phase composition	X-Ray Diffraction (XRD)	Rigaku ULTIMA IV diffractometer	[III]
Conductivity type	Hot probe measurements	Potentiometer/ Multimeter Brymen BM 338	[I-III]
Electrical grain resistance	2 point contacting with In contacts	Potentiometer/ Multimeter Brymen BM 338	[I-IV]
Solar cell quality	Quantum efficiency (QE)	Autolab PGSTAT 30	[III-V]
Solar cell characteristics	Current density versus voltage (*I-V*)	Keithley 2400	[III-V]

2.4.1   Current-voltage characteristics

The output parameters of MGL solar cells were deduced from *I-V* characteristics. *I-V* curves of solar cells were measured in dark and under the white light illumination of 100 mW/cm^2 (AM 1.5) using AUTOLAB PGSTAT 30 set-up. Solar cell efficiency was calculated by Eq. 2.1.

$$\eta = \frac{j_{SC} \cdot V_{OC} \cdot FF}{P_{st}} \cdot 100\% ,$$
(2.1)

where
η - efficiency;
j_{SC} - short circuit current density;
V_{OC} - open circuit voltage;
FF - fill factor;
P_{st} - power of the standard illumination of AM1.5 (100 mW/cm^2).

The fill factor of the solar cell was calculated by Eq. 2.2.

$$FF = \frac{j_{eff} \cdot V_{eff}}{j_{SC} \cdot V_{OC}} ,$$
(2.2)

where
FF - fill factor;
j_{eff} - current density at maximum power output;
V_{eff} - voltage at maximum power output;
V_{OC} - open circuit voltage;
j_{SC} - short circuit current density.

3 Results and discussion

The experimental work is divided into two main parts. The first part is dedicated to the compositional, structural and electrical properties of the synthesized $Cu_2ZnSn(S_{1-x}Se_x)_4$ (x = 0, 0.3, 1) monograins. The second part presents the results of post growth annealing studies on the properties of $Cu_2ZnSn(S_{1-x}Se_x)_4$ (x = 0, 0.3, 1) monograins and on the parameters of MGL solar cells based on these monograins.

3.1 Properties of as-grown monograin powders

There are only few papers in the literature describing the phase diagrams of Cu_2S-ZnS-SnS_2 and Cu_2Se-$ZnSe$-$SnSe_2$ systems, furthermore, no data are available about the phase diagrams of Cu_2ZnSnS_4 - $Cu_2ZnSnSe_4$ solid solution systems. Kesterite monograin powders are formed in closed ampoules, in the presence of liquid phase of KI. During the synthesis, some part of the binaries and of the formed kesterite dissolves in KI forming an equilibrium distribution of the material between the solid and liquid phases. When the material is cooled down after the synthesis, part of the dissolved material can form precipitates on the surface of monograin powder crystals. These precipitates change the surface composition of the monograins, which could lead to the change in *p-n* junction properties. As these precipitates are formed from initial precursors, the bulk composition of the synthesized monograins could also be changed. Therefore, additional studies must be conducted to study the compositional limits in the kesterite monograin systems.

In order to determine the exact compositional limits to obtain single phase monograin powders, the influence of the initial precursor composition on the final composition and on the properties of Cu_2ZnSnS_4, $Cu_2ZnSnSe_4$ and $Cu_2ZnSn(S_{0.7}Se_{0.3})_4$ monograin powders was investigated.

The compositional variations are mainly expressed by two parameters: [Cu]/([Zn]+[Sn]) and [Zn]/[Sn], where [Cu], [Zn] and [Sn] are atomic concentrations (at%) of the elements in the kesterite compound.

The precise initial precursor compositions and growth conditions are described in section 2.1.

3.1.1 The effect of concentration ratios of precursors on the elemental and phase composition of monograin powders

In the present study two experimental series were made with all three types of materials: Cu_2ZnSnS_4 (CZTS), $Cu_2ZnSnSe_4$ (CZTSe) and $Cu_2ZnSn(S_{0.7}Se_{0.3})_4$ (CZTSSe). In the first series the concentration ratio of Zn/Sn was kept constant and equal to 1.03, while the concentration ratio of Cu/Sn was varied. In the second series, the concentration ratio of Zn/Sn was changed, while the Cu/Sn concentration ratio was kept constant at 1.83. The initial compositions of precursors for synthesis of CZTS, CZTSe and CZTSSe monograin powders are presented in Table 2.1,

Table 2.2 and Table 2.3, respectively. Current study was focused mainly on the "Cu-poor" ([Cu]/([Zn]+[Sn]) < 1) and "Zn-rich" ([Zn]/[Sn] > 1) regions, but some powders were synthesized outside of those regions in order to clarify the compositional limits of the system.

In this study, the bulk chemical and phase composition of the synthesized monograin powders was determined from mechanically polished crystals using EDX and Raman analysis [I, II, III]. In this section, the compositional limits for single phase CZTS, CZTSe and CZTSSe monograin powders will be determined.

3.1.1.1 Elemental and phase composition of Cu_2ZnSnS_4 monograin powders

Figure 3.1 gives the values of Cu/(Zn+Sn) and Zn/Sn compositional ratios of the synthesized monograins, calculated from initial precursor compositions (Table 2.1) and from EDX analysis results of the produced powders. The hollow dots represent the initial metal compositions of the materials investigated in this study. The filled squares and dots represent metal compositional ratios of the synthesized powders. Figure 3.1a represents the series where Cu content was changed and the Zn/Sn concentration ratio was kept constant at 1.03. Figure 3.1b represents the series where Zn content was varied while Cu/Sn concentration ratio was kept constant at 1.83. More detailed description of the study is reported in paper [I].
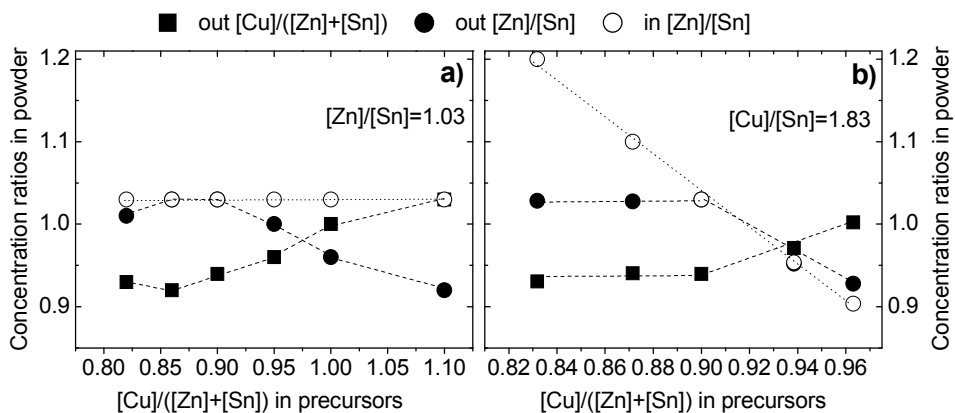
Figure 3.1 [Cu]/([Zn]+[Sn]) (filled squares) and [Zn]/[Sn] (filled dots) ratios of Cu_2ZnSnS_4 monograin powders depending on the [Cu]/([Zn]+[Sn]) ratio in precursors when a) [Zn]/[Sn] was kept constant and b) [Cu]/[Sn] was kept constant. Hollow dots represent the Zn to Sn concentration ratio in precursors

EDX analysis showed that the final composition of the Cu_2ZnSnS_4 monograin powders can be adjusted only in the following regions: Cu content between 23.9 and 25.3 at%, Zn content between 11.9 and 13.2 at% and Sn content between 12.7

and 13.0 at%. Thus, the variation in the compositional ratio of Cu/(Zn+Sn) and Zn/Sn in the synthesized powders remained between 0.92 and 1.03. When the Cu content in the initial precursor mixture was increased, but the Zn/Sn ratio was kept constant at 1.03 (see Figure 3.1a), the compositional ratio Zn/Sn in the synthesized materials decreased from 1.03 to 0.92. When the Cu/(Zn+Sn) concentration ratio was below 0.9, the Zn/Sn ratio remained constant in the synthesized materials. A similar trend was seen in the case where the Cu/Sn concentration ratio was kept constant at 1.83 while changing the Zn content in the precursor mixture (see Figure 3.1b). If the concentration ratio of Zn/Sn in precursor mixture was increased, the Cu/(Zn+Sn) concentration ratio in the synthesized powders decreased. When the Zn/Sn ratio was increased beyond 1.03, the Zn/Sn ratio in the synthesized powders remained unchanged and the Cu/(Zn+Sn) concentration ratio also remained almost constant (around 0.93 - 0.95).

The differences between the composition of precursor mixtures and the composition of synthesized powders lead to an assumption, that both Zn and Cu are forming also separate phases in the material. SEM images of polished CZTS crystals are shown in Figure 3.2. According to SEM results, some CZTS crystals contained areas of secondary phases. In Cu-rich conditions (concentration ratio of Cu/(Zn+Sn) $\geq$ 1.0), regions with composition characteristic of the $Cu_{2-x}S$ phase were detected also by the EDX analysis (see Figure 3.2b).
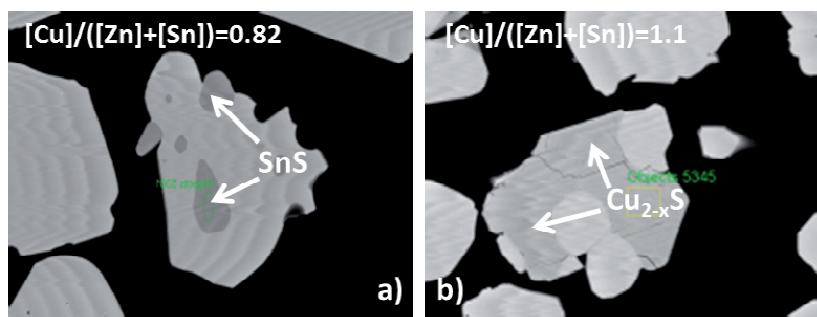
Figure 3.2 SEM images of mechanically polished a) Sn-rich and b) Cu-rich Cu_2ZnSnS_4 crystals

The presence of $Cu_{2-x}S$ compound was confirmed by its Raman peak at 473 cm^{-1} [65] (see Figure 3.3b)). The formation of $Cu_{2-x}S$ on the Cu-rich side of compositions is in agreement with the phase diagram assembled by Olekseyuk *et al* [25]. The SEM, EDX and Raman investigations showed that powders with initial compositional ratio of Cu/(Zn+Sn) below 0.95 and Zn/Sn > 1.03 contain a separate phase of ZnS. The results of Raman analysis confirmed the presence of this separate ZnS phase in crystals by its Raman peak at 351 - 353 cm^{-1} [65] (see Figure 3.3d).
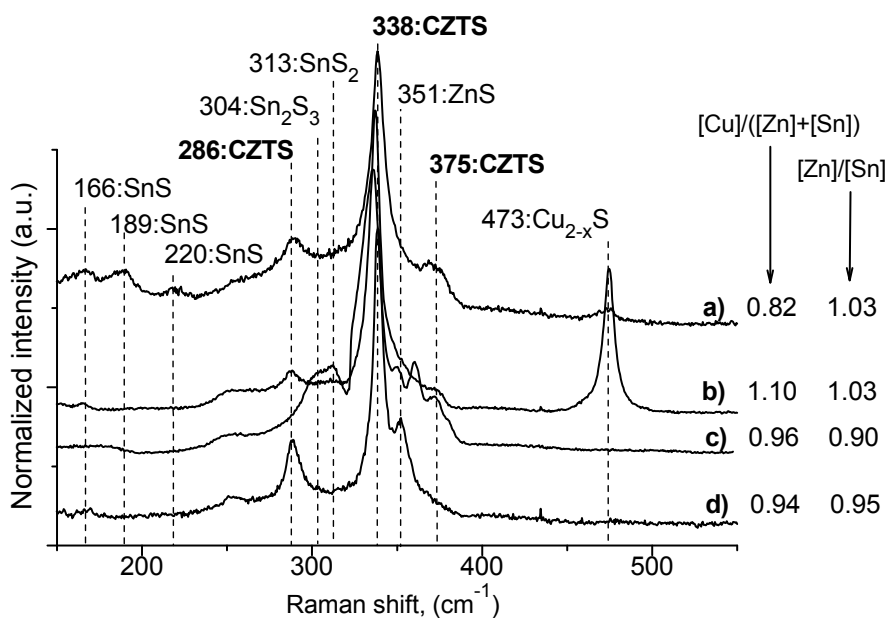
Figure 3.3 RT Raman spectra of Cu_2ZnSnS_4 (CZTS) powders with different initial [Cu]/([Zn]+[Sn]) and [Zn]/[Sn] compositions a) 0.82 and 1.03, b) 1.10 and 1.03, c) 0.96 and 0.9, d) 0.94 and 0.95, respectively

All Raman spectra of CZTS powders independent of the Cu- and Zn-content showed (Figure 3.3) the characteristic Raman peaks of CZTS at 286, 338, and 375 cm^{-1} [65]. In the case of the lowest Cu content in the precursors (Cu/(Zn+Sn) = 0.82), additional phases of SnS and SnS$_2$ were detected by their Raman peaks at 166, 189, 220, and 313 cm^{-1} [66], respectively (see Figure 3.3a). Regions with composition characteristic of the SnS phase were detected also by the EDX analysis (see Figure 3.2a). An additional Sn$_2$S$_3$ phase with the characteristic Raman mode at 304 cm^{-1} [65] was detected. The powder with the highest Sn content in the initial composition has the CZTS peak at 338 cm^{-1} with a shoulder peak at lower wave numbers at around 330 cm^{-1} (see Figure 3.3c), which could be assigned to some separate ternary Cu-Sn-S phases [67] among the powder crystals.

From the results it can be concluded, that the composition region for the single phase CZTS monograin powder synthesis is narrow. Already a slight deviation from this area leads to the formation of separate phases in addition to the CZTS compound. In the case of excess Zn (concentration ratio of Zn/Sn > 1.03), ZnS forms as a secondary phase. In the opposite case, under Zn-poor conditions, separate Sn-S phases are present in addition to the ZnS phase. A Cu-rich composition results in an additional Cu$_{2-x}$S phase on the powder crystal surfaces.

In conclusion, single phase Cu$_2$ZnSnS$_4$ monograin powders could be synthesized from a precursor mixture comprising metal ratios of Cu/(Zn+Sn) = 0.90 - 0.95 and

Zn/Sn = 1.0 - 1.03. In atomic percentages, these ratios correspond to the Cu content of 23.8 ± 0.5 at%, the Zn content of 13.3 ± 0.7 at% and the Sn content of 13 ± 0.2 at%.

3.1.1.2 Elemental and phase composition of $Cu_2ZnSnSe_4$ monograin powders

To study the influence of Cu and Zn content in $Cu_2ZnSnSe_4$ (CZTSe) monograin powders, several powders were grown with different Cu and Zn content in precursors (Table 2.2). The metal composition ratios of the initial (hollow dots) and synthesized (filled squares and dots) monograins are shown in Figure 3.4. Figure 3.4a presents the series where Cu content was changed and the Zn/Sn concentration ratio was kept constant at 1.03. Figure 3.4b presents the series where Zn content was varied while the Cu/Sn concentration ratio was kept constant at 1.83. More detailed description of the work is reported in paper [II].
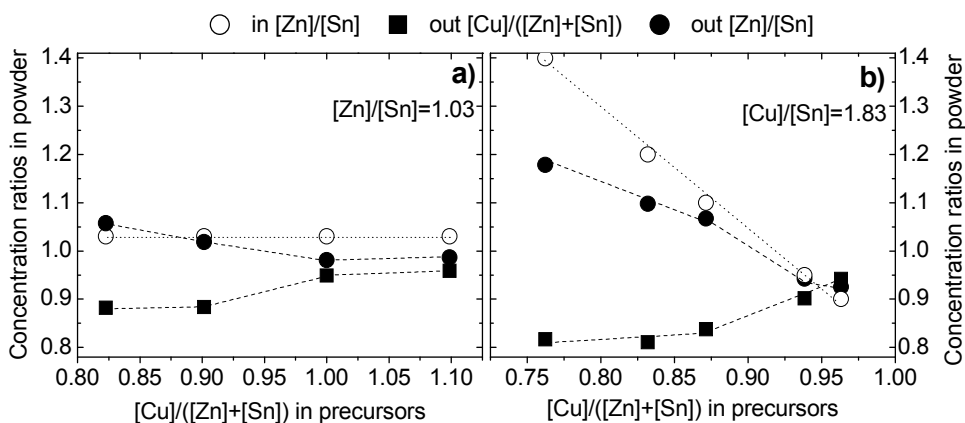
Figure 3.4 [Cu]/([Zn]+[Sn]) (filled squares) and [Zn]/[Sn] (filled dots) ratios of $Cu_2ZnSnSe_4$ monograin powders depending on the [Cu]/([Zn]+[Sn]) ratio in precursors when a) [Zn]/[Sn] was kept constant and b) [Cu]/[Sn] was kept constant. Hollow dots represent the Zn to Sn concentration ratio in precursors

It was found that the Cu content could be changed only by 2 at% (from 22.4 - 24.5 at%), although the initial Cu content in the precursors was changed almost by 5 at%. Thus, the variation in the compositional ratio of Cu/(Zn+Sn) in the synthesized powders was only between 0.8 and 1.0. The Zn content in synthesized powders changed from 12.4 to 14.9 at% and the Sn content from 12.6 and 13.5 at%, which corresponds to the change in the Zn to Sn ratio of 0.9 to 1.2. It was observed that when the Zn content in the precursors was increased while Cu/Sn was kept constant at 1.83, the Cu/(Zn+Sn) concentration ratio in the synthesized powders decreased. Further, if the Cu content was increased while the Zn/Sn ratio was kept constant at

1.03, the Zn to Sn concentration ratio in the synthesized materials decreased. When the compositional ratio of Cu/(Zn+Sn) in the precursors was greater than 1, the concentration ratio of the metals in the synthesized materials did not change further. When the Cu/(Zn+Sn) concentration ratio in the precursors decreased, the Zn/Sn ratio in the powders was still increased. Thus, it can be assumed that in the latter case Cu vacancies are formed, which are then occupied by Zn atoms.
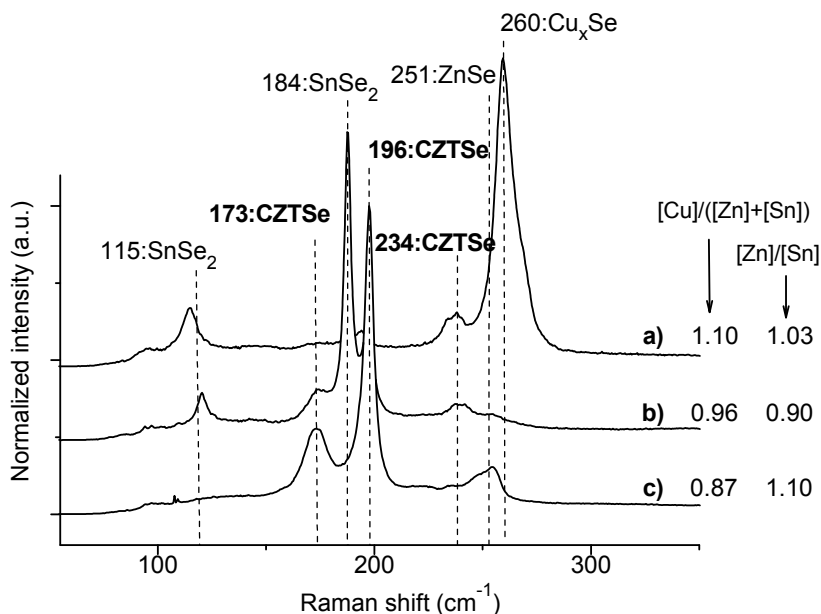
Figure 3.5 RT Raman spectra of $Cu_2ZnSnSe_4$ (CZTSe) powders with different initial [Cu]/([Zn]+[Sn]) and [Zn]/[Sn] compositions a) 1.10 and 1.03, b) 0.96 and 0.90, c) 0.87 and 1.10, respectively

RT Raman spectra of CZTSe powder crystals (Figure 3.5) revealed three main peaks at 196, 173 and 234 cm^{-1}, which are characteristic of CZTSe [68]. At Cu-poor (Cu/(Zn+Sn) < 1.0) and Zn-rich conditions (Zn/Sn ≥ 1.1), the presence of ZnSe secondary phase was detected by its Raman peak at 251 cm^{-1} [69] (see Figure 3.5c). In the growth process of monograins, part of the precursors and the CZTSe already formed are dissolved in the flux at the growth temperature. During the cooling period, the material dissolved in the flux precipitates from the flux and deposits on the surface of powder crystals. We suppose that very weak Raman peaks of ZnSe in the Raman spectra originate from these deposits. In Cu-rich (Cu/(Zn+Sn) ≥ 1.0) conditions, a Cu_xSe secondary phase was detected by Raman peaks at 260 cm^{-1} (Figure 3.5a). $SnSe_2$ secondary phases were also detected by Raman peaks at 115 cm^{-1} and 184 cm^{-1} [70, 71] in Cu-rich (Cu/(Zn+Sn) ≥ 0.96) and Zn-poor conditions (Zn/Sn ≤ 1.03) (see Figure 3.5a and b).

The results showed that single phase CZTSe monograin powders could be synthesized from precursor mixtures, where the ratio of Zn/Sn $\geq$ 1.03, and the ratio of Cu to other metals is in the range of 0.83 - 0.92. Already in the case of Cu/(Zn+Sn) > 0.95 and Zn/Sn $\geq$ 1.1, other phases were clearly detectable by Raman analysis.

In summary, the results of both of the experimental series confirm that the composition of the powders can be tailored by changing the initial Cu and Zn content taking into account that an increase of one of the components at the same time causes ta decrease of the other.

3.1.1.3 Elemental and phase composition of $Cu_2ZnSn(S_{0.7}Se_{0.3})_4$ monograin powders

So far, phase diagrams only for $Cu_2ZnSnSe_4$ [27] and Cu_2ZnSnS_4 systems have been published [25]. The borders of single phase $Cu_2ZnSn(S_{1-x}Se_x)_4$ (0 < x < 1) formation for solid solutions have still not been determined.

Figure 3.6 gives the values of Cu/(Zn+Sn) and Zn/Sn compositional ratios of the synthesized $Cu_2ZnSn(S_{0.7}Se_{0.3})_4$ (CZTSSe) monograins calculated from initial precursor compositions (Table 2.3) and from EDX analysis results of the produced powders.
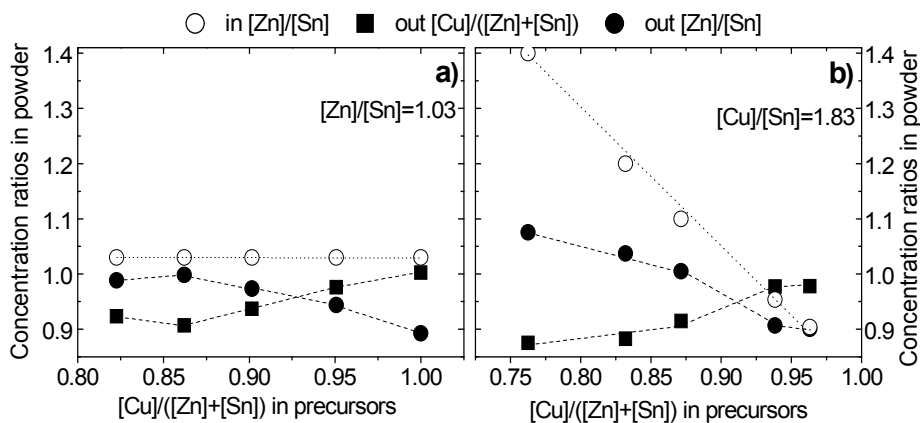
Figure 3.6 [Cu]/([Zn]+[Sn]) (filled squares) and [Zn]/[Sn] (filled dots) ratios of $Cu_2ZnSn(S_{0.7}Se_{0.3})_4$ monograin powders depending on the [Cu]/([Zn]+[Sn]) ratio in precursors when a) [Zn]/[Sn] was kept constant and b) [Cu]/[Sn] was kept constant. Hollow dots represent the Zn to Sn concentration ratio in the precursors

The hollow dots represent the initial metal compositions of the materials investigated in this study. The filled squares and dots represent metal compositions of the synthesized powders. Figure 3.6a presents the series where Cu-content was changed and Zn/Sn concentration ratio was kept constant at 1.03. Figure 3.6b

present the series, where Zn-content was varied while Cu/Sn concentration ratio was kept constant at 1.83. More detailed description of the work is reported in paper [III].

It was found that even though the initial Cu content in the precursors was changed from 21.6 at% to 25.0 at%, the Cu content in the final CZTSSe monograins changed only between 23.3 and 25.0 at%. This corresponds to the Cu/(Zn+Sn) concentration ratio of 0.9 - 1.0, probably the Cu deviation range of the single phase $Cu_2ZnSn(S_{0.7}Se_{0.3})_4$ compound. The Zn content in the final powders changed between 11.8 at% and 13.8 at%, which is only 2 at%, even though the Zn content in the initial precursor mixture was changed over 4 at%. The Sn content in the final products deviates only 0.5 at% (12.8 - 13.3 at%), which is only a third of the initial variation. Hence, the Zn/Sn concentration ratio was only changeable between 0.9 and 1.1. When the Cu/(Zn+Sn) concentration ratio in the precursor mixture was decreased below 0.85 or the Zn/Sn ratio increased above 1.2, the Cu/(Zn+Sn) and Zn/Sn concentration ratios in the synthesized materials did not change further. Considering both the Cu_2ZnSnS_4 and $Cu_2ZnSnSe_4$ systems, the monograin powder with the lowest Cu content was synthesized in the region, where ZnS(Se), SnS(Se)$_2$ and $Cu_2ZnSn(S_{0.7}Se_{0.3})_4$ coexist together. Results of EDX analysis confirmed, that the powder contained also different binaries (Sn$_2$S(Se)$_3$, ZnS(Se), ZnS(Se), SnS(Se$_2$)) and ternary compounds (Cu$_3$SnS(Se)$_4$, Cu$_2$SnS(Se)$_3$). Raman spectroscopy is useful to analyze the phase composition of Cu_2ZnSnS_4 and $Cu_2ZnSnSe_4$ samples, but Raman spectra of $Cu_2ZnSn(S_{1-x}Se_x)_4$ (0 < x < 1) solid solutions are complicated to read due to the bimodal behavior of the spectra [10]. The RT Raman spectra of $Cu_2ZnSn(S_{0.7}Se_{0.3})_4$ monograins are shown in Figure 3.7. The dominating CZTSSe Raman peaks were detected at 163, 195, 226, 234, 285, and 336 cm^{-1}. In the case of Zn-rich materials (Figure 3.7b), the presence of ZnS(Se) secondary phases were detected from their Raman peaks at 205, 251 and 350 cm^{-1}. SnS(Se)$_2$ phase with a characteristic Raman mode at 299 cm^{-1}, and Cu$_x$S(Se) phase with a Raman peak at 259 cm^{-1} was found in Cu-rich (Figure 3.7c) and Sn-rich (Figure 3.7a) materials. However, the intensity of the Cu$_x$S(Se) peak is very low. The Raman peaks of secondary phases, in general, have quite low intensities in comparison with those of CZTSSe peaks.

There was a slight change in the Raman peak positions in Figure 3.7 indicating a variation in the S/Se concentration ratio in the materials, which is characteristic of solid solutions of $Cu_2ZnSn(S_{1-x}Se_x)_4$ (0 < x < 1) [10]. EDX analysis results of CZTSSe samples confirmed that in most of the materials, the S/(S+Se) concentration ratio in the final material was slightly increased (2 - 6 at% depending on the powder) compared to the initial ratio in the precursors. The increase of the S/(S+Se) concentration ratio was the highest in a Sn-rich material, thus the peaks of Raman spectra are slightly shifted to the higher wave numbers towards to the peak positions of the pure Cu_2ZnSnS_4. The quite broad Raman peaks of $Cu_2ZnSn(S_{0.7}Se_{0.3})_4$ solid solutions are in correlation with the increasing structural disorder due to the random distribution of S and Se atoms in the lattice that leads to fluctuations in the masses and force constants in the neighborhood [10].
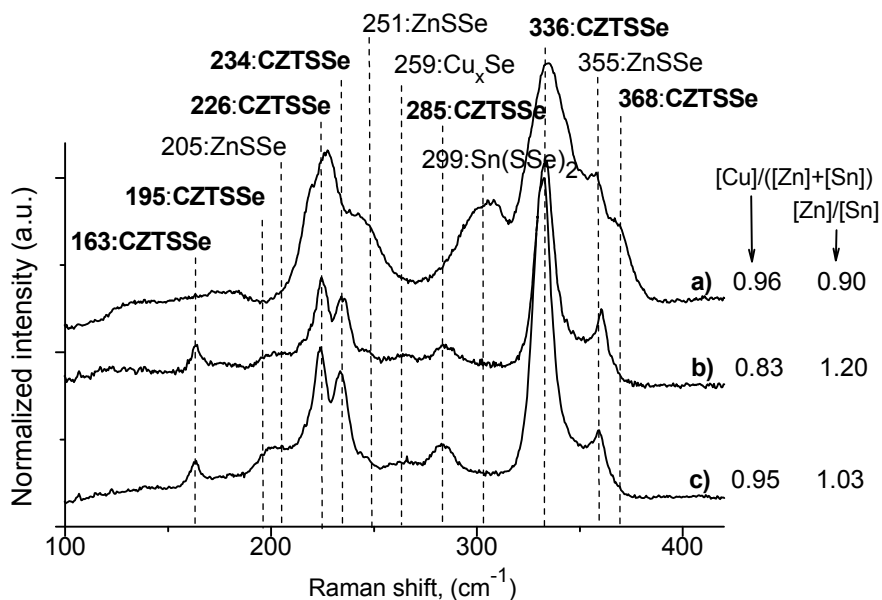
Figure 3.7 RT Raman spectra of $Cu_2ZnSn(S_{0.7}Se_{0.3})_4$ (CZTSSe) monograin powders with different initial $[Cu]/([Zn]+[Sn])$ and $[Zn]/[Sn]$ compositions a) 0.96 and 0.90, b) 0.83 and 1.20, c) 0.95 and 1.03, respectively

It can be concluded that the boarders of single phase area in $Cu_2ZnSn(S_{0.7}Se_{0.3})_4$ solid solutions are hard to distinguish. Cu-rich and Sn-rich compositions in precursor mixture led to the formation of $Cu_xS(Se)$ and $SnS(Se)$ secondary phases in the synthesized monograins. Zn-rich precursor mixtures resulted in $ZnS(Se)$ secondary phases in the synthesized crystals.

3.1.1.4 The effect of Se deviation from the stoichiometry on the $Cu_2ZnSnSe_4$ monograin powder composition

We investigated the composition of $Cu_2ZnSnSe_4$ monograins by varying the concentration ratio of $Se/(Cu+Zn+Sn)$ in the precursors between 0.96 and 1.09 while the molar ratios of $Cu/(Zn+Sn)$ and Zn/Sn were kept constant at 0.9 and 1.03, respectively. The obtained results of EDX and Raman analyses allow us to conclude that a slight excess of chalcogen (Se/Metals = 1.03) does not lead to major changes in the bulk composition of the monograins. However, lack of chalcogen (Se/Metals = 0.96) leads to the presence of additional Cu_xSe phases, which were not present in the materials with a slight excess of chalcogen (Se/Metals = 1.03). At the same time, at the highest Se to metals concentration ratios applied (1.09), separate ZnSe and $SnSe_2$ phases were detected. The study is published in paper (II).

3.1.2 Structural analysis of as-grown monograin powders by XRD

XRD study was applied to characterize the crystal structure of powder crystals. The results are published in paper [III]. In general, the identification of secondary phases in the bulk of kesterite materials by XRD is more complicated than Raman measurements. In Raman analysis, the spectrum is taken from the bulk of the material (from mechanically polished samples). In XRD the monograins are crushed, so the XRD pattern is a mixture of bulk and surface of the monograins. Therefore, separate crystalline phases left on the surface of the monograins during the cooling period are also shown on the pattern.

In Figure 3.8, XRD patterns of the synthesized Cu_2ZnSnS_4, $Cu_2ZnSnSe_4$, and $Cu_2ZnSn(S_{0.7}Se_{0.3})_4$ monograins are shown. XRD patterns of CZTS (Figure 3.8c) and CZTSe (Figure 3.8a) exhibited diffraction peaks belonging to the kesterite Cu_2ZnSnS_4 (ICDD: 01-075-4122) and $Cu_2ZnSnSe_4$ (ICDD: 01-070-8930), respectively. Main characteristic peaks of planes (101), (112), (240/220), (312/116), (008) and (332) and the other less dominant peaks seen in Figure 3.8 can be attributed to the kesterites [72]. In addition to the main reflections, the Rietveld analysis also suggested the presence of SnS (ICDD: 00-053-0526) in CZTS materials, $SnSe_2$ (ICDD: 01-089-2939) in CZTSe materials and ZnS (ICDD: 01-074-4981) in CZTSSe monograins. Also the presence of the Cu-Sn-S secondary phase was suggested in CZTS and CZTSSe. However, Cu_2SnS_3 and ZnS phases are generally not well distinguishable from the kesterite phase because their diffraction peaks overlap [44]. In CZTSe and CZTSSe monograins, also Cu_2Se_x (ICDD: 00-047-1448) and Cu_4Se_3 (ICDD: 00-042-0925) were present according to the Rietveld analysis.
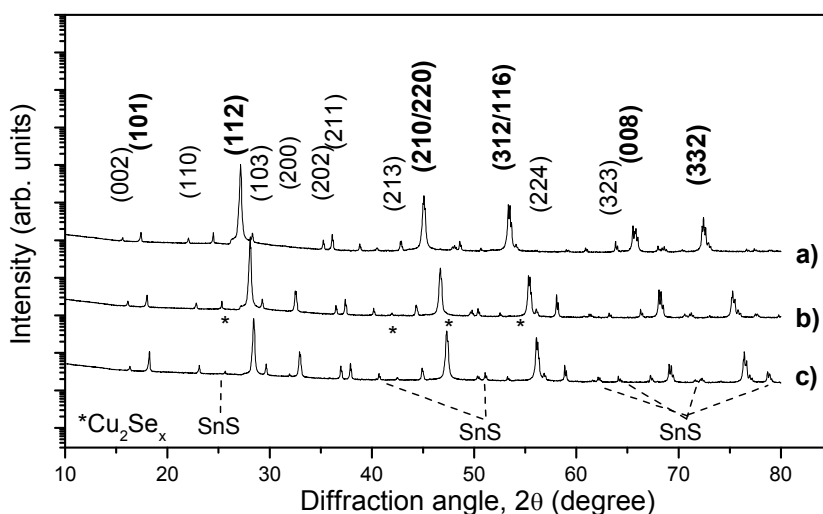
Figure 3.8 XRD pattern of a) $Cu_2ZnSnSe_4$, b) $Cu_2ZnSn(S_{0.7}Se_{0.3})_4$ and c) Cu_2ZnSnS_4 monograin powders

Lattice constants a, b and c of the monograins calculated from the XRD patterns were in good correlation with literature data (see section 1.2). For Cu_2ZnSnS_4 monograins $a = b = 5.436$ Å and $c = 10.844$ Å. For $Cu_2ZnSnSe_4$ monograins, lattice constants a and c were 5.696 Å and 11.350 Å, respectively. As expected, values of lattice constants for $Cu_2ZnSn(S_{0.7}Se_{0.3})_4$ monograins lay between those of CZTS and CZTSe ($a = b = 5.528$ Å and $c = 10.985$ Å).

In Figure 3.9, XRD peaks at $2\theta \sim 28.08°$ corresponding to the (112) plane of two $Cu_2ZnSn(S_{0.7}Se_{0.3})_4$ monograin powders are shown. Similarly to Raman spectroscopy, the shift of XRD peak position is caused by a change in the S/Se concentration ratio in a solid solution [58]. Though both of the materials were synthesized with the same initial S concentration (70 mole%) and they differ only by the metal ratios, the final materials had higher sulfur content (74 mole%) according to the EDX analysis taken from the bulk of the monograins. The observed shift of the peak of the XRD pattern in Figure 3.9, assigned to the change in the S/(S+Se) ratio, and the formation of secondary phases (confirmed in Figure 3.8) are most probably caused by the secondary phases left on the surfaces of the monograins.
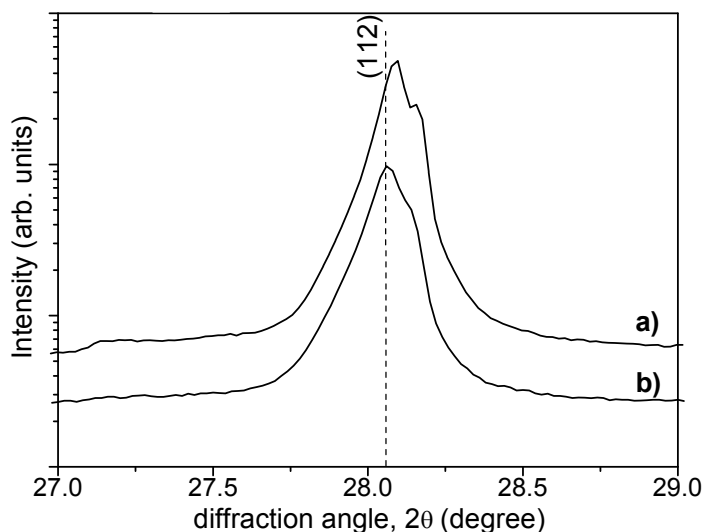
Figure 3.9 The X-ray diffraction pattern of $Cu_2ZnSn(S_{0.7}Se_{0.3})_4$ monograin powders with different metal ratios in the powder a) [Cu]/([Zn]+[Sn]) = 0.88 and [Zn]/[Sn] = 1.04 and b) [Cu]/([Zn]+[Sn]) = 0.98 and [Zn]/[Sn] = 0.91

3.1.3 Electrical measurements of synthesized monograin powders

In the current work the electrical resistance of individual powder grains was measured and the type of conductivity was determined to study the influence of changes in the composition of the electrical properties of the synthesized materials.

The monograins used for measurements were around 150 - 200 μm in diameter. Due to the small size and tetragonal shape of the crystals, the approximate values of grain resistance were gained and only technological trends could be observed from the grain resistance measurements. The electrical measurements were performed by contacting single grains of possibly uniform size between two indium contacts. The ohmic behavior of the contacts was confirmed from the linearity of the *I-V* curves. The conductivity type of the materials was determined by the hot-probe method by heating one of the In contacts. The results are published in paper [I-IV].

All the synthesized $(Cu_2ZnSnS_{1-x}Se_x)_4$ (x = 0, 0.3 and 1) monograin materials exhibited *p*-type conductivity regardless of the Cu/(Zn+Sn) and the Zn/Sn concentration ratios.
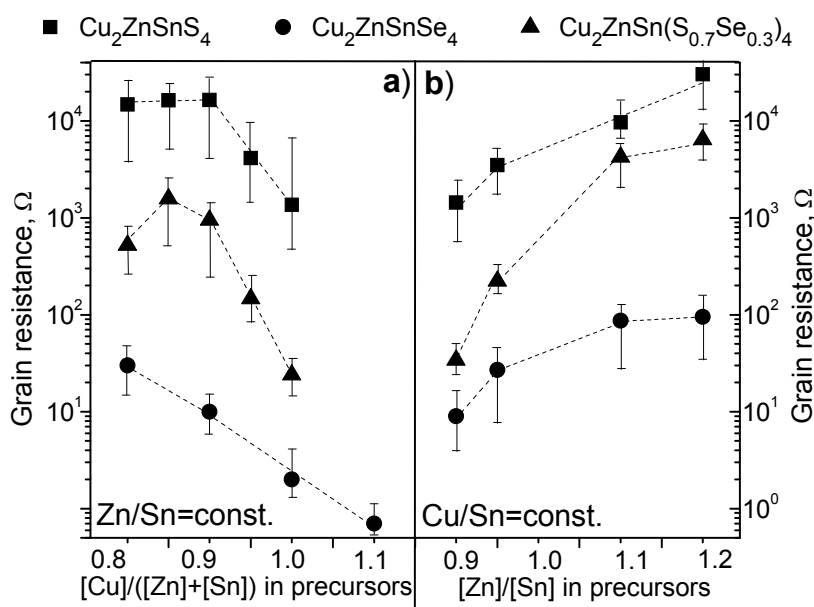
Figure 3.10 The average grain resistance of synthesized Cu_2ZnSnS_4 (squares), $Cu_2ZnSnSe_4$ (dots) and $Cu_2ZnSn(S_{0.7}Se_{0.3})_4$ (rectangular) monograins according to the concentration ratios of a) Cu/(Zn+Sn) and b) Zn/Sn

The dependence of the average grain resistance on the initial Cu/(Zn+Sn) concentration ratio is shown in Figure 3.10a. The measured values of the grain resistances decrease with an increasing Cu content in the precursor mixtures. Cu-rich and Sn-rich powders have the lowest grain resistance for all types of kesterites. This could be attributed to the presence of the highly conductive $Cu_xS(Se)$ or ternary Cu-Sn-S(Se) phases that probably precipitated on the grain surfaces during the cooling of the materials [60]. Due to the high surface conductivity, these materials may not be suitable for fabricating solar cells [73].

Keeping the Cu/Sn concentration ratio constant in the initial composition while decreasing the Zn content, the average grain resistance decreases (see Figure 3.10b). The most conductive are CZTSe monograins. The resistance of CZTS monograins is nearly four orders of magnitude higher than that of the CZTSe materials and the grain resistance of $Cu_2ZnSn(S_{0.7}Se_{0.3})_4$ materials is between that of the CZTS and CZTSe materials. The highest grain resistance of Zn-rich powders could be attributed to the precipitates of high resistivity ZnS(Se) phase [74, 75] on the crystal's surface, as detected by Raman measurements (see Figure 3.3d, Figure 3.5c and Figure 3.7b).

3.1.4 Morphology of the monograins depending on initial powder composition and amount of flux

In addition to the compositional and electrical investigations, a morphological analysis of the synthesized monograin materials was performed. Results of the morphology studies of monograins are published in paper [II]. SEM micrographs showed that the grown powder crystals had tetragonal shape with either sharp or rounded edges. It was found that there is no clear dependence of the shape of the crystals on the Cu/(Zn+Sn) or Zn/Sn concentration ratios. However, the shape of the kesterite powder crystals depends strongly on the volume ratio of flux to material (cm^3/cm^3).
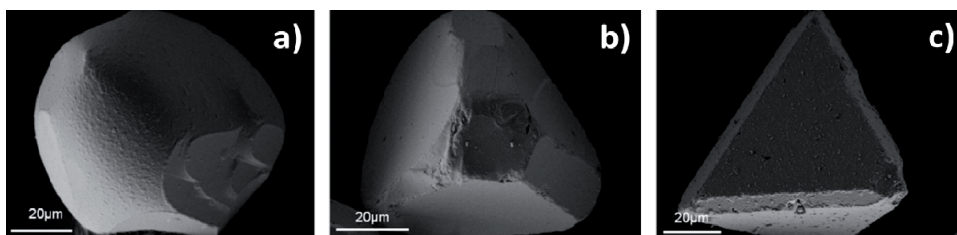
Figure 3.11 SEM images of $Cu_2ZnSnSe_4$ crystals grown with different ratios (cm^3/cm^3) of flux to material a) 0.4, b) 1.6 and c) 4.9

The dependence of the CZTSe monograin shape on the volume ratio of the flux to CZTSe is presented in Figure 3.11. In the case of excess of the flux (flux/CZTSe > 1.6), the powder crystals had a tetragonal shape with very well formed crystal planes (Figure 3.11b and c) as compared to powders grown in a lack of flux material (CZTSe/flux < 0.54), which had crystals with rounded edges (Figure 3.11a). In the latter case, with the lowest amount of KI between the monograins formed, the neighboring crystals start to implicate each other hindering the formation of individual crystals. Also, some of precursors for CZTSe formation (CuSe and Se) could act as flux material after melting and as a result the formed powder crystals have more rounded edges due to the much higher solubility of the material in

CuSe-Se than in KI [26]. In the case of KI surplus, the monograins have more space to grow and therefore can obtain more regular-shaped planes and form tetragonal crystals. EDX analysis of the powders grown with different amounts of flux material indicate that in the case of KI deficiency (CZTSe/KI = 0.4), powders with increased Cu/(Zn+Sn) and decreased Zn/Sn concentration ratios are obtained. All the other CZTSe/KI ratios showed no significant changes in their compositional ratios.

3.1.5 Comparison of compositional limits of $Cu_2ZnSn(S_{1-x}Se_x)_4$ (x = 0, 0.3 and 1) monograin powders and summary of the results

In Figure 3.12a compositional limits of three different types of synthesized kesterite monograin powders are compared. As can be seen, the compositional region of the single phase monograin powders (striped area) is very narrow in the case of Cu_2ZnSnS_4 and $Cu_2ZnSn(S_{0.7}Se_{0.3})_4$ and slightly wider for $Cu_2ZnSnSe_4$. If the Zn concentration is higher than on the single phase border, ZnS(Se) forms as a secondary phase. In the opposite case, under Zn-poor conditions, separate Sn-S(Se) phases are present in addition to the ZnS(Se) phase. Cu-rich composition results in an additional $Cu_{2-x}S(Se)$ phase on the powder crystal surfaces. Thus, although the initial Cu and Zn content in monograins was changed in wide limits (up to 5 at%), the final composition of materials only changed around 2 at%. The Sn content was changeable only up to 1 at%.

In conclusion, based on the experiments in the current study, the single phase Cu_2ZnSnS_4 monograin powders could be synthesized from precursor mixtures with the Cu/(Zn+Sn) ratio in the range 0.9 - 0.95 and the ratio of Zn/Sn between 1.0 and 1.03. The compositional area of single phase $Cu_2ZnSnSe_4$ monograin powders is extending towards more Cu-poor side in comparison to Cu_2ZnSnS_4. The single phase $Cu_2ZnSnSe_4$ can be synthesized from precursor mixtures with metal concentration ratios of Cu/(Zn+Sn) = 0.83 - 0.92 and Zn/Sn = 1.03 - 1.1. The single phase area of $Cu_2ZnSn(S_{0.7}Se_{0.3})_4$ lies between the single phase area of Cu_2ZnSnS_4 and the single phase area of $Cu_2ZnSnSe_4$, depending on the sulfur to selenium ratio. The single phase area of $Cu_2ZnSn(S_{0.7}Se_{0.3})_4$ is slightly wider than that of Cu_2ZnSnS_4 and remarkably narrower than that of $Cu_2ZnSnSe_4$.

It was also observed, that by changing the initial metal ratios in the precursors, the S/Se ratio in the synthesized powders increases up to 5%, which leads to slight peak shifts in XRD and Raman spectra towards the peak positions of the pure Cu_2ZnSnS_4. All the as-grown monograin powders exhibited *p*-type conductivity. The grain resistance increases with the decreasing concentration ratio of Cu/(Zn+Sn) and with the increasing ratio of Zn/Sn. The shape of kesterite powder crystals depends mostly on the volume ratio of the flux to material.
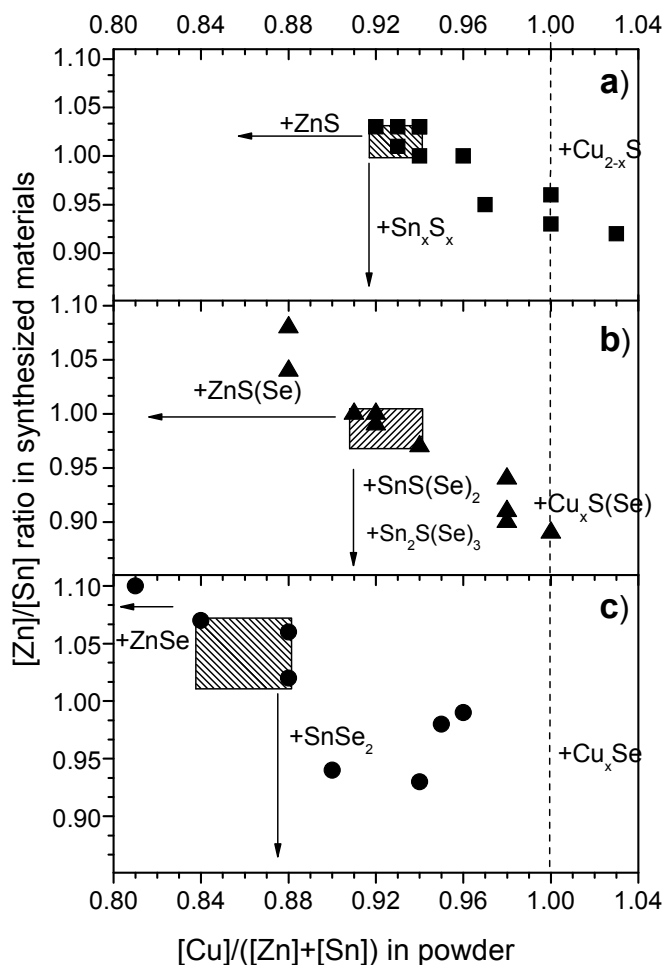
Figure 3.12 Comparison of the single phase areas of a) Cu_2ZnSnS_4, b) $Cu_2ZnSn(S_{0.7}Se_{0.3})_4$ and c) $Cu_2ZnSnSe_4$ monograin powders. Striped rectangle marks the single phase area of the materials, arrows show the composition, where secondary phases appear and the dashed line marks the stoichiometric composition of $Cu_2ZnSn(S_{1-x}Se_x)_4$ (x = 0, 0.3, 1)

3.2 Thermal treatment of monograins and characterization of the MGL solar cell devices

Monograin powders need thermal treatment after the synthesis to modify the crystal surfaces for effectively working *p-n* junctions in MGL solar cells. Post-growth thermal treatments usually need high temperatures up to 740°C, but as reported earlier by different authors [43, 76, 42], kesterites start to decompose already at temperatures higher than 400°C. Although the post-growth annealing step of monograin powders takes place in closed ampoules, the material to ampoule volume ratio in the ampoules is much larger than it is in the synthesis process. Therefore material decomposition can occur to some extent, which leads to tin loss. Thus, in order to keep the material from decomposing, external vapor pressure needs to be applied. It has been shown [43, 44] by different kinetic models that ambient vapor phase with both chalcogen and tin containing compound, is a prerequisite for stability of the kesterite surface. These models predict that if the product of the sulfur (or selenium) and SnS(Se) vapor pressures exceeds a certain value, the kesterite surface would be completely stabilized. It is therefore important to determine these critical values of the sulfur (or selenium) and SnS(Se) vapor pressures for monograins, in order to produce $Cu_2ZnSn(S_{1-x}Se_x)_4$ (x = 0 - 1) monograins with good surface quality that is vital for solar cell performance. To study the effect of different ambient vapor phases and to optimize the time and temperature of the thermal treatments, post-growth thermal treatments were carried out using either isothermal or two-temperature zone conditions. The conditions of these treatments are described more precisely in section 2.2.

In the next sections, the effect of sulfur, selenium, SnS_2 and $SnSe_2$ vapor treatments on the elemental and phase composition of the monograins and on the properties of monograin layer (MGL) solar cells was studied by systematically varying the annealing atmosphere, annealing temperature and applied vapor pressure. As a result, the optimal post-treatment conditions were found.

3.2.1 The effect of sulfur and SnS_2 vapor pressure treatments on the properties of Cu_2ZnSnS_4 monograin powders and solar cells

To prevent the decomposition of Cu_2ZnSnS_4 (CZTS) and the sulfur and tin loss at high temperatures, we investigated the influence of sulfur and SnS_2 vapor pressure treatments on the CZTS absorber materials properties. The concentration ratios of metals in the initial material were Cu/(Zn+Sn) = 0.89 and Zn/Sn = 1.1. The heat-treatment was carried out using a two-temperature zone setup (Figure 2.2c). The study is reported in paper [IV].

EDX analysis of monograins confirmed that no changes occurred in the bulk composition of materials under the applied conditions during either sulfurization or SnS_2-annealing studies. It is believed that the annealing in SnS_2 vapor is a self-limiting process and it has no influence on the CZTS bulk composition if it already corresponds to the composition of the single phase border in the phase diagram. We

can also assume that the unchanged values of the compositional ratios correlate to the border of the homogeneous phase composition.

Raman spectra of the sulfurized powders exhibit main peaks of CZTS at 287, 338 and 373 cm^{-1} [74]. Also, the ZnS secondary phase was found by its Raman peak at 353 cm^{-1} [74]. Based on the solar cell performance, we believe that ZnS is acting as an insulator and it reduces the active area and the current density of MGL solar cells due to its high band gap value (3.54 eV) and high resistivity.

To find optimal conditions for producing a well working absorber material, the parameters of heat-treatments were varied. For sulfur treatments, the annealing temperatures in the material zone were varied between 550 and 740°C and the temperature of the component zone was varied from 280 to 465°C. At these temperatures, the vapor pressure of sulfur varies from 30 Torr to 1000 Torr. To find an optimum SnS_2 annealing temperature, powders were annealed at temperatures between 330 and 740°C for a constant time (10 min). The temperature of the CZTS zone was kept constant ($T_{mat} = 740$°C). Annealing parameters are described in section 2.2. MGL solar cells were made on the base of these heat-treated powder materials.

Table 3.1 Parameters of MGL solar cells based on monograins annealed using different sulfur vapor pressures and temperatures of the Cu_2ZnSnS_4 zone (active area of MGL solar cell is around 75%)

T_{mat} [°C]	p_S [Torr]	V_{oc} [mV]	j_{sc}, [mA/cm^2]	FF, [%]	η_{max}, [%]
untreated		184	1.8	27	0.1
550	100	645	15.8	56	5.6
600	100	661	17.4	61	6.2
650	100	627	13.5	55	6.1
700	100	665	18.0	62	6.6
700	30	542	10.9	47	2.6
700	300	637	14.6	56	4.6
700	1000	644	16.0	57	5.8

Table 3.1 gives the maximum parameters of CZTS solar cells prepared from sulfurized materials. These MGL solar cells show V_{oc} values of up to 665 mV and FF of up to 62 %. The efficiencies of CZTS MGL solar cells increase continuously with the temperature increasing from 550 to 700°C after annealing in sulfur vapor pressures of 100 Torr. The annealing of the absorber powders under higher S vapor pressures did not lead to further improvements of the solar cell parameters. If the vapor pressure of sulfur was lower than 100 Torr, the precipitation of SnS_2 on the walls of the ampoules was visible. Relatively low S vapor pressure ($P_S \leq 30$ Torr) did not prevent any tin loss from CZTS, which probably led to a Sn-poor surface region. The electronic structure of a Sn-depleted surface is not favorable for the formation of a well working *p-n* junction, as indicated by the poor solar cell efficiencies in Table 3.1.

Table 3.2 shows the best output parameters achieved from MGL solar cells based on SnS_2-annealed absorbers. The results show that by changing annealing temperatures the photovoltaic behavior can be significantly affected. The highest $j_{sc} = 18.4$ mA/cm^2 and $V_{oc} = 720$ mV values were obtained from the devices with the CZTS powder being annealed at 740°C in SnS_2 vapor. Improvements obtained in V_{oc} and j_{sc} values were the largest for materials annealed at temperatures higher than 650°C. The best V_{oc} is close to the highest value reported for CZTS so far [77]. A major drawback of solar cell structures is their low j_{sc} values, which may be due to recombination losses at the active interface, i.e. between CZTS and CdS.

Table 3.2 Electrical characteristics of MGL solar cells based on Cu_2ZnSnS_4 monograins annealed at various temperatures of the SnS_2 zone ($T_{CZTS} = 740$°C, active area of MGL solar cell ~ 75%)

$T_{comp.}$ [°C]	V_{oc} [mV]	j_{sc} [mA/cm^2]	FF [%]	η_{max} [%]
330	473	3.1	29	0.4
560	442	1.5	38	0.1
600	440	2.7	43	0.4
625	553	2.0	56	0.4
650	645	16.0	56	5.2
700	680	11.7	60	4.7
740	720	18.4	60	7.4
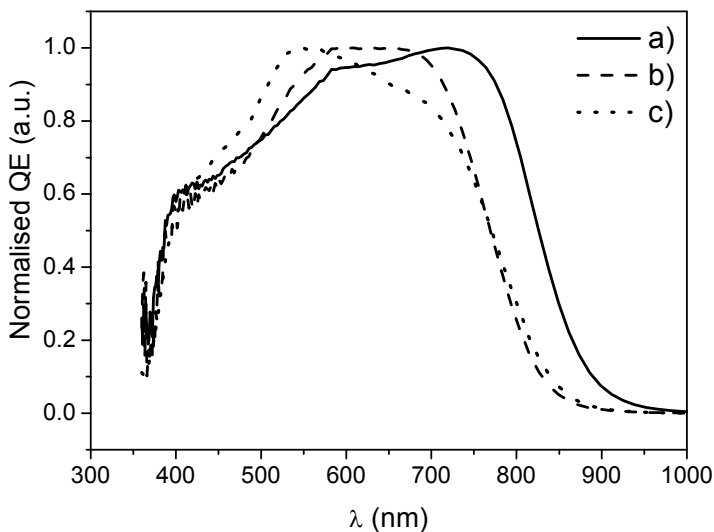
Figure 3.13 QE of Cu_2ZnSnS_4 MGL solar cells using the a) untreated, b) sulfurized and c) annealed under SnS_2 vapor

Figure 3.13 shows the relative quantum efficiencies of the CZTS MGL solar cells that are based on untreated, sulfur-annealed and SnS_2-annealed samples. As the result of the treatments, the absorption edge of the annealed CZTS shifts to shorter wavelengths. The derivatives of the QE with respect to the wavelength give a rough estimation of the effective band gap of the absorber material. The estimated band gap for an annealed CZTS material is around 1.5 eV and it is for as-grown material around 1.4 eV. Although we used Cu-poor and Zn-rich powders, it is possible that some secondary phases precipitate from the flux on the grain surface during the powder quenching processes. Thus, we assume that chemical pre-treatment and heat-treatment under SnS_2 vapor remove the secondary phases from the CZTS monograin surface.

3.2.2 The influence of selenium and $SnSe_2$ vapor pressure treatments on the properties of $Cu_2ZnSnSe_4$ monograin powders and solar cells

For pure $Cu_2ZnSnSe_4$ (CZTSe) monograin powders, $SnSe_2$ or selenium sources were used to produce and regulate the gas phase composition. The following reactions (Eqs. 3.1 - 3.4) describe the decomposition of CZTSe (Eq. 3.1) and formation of gas phase above CZTSe by heating. $SnSe_2$ as a separate source decomposes at high temperatures according to reactions (Eq. 3.2) and (Eq. 3.3), providing SnSe and Se into a gas phase. Se in a saturated gas phase consists of oligomers Se_n (g), where n = 2, 3, 5, 6, 7, 8, and the proportions of them depend on the temperature [61].

$$Cu_2ZnSnSe_4 \text{ (s)} \leftrightarrow Cu_2Se \text{ (s)} + ZnSe \text{ (s)} + SnSe_2 \text{ (s)} \tag{3.1}$$

$$SnSe_2 \text{ (s)} \leftrightarrow SnSe \text{ (s)} + 1/n\ Se_n \text{ (g)} \qquad K_p = P_{Sen}^{1/n} \tag{3.2}$$

$$SnSe \text{ (s)} \leftrightarrow SnSe \text{ (g)} \qquad K_{SnSe} = P_{SnSe} \tag{3.3}$$

$$Cu_2ZnSnSe_4 \text{ (s)} \leftrightarrow Cu_2Se \text{ (s)} + ZnSe \text{ (s)} + SnSe \text{ (g)} + 1/n\ Se_n \text{ (g)}$$

$$K_{CZTSe} = P_{SnSe}\ P_{Sen}^{1/n} \tag{3.4}$$
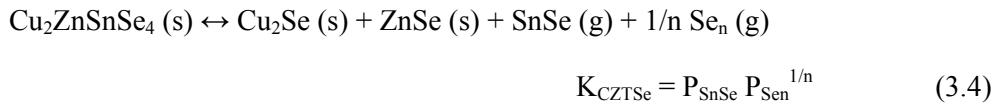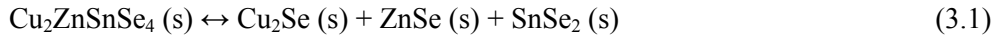
where
K - equilibrium constant;
P - partial pressure of components.

It results from a mass-spectrometry analysis [78] that the vapor phase above the solid SnSe(s) (melting point 861°C) consists mainly from SnSe atoms described by the equilibrium (Eq. 3.3). The equilibrium vapor pressure of pure SnSe is more than four orders of magnitude lower than the vapor pressure on pure $SnSe_2$ or pure Se, as can be seen in Figure 2.3. From the Eq. 3.4 of equilibrium it can be derived that the

reaction is shifted to the left side if $lgP_{Sen} > 1/n$ (lgK_{CZTSe} - lgP_{SnSe}) and the incorporation of Sn from the gas phase of $SnSe_2$ into the crystal of CZTSe could occur. If in a closed ampoule with CZTSe the applied vapor pressure of Se is lower than determined by the equilibrium of the reaction (Eq. 3.4), Se vapor pressure is not high enough to avoid the decomposition process of CZTSe. Thus the composition of CZTSe changes by an extent determined by the applied Se pressure.

To find optimal post-annealing conditions for CZTSe MGL solar cells, different Se or $SnSe_2$ vapor pressures were applied for several periods, while the temperature of material zone was varied from 550°C to 740°C. The ratios of metal concentrations in the used as-grown CZTSe powder were Cu/(Zn+Sn) = 0.81 and Zn/Sn = 1.13.

As seen in Figure 3.14, Se-vapor treatment of the CZTSe absorber in the temperature range 550 - 650°C was beneficial for the values of V_{oc} and FF. Although the values of V_{oc} and FF of solar cells based on $SnSe_2$-treated absorbers were lower than those of MGL solar cells based on Se-treated CZTSe absorbers, the values of j_{sc} increased continuously with the temperature of the material zone increasing up to 740°C.
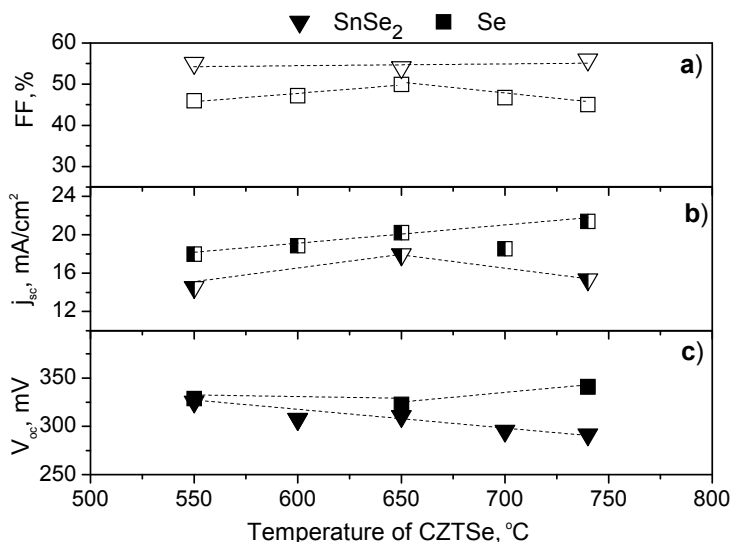
Figure 3.14 The values of a) FF, b) j_{sc} and c) V_{oc} of $Cu_2ZnSnSe_4$ (CZTSe) MGL solar cells depending on the annealing temperature in the material zone

Figure 3.15 displays Raman spectra of the CZTSe monograin powder with the compositional ratios of Cu/(Zn+Sn) = 0.81 and Zn/Sn = 1.13 after annealing in the $SnSe_2$ vapor at 740°C. Raman analysis revealed that a secondary phase with the Raman peak at 186 cm^{-1} had formed on the surface of CZTSe monograins. It can be attributed to the $SnSe_2$ compound [71]. EDX analysis from the surface layer of powder crystals showed that the Cu/(Zn+Sn) concentration ratio decreased from

0.81 to 0.79 and the Zn to Sn concentration ratio from 1.13 to 1.08 after annealing in the $SnSe_2$ vapor. In order to remove the formed secondary phase, the sequential etching with bromine in methanol and with cyanide solution on the annealed CZTSe monograins was performed.
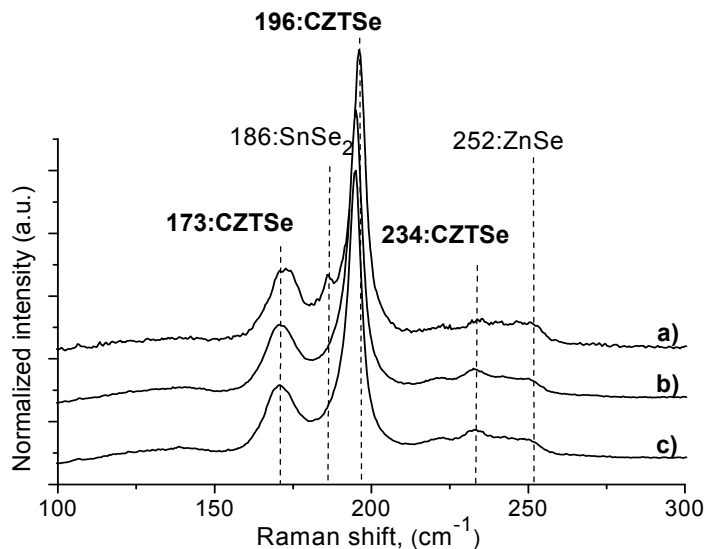
Figure 3.15 Raman spectra of $Cu_2ZnSnSe_4$ (CZTSe) monograin powders: a) $SnSe_2$-annealed, b) annealed and subsequently etched with bromine-in-methanol etchant and c) annealed and subsequently etched with bromine-in-methanol etchant followed by KCN etching
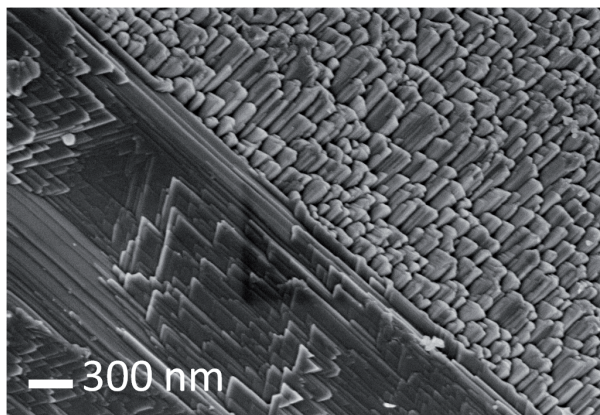
Figure 3.16 SEM photo of a $Cu_2ZnSnSe_4$ monograin surface after etching with bromine solution in methanol

Figure 3.16 illustrates a typical etch pattern observed on the monograin surface after the sequential etching. The bromine etchant produced well-defined triangular pits on some faces of crystals and crystal columns on the other type of faces. After bromine etching, a dark red liquid is usually visible on the surface of the monograins. This liquid could be either Br_2Se_3 or Br_4Se_2 [79]. Before the second etching, the powder was washed in water. Se excess from the surface was etched off in a potassium cyanide solution. The Raman scattering peak at 186 cm^{-1} (Figure 3.15c) completely disappeared after the sequential chemical etching while no change was observed in the main peaks of CZTSe at 173, 196 and 234 cm^{-1}. Also, ZnSe peak at 252 cm^{-1} remained [78].

3.2.2.1 The influence of $Cu_2ZnSnSe_4$ monograin powder composition on the performance of MGL solar cells

The composition of $Cu_2ZnSnSe_4$ (CZTSe) absorber has strong influence on the performance of solar cells. Therefore, to confirm clearly the effect of absorber composition on CZTSe MGL device performance, we annealed powders with a large deviation of compositional ratios: $0.79 < Cu/(Zn+Sn) < 0.95$ and $0.93 < Zn/Sn < 1.2$. Figure 3.17 presents the dependence of powder composition on the device performance after annealing in Se or $SnSe_2$ atmospheres. The values of V_{oc} shown depend on the Cu/(Zn+Sn) and Zn/Sn concentration ratios in the initial powder. The highest value $V_{oc} = 350$mV was gained with Cu-poor (Cu/(Zn+Sn) = 0.81 - 0.83) and Zn-rich (Zn/Sn = 1.1) powders.
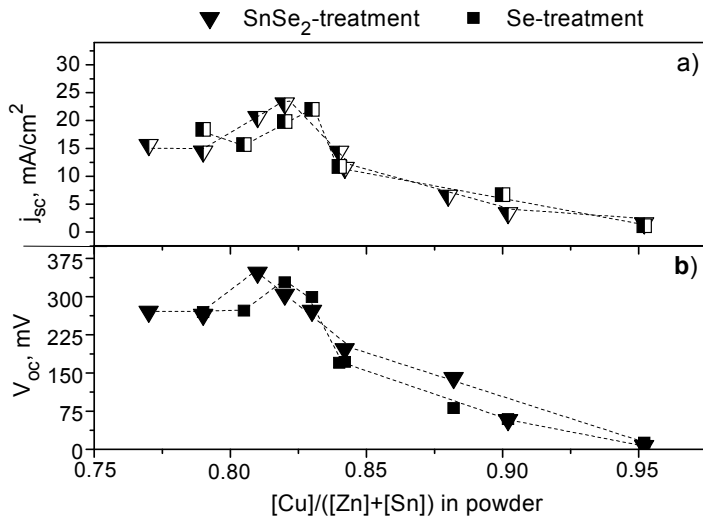
Figure 3.17 a) short circuit current (j_{sc}) and b) open circuit voltage (V_{oc}) of $Cu_2ZnSnSe_4$ MGL solar cells based on $SnSe_2$- and Se-treated absorbers as functions of the [Cu]/([Zn]+[Sn]) ratio in the absorber material

The values of j_{sc} = 23.8 mA/cm^2 were also the highest in these regions of CZTSe composition. The performance of solar cells is very poor if the powder's compositional ratio is Cu/(Zn+Sn) > 0.85. It was found in section 3.1.1.2, that by increasing the Cu content in powders, the Zn/Sn concentration ratio decreased and the CZTSe materials were Sn-rich (Zn/Sn < 1). There is a high probability that Cu- and Sn-rich materials contain secondary phases and due to this the solar cells showed very low performance.

The highest Cu$_2$ZnSnSe$_4$ MGL solar cell efficiency, 4.4%, was achieved with SnSe$_2$-annealed monograin powders with concentration ratios of Cu/(Zn+Sn) = 0.81 and Zn/Sn = 1.12. During thermal treatment, the temperature in the material zone was 650°C and the temperature of the SnSe$_2$ zone was 600°C.

3.2.3 The influence of thermal treatments on the properties of Cu$_2$ZnSn(S$_{0.7}$Se$_{0.3}$)$_4$ monograin powders and solar cells

3.2.3.1 The effect of isothermal annealing with additional SnS$_2$ in ampoule on the output parameters of Cu$_2$ZnSn(S$_{0.7}$Se$_{0.3}$)$_4$ MGL solar cells

In this section, an isothermal annealing at 740°C without (Figure 2.2a) and with an additional source of SnS$_2$ (Figure 2.2b) was used. Previous studies report only isothermal treatment without additional vapor pressure sources [60]. It was believed that the equilibrium vapor pressure formed inside sealed ampoules with Cu$_2$ZnSn(S$_{0.7}$Se$_{0.3}$)$_4$ (CZTSSe) would be enough to prevent any material loss and to guarantee effective surface layer of the absorber material. Unfortunately, the characteristics of solar cells based on the isothermally annealed CZTSSe monograins with different initial compositions were not reproducible. To avoid any possible tin or sulfur (selenium) loss from the material and to provide the equilibrium between the solid and the gas phase in the ampoule, a separate SnS$_2$ source in the isothermal ampoule (Figure 2.2b) was used.

Figure 3.18 shows that the influence of the isothermal treatment in the SnS$_2$ vapor depends on the composition of the CZTSSe. An improvement in solar cell parameters is remarkable if the concentration ratio of Cu/(Zn+Sn) is in the range of 0.91 - 0.94 and the concentration ratio of Zn/Sn is equal or higher than one (Zn-rich samples). If the initial composition of the material is more Cu- and Sn-rich (Zn/Sn < 1), the output parameters of these MGL solar cells are extremely poor. This could be due to the very low grain resistance (~ 100 Ω) of the Cu-rich and Sn-rich materials compared with the resistances of Cu-poor and Zn-rich materials (~ 1000 Ω) (see Figure 3.10). Raman studies reveal that these low resistance materials contain CuS(Se) and SnS(Se) separate phases. Binary copper chalcogenides CuS(Se) have semi-metallic nature and therefore have a tendency to degrade the open circuit voltage [80]. Another possibility is that ternary Cu-Sn-S(Se) compound forms in the presence of copper chalcogenide and sufficient source of SnS$_2$. Cu$_2$SnS$_3$ with a band

gap of about 0.95 eV that results in a lowered value of open circuit voltage [65]. Therefore, materials with the concentration ratio of Zn/Sn < 1 are not suitable for manufacturing solar cells.
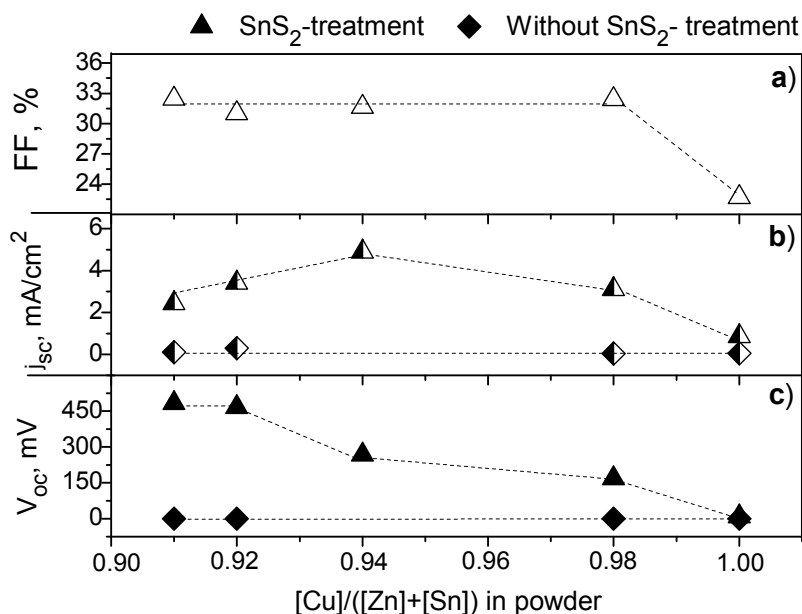
Figure 3.18 Parameters of MGL solar cells depending on [Cu]/([Zn]+[Sn]) ratios in the synthesized powders. $Cu_2ZnSn(S_{0.7}Se_{0.3})_4$ powders with [Zn]/[Sn] $\geq$ 1 were isothermally heat-treated in the presence of SnS_2

Depth of sulfur diffusion into monograins during the annealing process

In order to clarify the depth of sulfur diffusion at different annealing temperatures (T_{mat} = 550 - 740°C), cross sections of $Cu_2ZnSnSe_4$ monograin powder crystals annealed in the sulfur vapor were analyzed by EDX. Figure 3.19a and b show SEM images of a $Cu_2ZnSnSe_4$ single grain and its surface, respectively. In Figure 3.19c the EDX profile of a crystal after isothermal SnS_2 treatment at 740°C is presented. It was found that the heat-treatment in the SnS_2 atmosphere results in rough surface monograins, probably due to a gas-phase surface re-crystallization [81]. The depth of the sulfur diffusion increases from 0.2 to 2 μm with the annealing temperature increasing from 550°C to 740°C for 30 minutes. The sulfur content increases in the $Cu_2ZnSnSe_4$ powder surface layer up to 10 mole% according to the EDX analysis.
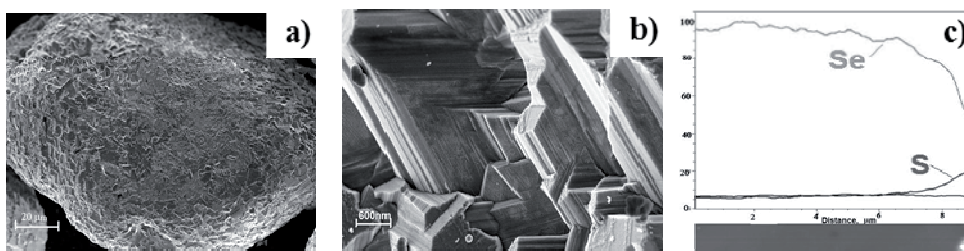
Figure 3.19 SEM images of a) $Cu_2ZnSnSe_4$ single monogain, b) its surface and c) EDX profile after isothermal SnS_2-treatment at 740°C

Next, the $Cu_2ZnSn(S_{0.7}Se_{0.3})_4$ monograins were analyzed with EDX and it was found that the bulk composition of the $Cu_2ZnSn(S_{0.7}Se_{0.3})_4$ monograins remained unchanged during the annealing processes in either S or SnS_2 atmospheres, while a slight increase in the S/(S+Se) concentration ratio on the surface layer of the monograins was detected regardless of the initial composition of the material treated. It was also detected that while the surface of as-grown monograins was slightly sulfur- and zinc-rich in comparison with the bulk of the material, the surface and bulk compositions of the crystals became similar to each other after heat-treatment.

3.2.3.2 The effect of two-temperature zone treatments in Se, S and SnS_2 vapors on the output parameters of $Cu_2ZnSn(S_{0.7}Se_{0.3})_4$ MGL solar cells

$Cu_2ZnSn(S_{0.7}Se_{0.3})_4$ (CZTSSe) monograin powders with various compositions were annealed in different atmospheres using a two-temperature zone treatment setup (Figure 2.2b) and subsequently MGL solar cells were prepared. Figure 3.20 shows the influence of selenium, sulfur and SnS_2 treatments on the solar cell parameters based on the absorber material with different Cu/(Zn+Sn) concentration ratios.

It is seen from the Figure 3.20c that the highest open circuit voltages (570 – 580 mV) were achieved for solar cells based on CZTSSe absorbers with Cu/(Zn+Sn) concentration ratios between 0.88 and 0.92 and Zn/Sn between 1.01 - 1.04. When the initial composition of the material is Cu- and Sn-rich (Cu/(Zn+Sn) $\geq$ 0.94) or very Zn-rich and Cu-poor, the output parameters were rather poor. This is most likely due to the secondary phases formed on the monogain surface, which could also be the cause of the low values of resistances of these materials. In the case of copper-rich materials, the surface of the grains contains $Cu_xS(Se)$ secondary phases, which results in their high conductivity. The measured grain resistance of these materials was around 100 Ω, opposite to slightly Cu-poor and Zn-rich materials, which had resistance over 4000 Ω. Heat-treatment of CZTSSe powders in the Se atmosphere resulted in solar cells with the lowest open circuit voltage values

regardless of the Cu/(Zn+Sn) concentration ratios. Compared to sulfurization, the open-circuit voltage of solar cells was up to 300 mV lower.

EDX analysis of CZTSSe crystals showed that the concentration ratio of S/(S+Se) = 0.71 in bulk of the crystals remained unchanged during heat-treatments in sulfur or selenium atmosphere, but the surface of the monograins became more selenium-rich (S/(S+Se) = 0.5) after selenization and more sulfur-rich after sulfur and SnS_2 treatments (S/(S+Se) = 0.77).
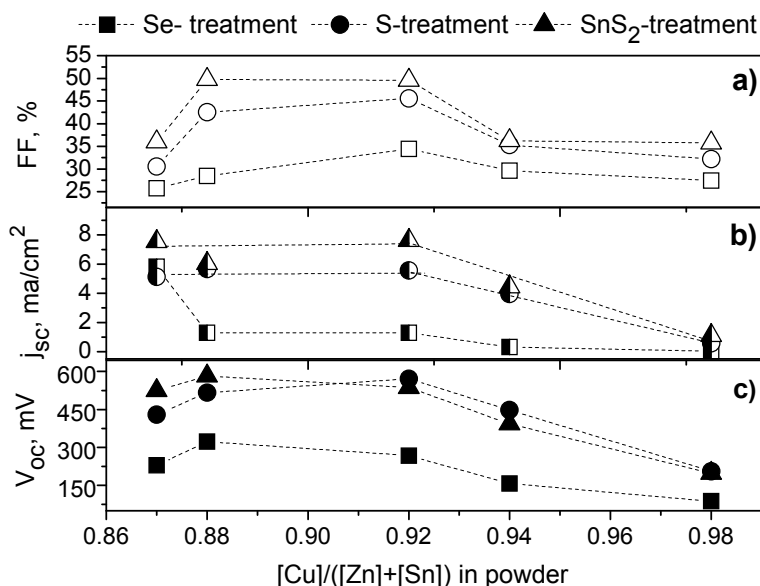
Figure 3.20 a) Fill factor (*FF*), b) Current density (*j$_{sc}$*) and c) Open circuit voltage (*V$_{oc}$*) values depending on different [Cu]/([Zn]+[Sn]) ratios in the synthesized $Cu_2ZnSn(S_{0.7}Se_{0.3})_4$ material after vapor treatments in Se (squares), S (dots) and SnS_2 (triangles)

Summary of post-treatments

Three different experimental arrangements were used for post-annealings of the as grown monograin powders.

- Cu_2ZnSnS_4 monograins were heat-treated in a two-temperature zone setup in SnS_2 and S vapors. The temperature of the Cu_2ZnSnS_4 material zone and the component zone was varied to find optimum annealing conditions. We studied the influence of the treatments on the Cu_2ZnSnS_4 material composition, electrical properties and on the MGL solar cell characteristics based on these absorber materials. It was observed that both annealing atmospheres improved solar cell performance, giving a maximum efficiency of 7.4% after annealing in the SnS_2 atmosphere. As the bulk composition of the initial material remained

unchanged during the thermal treatments, it is probable that the composition of the used Cu_2ZnSnS_4 material was already close to the optimal. The S and SnS_2 vapor treatment in the two temperature zone arrangement is a self-limiting process determined by the equilibrium between solid and gas phases and can be used to tune the surface composition of the monograin powders.

- $Cu_2ZnSnSe_4$ monograins were annealed in Se or $SnSe_2$ atmospheres using a two-temperature zone setup. It was observed that after annealing in $SnSe_2$ atmosphere, the surface of the monograins contained a separate $SnSe_2$ phase, which was successfully removed by etching. The characteristics of MGL solar cells were found dependent on the composition of the initial materials used. The best efficiency of the solar cells, 4.4%, was achieved using $Cu_2ZnSnSe_4$ monograin powders heat-treated in $SnSe_2$ vapors. As the initial composition of monograin powders changed slightly during the annealing, it is probable that the used composition of the monograins is not yet optimal and needs further investigation.

- In the case of $Cu_2ZnSn(S_{0.7}Se_{0.3})_4$ monograin powders, isothermal post-annealing has been used in previous studies, but the characteristics of solar cells based on the isothermally annealed $Cu_2ZnSn(S_{0.7}Se_{0.3})_4$ monograins were not reproducible. Additional sulfur, selenium, or SnS_2 in the isothermal ampoule or using a two-temperature zone setup improved the characteristics of MGL solar cells. The two-temperature zone treatment was found to be the most effective approach. After the selenization process, the material surface became more selenide-rich and after sulfur or SnS_2 annealing more sulfur-rich, which was not observed in the case of Cu_2ZnSnS_4 or $Cu_2ZnSnSe_4$. Further investigations should be conducted to find optimal annealing conditions for $Cu_2ZnSn(S_{0.7}Se_{0.3})_4$ monograin powders.

CONCLUSIONS

In the present thesis, Cu_2ZnSnS_4, $Cu_2ZnSnSe_4$ and $Cu_2ZnSn(S_{0.7}Se_{0.3})_4$ monograin powders were grown in a molten KI flux, varying the initial compositions of precursor mixtures. The as-grown materials were annealed in sulfur, selenium, SnS_2 or $SnSe_2$ atmospheres at various temperatures using either an isothermal (with or without additional vapor source) or a two-temperature zone arrangement. The heat-treated monograins were used as absorber layers in monograin layer solar cells. On the basis of the thesis, following conclusions can be made:

1. The composition of the single phase $Cu_2ZnSn(S_{1-x}Se_x)_4$ (x = 0 - 1) monograin powders can be adjusted in the narrow concentration regions and can be controlled by the Cu and Zn content in precursors. Inside the concentration region for single phase monograin powders, the Cu and Zn content in the synthesized material is interchangeable to some extent: higher copper content in the initial precursors is always accompanied by a lower Zn content in the product material and vice versa – a higher Zn content in the precursors allows us to produce monograin powders with lower Cu concentration in the product material. The single phase region of $Cu_2ZnSn(S_{1-x}Se_x)_4$ (x = 0 - 1) monograins widens with increasing Se content.

2. All the synthesized monograin powders exhibit *p*- type conductivity. The grain resistance of the monograins depends on the composition of the CZTSSe, increasing both with the decreasing concentration ratio of Cu/(Zn+Sn) and the increasing ratio of Zn/Sn. At the same time, the morphology (the shape of $Cu_2ZnSn(S_{1-x}Se_x)_4$ (x = 0 - 1) powder crystals) does not depend on the initial composition of the material.

3. The precise adjustment of the composition of kesterites can be performed in the gas-solid equilibrium conditions during post growth gas-phase annealing process in sulfur, SnS_2, selenium or $SnSe_2$ vapors under controlled conditions. The annealing temperature and atmosphere were found to be crucial for the final performance of the kesterite monograin layer solar cells. Monograin layer solar cells based on copper-poor and zinc-rich monograins annealed in $SnS(Se)_2$ vapors resulted in the highest conversion efficiencies.

4. Applying the knowledge gained from compositional and annealing studies to monograin absorber preparation processes, allowed to prepare $Cu_2ZnSnSe_4$ and Cu_2ZnSnS_4 based monograin layer solar cells with efficiencies of 4.4% and 7.4%, respectively.

REFERENCES

[1] T. M. Razykov, C. S. Ferekides, D. Morel, E. Stefanakos, H. S. Ullar and H. M. Upadhyaya, *Solar Energy 85,* p. 1580–1608, 2011.

[2] K. Zweibel, *Technical Report NREL/TP-520-38350,* 2005.

[3] J. Krustok and E. Mellikov, "Päikeseenergeetikal on tulevikku ka Eestis," [Online]. Available: http://www.loodusajakiri.ee/eesti_loodus/index.php?artikkel=1549.

[4] "Web of Knowledge," [Online]. Available: http://apps.webofknowledge.com.

[5] M. Altosaar, A. Jagomägi, M. Kauk, M. Krunks, J. Krustok, E. Mellikov, J. Raudoja and T. Varema, *Thin Solid Films 431-432,* pp. 466-469, 2003.

[6] J. Nelson, The Physics of Solar Cells, Imperial College Press, 2003.

[7] H. Katagiri, K. Saitoh, T. Washio, H. Shinohara, T. Kurumadani and S. Miyajima, *Solar Energy Materials & Solar Cells 65,* pp. 141-148, 2011.

[8] K. Ito and T. Nakazawa, *Japanese Journal of Applied Physics,* vol. 27, pp. 2094-2097, 1988.

[9] I. Repins, N. Vora, C. Beall, S.-H. Wei, Y. Yan, M. Romero, G. Teeter, H. Du, B. To, M. Young and R. Noufi, in *Proceedings of the Materials Research Society Symposium, 25 - 29 April 2011, San Francisco, California. Materials Research Society Symposium Proceedings, Vol. 1324.*, 2011.

[10] M. Grossberg, J. Krustok, J. Raudoja, K. Timmo, M. Altosaar and T. Raadik, *Thin Solid Films 519,* pp. 7403-7406, 2011.

[11] S. Chen, A. Walsh, J. Yang, X. G. Gong, L. Sun, P.-X. Yang, J.-H. Chu and S.-H. Wei, *Physical Review B 83, 125201,* 2011.

[12] T. Unold and H. W. Schock, *Annual Review of Materials Research 41,* pp. 297-321, 2011.

[13] H. Flammersberger, Masters thesis. Department of Engineering Sciences, Uppsala University, 2010.

[14] H. Katagiri, K. Jimbo, W. S. Maw, K. Oishi, M. Yamazaki, H. Araki and A. Takeuchi, *Thin Solid Films 517 ,* pp. 2455-2460, 2009.

[15] H. Wang, *International Journal of Photoenergy, 801292,* vol. 2011, 2011.

[16] B. Shin, O. Gunawan, Y. Zhu, N. Bojarczuk, S. J. Chey and S. Guha, *Progress in Photovoltaics: Research & Applications,* 2011.

[17] W.-C. Hsu, B. Bob, W. Yang, C.-H. Chung and Y. Yang, *Energy & Environmental Science 5,* pp. 8564-8571, 2012.

[18] S. Bag, O. Gunawan, T. Gokmen, Y. Zhu, T. K. Todorov and D. B. Mitzi, *Energy & Environmental Science 5,* pp. 7060-7065, 2012.

[19] T. K. Todorov, J. Tang, S. Bag, O. Gunawan, T. Gokmen, Y. Zhu and D. B. Mitzi, *Advanced Energy Materials., doi: 10.1002/aenm.201200348,* 2012.

[20] S. Schorr, *Solar Energy Materials & Solar Cells 95,* pp. 1482-1488, 2011.

[21] A. Khare, B. Himmetoglu, M. Johnson, D. J. Norris, M. Cococcioni and E. S. Aydil, *Journal of Applied Physics 111, 129901,* vol. 111, 2012.

[22] S. Chen, H. G. Gong, A. Walsh and S.-H. Wei, *Applied Physics Letters 94, 041903,* 2009.

[23] C. Persson, *Journal of Applied Physics 107, 053710,* 2010.

[24] S. Botti, D. Kammerlander and M. A. L. Marques, *Applied Physics Letters 98, 241915,* 2011.

[25] I. D. Olekseyuk, I. V. Dudchak and L. V. Piskach, *Journal of Alloys and Compounds 368,* p. 135–143, 2004.

[26] I. Д. Олексеюк, I. В. Дудчак and Л. В. Піскач, *Physics and Chemistry of Solid State,* vol. 1, pp. 195-200, 2001.

[27] I. V. Dudchak and L. V. Piskach, *Journal of Alloys and Compounds 351,* p. 145–150, 2003.

[28] T. Maeda, S. Nakamura and T. Wada, *Thin Solid Films 519,* pp. 7513-7516, 2011.

[29] A. Walsh, S. Chen, S.-H. Wei and X.-G. Gong, *Advanced Energy Materials 2,* p. 400–409, 2012.

[30] R. Schurr, A. Hölzing, S. Jost, R. Hock, T. Vob, J. Schulze, A. Kirbs, A. Ennaoui, M. Lux-Steiner, A. Weber, I. Kötschau and H.-W. Schock, *Thin Solid Films 517,* pp. 2465-2468, 2009.

[31] S. Shorr, A. Weber, V. Honkimäki and H.-W. Schock, *Thin Solid Films 517,* pp. 2461-2464, 2009.

[32] R. B. V. Chalpathy, G. S. Jung and B. T. Ahn, *Solar Energy Materials & Solar Cells 95,* pp. 3216-3221, 2011.

[33] R. A. Wibowo, W. H. Jung, M. H. Al-Faruqi, I. Amal and K. H. Kim, *Materials Chemistry and Physics 124,* pp. 1006-1010, 2010.

[34] R. A. Wibowo, W. H. Jung and K. H. Kim, *Journal of Physics and Chemistry of Solids 71,* pp. 1702-1706, 2010.

[35] S. Chen, X. G. Gong, A. Walsh and S. H. Wei, *Applied Physics Letters 96, 021902,* 2010.

[36] A. Nagoya, R. Asahi, R. Wahl and G. Kresse, *Physical Review B 81, 113202,* 2010.

[37] T. Maeda, S. Nakamura and T. Wada, *Japanese Journal of Applied Physics 50, 04DP07,* 2011.

[38] S. Chen, J.-H. Yang, X. G. Gong, A. Walsh and S.-H. Wei, *Physical Review B 81, 245204,* 2010.

[39] A. R. Jeong, W. Jo, S. Jung, J. Gwak and J. H. Yun, *Applied Physics Letters 99, 082103,* 2011.

[40] J. J. Scragg, P. J. Dale, D. Colombara and L. M. Peter, *ChemPhysChem 13,* no. 12, p. 3035–3046, 2012.

[41] A. Redinger and S. Siebentritt, *Applied Physics Letters 97, 092111,* 2010.

[42] A. Weber, R. Mainz and H. W. Schock, *Journal of Applied Physics 107, 013516,* 2010.

[43] J. J. Scragg, T. Ericson, T. Kubart, M. Edoff and C. Platzer-Björkman, *Chemistry of Materials 23,* pp. 4625-4633, 2011.

[44] A. Redinger, D. M. Berg, P. J. Dale and S. Siebentritt, *Journal of the American Chemical Society 133,* pp. 3320-3323, 2011.

[45] T. S. Velde and G. W. M. T. Helden, *Philips Technical Review 29,* p. 238, 1968.

[46] D. Meissner, R. Memming and B. Kastening, *Chemical Physics Letters 96,* p. 34, 1983.

[47] M. Altosaar, J. Hiie, E. Mellikov and J. Mädasson, *Crystal Research and Technology 31,* pp. 505-508, 1996.

[48] E. Mellikov, J. Hiie and M. Altosaar, *SPIE Proceedings 222,* pp. 177-185, 1994.

[49] J. Hiie, M. Altosaar and E. Mellikov, *Solid State Phenomena 67-68,* pp. 303-308, 1999.

[50] K. Timmo, M. Altosaar, M. Kauk, J. Raudoja and E. Mellikov, *Thin Solid Films 515,* pp. 5884-5886, 2007.

[51] M. Altosaar, J. Raudoja, M. Danilson, K. Timmo, M. Krunks and E. Mellikov, in *IEEE Electron Devices Society, pp. 468-470,* 2006.

[52] I. Leinemann, J. Raudoja, M. Grossberg, R. Traksmaa, T. Kaljuvee, M. Altosaar and D. Meissner, in *Conference Proceedings of the Conference of Young Scientists on Energy Issues; Kaunas, Lithuania,* 2011.

[53] I. Klavina, T. Kaljuvee, K. Timmo, J. Raudoja, R. Traksmaa, M. Altosaar and D. Meissner, *Thin Solid Films 519,* pp. 7399-7402, 2011.

[54] I. Leinemann, T. Kaljuvee, R. Traksmaa, J. Raudoja, M. Grossberg, M. Altosaar and D. Meissner, *Journal of Alloys and Compounds,* 2011.

[55] A. S. Ionkin, B. M. Fish, W. J. Marshall and R. H. Senigo, *Solar Energy Materials & Solar Cells 104,* p. 23–31, 2012.

[56] S.-J. L. Kang, Sintering. Densification, Grain Growth and Microstructure, Elsevier Butterworth-Heinemann, 2005.

[57] T. Bergfors, "Tutorial 6: Ostwald Ripening," [Online]. Available: http://xray.bmc.uu.se/terese/crystallization/tutorials/tutorial6.html.

[58] K. Timmo, M. Altosaar, J. Raudoja, K. Muska and M. Kauk, *Solar Energy Materials & Solar Cells 94,* pp. 1889-1892, 2010.

[59] K. Timmo, Doctoral thesis. Department of Materials Science, Tallinn

University of Technology, 2011.

[60] K. Timmo, M. Altosaar, J. Raudoja, M. Grossberg, M. Danilson, O. Volobujeva and E. Mellikov, in *35th IEEE Photovoltaic Specialists Conference, Honolulu, Hawaii, June 20-25, 2010: Conference Proceedings 1982-1985.*, 2010.

[61] Я.И.Герасимов, А. Крестовников and С. Горбов, Химическая термодинамика в цветной металлургии, Металлургия, 1974.

[62] Справочник химика (том I), Ленинград, Москва, "ГХИ", 1962.

[63] R. C. Sharma and Y. A. Chang, *Bulletin of Alloy Phase Diagrams 7, 269273,* no. 3, 1986.

[64] Н. Х. Абрикосов and Л. Е. Шелимова, Полупроводниковые материалы на основе соединений A(IV)B(VI), Издательство "Наука" Москва, 1975.

[65] K. Wang, B. Shin, K. B. Reuter, T. Todorov, D. B. Mitzi and S. Guha, *Applied Physics Letters 98, 01912,* 2011.

[66] L. S. Price, I. P. Parkin, A. M. E. Hardy and R. J. H. Clark, *Chemistry of Materials 11,* pp. 1792-1799, 1999.

[67] P. A. Fernandes, P. M. P. Salome and A. F. Cunha, *Journal of Physics D: Applied Physics 43, 215403,* 2010.

[68] M. Grossberg, J. Krustok, K. Timmo and M. Altosaar, *Thin Solid Films 517,* p. 2489–2492, 2009.

[69] G. Perna, M. Lastella, M. Ambrico and V. Capozzi, *Applied Physics A 83: Materials Science & Processing,* pp. 127-130, 2006.

[70] G. Morell, R. S. Katiyar, S. Z. Weisz, T. Walter, H. W. Schock and I. Balberg, *Applied Physics Letters 69,* pp. 987-989, 1996.

[71] G. Lucovsky, J. C. Mikkelsen, W. Y. Liang, R. M. White and R. M. Martin, *Physical Review B 14,* no. 4, pp. 1663-1669, 1976.

[72] J. He, L. Sun, S. Chen, Y. Chen, P. Yang and J. Chu, *Journal of Alloys and Compounds 511,* pp. 129-132, 2012.

[73] T. Tanaka, A. Yoshida, D. Saiki, K. Saito, Q. Guo, M. Nishio and T. Yamaguchi, *Thin Solid Films 518,* pp. 29-33, 2010.

[74] K. Wang, O. Gunawan, T. Todorov, B. Shin, S. J. Chey, N. A. Bojarczuk, D. B. Mitzi and S. Guha, *Applied Physics Letters 97, 143508,* 2010.

[75] A. Redinger, K. Hönes, X. Fontane, V. Izquierdo-Roca, E. Saucedo, N. Valle, A. Perez-Rodrigez and S. Siebentritt, *Applied Physics Letters 98, 101907,* 2011.

[76] A. Redinger, D. M. Berg, P. J. Dale, R. Djemour, L.Gütay, T.Eisenbarth, N. Valle and S. Siebentritt, *IEEE Journal of Photovoltaics,* vol. 1, no. 2, 2011.

[77] H. Katagiri, N. Ishigaki and K. S. T. Ishida, *Japanese Journal of Applied Physics 40,* pp. 500-504, 2011.

[78] R. F. Brebrick and A. J. Strauss, *Journal of Chemical Physics 40,* p. 3230, 1964.

[79] S. Gezci and J. Woods, *Journal of Materials Science 7,* pp. 603-608, 1972.

[80] H. Katagiri, K. Jimbo, M. Tahara, H. Araki and K. Oishi, *Materials Research Society Symposium Proceedings 1165,* 2009.

[81] Y. Saito, Statistical Physics of Crystal Growth, World Scientific Publishing Co. Pte. Ltd., 1996.

ABSTRACT

Study of Composition and Thermal Treatments of Quaternary compounds for Monograin Layer Solar Cells

The aim of the present thesis was to investigate the influence of the initial composition of precursors on the properties and composition of synthesized kesterite monograin powders: Cu_2ZnSnS_4 (CZTS), $Cu_2ZnSnSe_4$ (CZTSe) and $Cu_2ZnSn(S_{0.7}Se_{0.3})_4$ (CZTSSe) and to study the effect of post-growth annealing in various gas atmospheres on the properties of monograins and monograin layer (MGL) solar cells.

Kesterites are promising absorber materials for solar cells due to their optimal direct band gap, high absorption ability and their abundant and non-toxic constituent elements. The best efficiency achieved with kesterite absorber materials is 11.1%. The performance of a solar cell depends strongly on the material composition, therefore tight control of the composition and the structure of kesterites is crucial to achieve high efficiency solar cells. Solar cell characteristics can also be improved by post-treatments, but during high temperature post-treatments, the decomposition of the kesterite can occur. The volatile products of kesterite decomposition are SnS_2 or $SnSe_2$ and sulfur or selenium. By applying vapor pressure of these volatile components in the post-growth heat treatments, the composition of the kesterite absorber material can be controlled.

In the current thesis, $Cu_2ZnSn(S_{1-x}Se_x)_4$ materials with x = 0, 0.3 and 1 were synthesized in monograin form in the liquid phase of KI as flux material with different Cu/(Zn+Sn) and Zn/Sn concentration ratios. Synthesized monograins were post-treated in sulfur, selenium, SnS_2 and/or $SnSe_2$ atmospheres at various temperatures using either an isothermal (with or without additional vapor source) or a two-temperature zone arrangement. Heat-treated monograins were used as absorber layers in MGL solar cells. The elemental composition, phase composition, and electrical and morphological properties of as-grown and post-treated monograin powders were studied by using EDX, SEM, Raman spectroscopy, XRD and hot probe measurements. The MGL solar cells were characterized by current-voltage (*I-V*) and *QE* measurements.

It was found that the bulk and phase composition of the synthesized monograins can be controlled by initial precursor composition. Experiments showed that Cu and Zn are to some extent interchangeable: higher copper content in initial precursor's mixture composition is accompanied by a lower Zn content in the product material and vice versa – a higher Zn content in precursors allows us to produce monograin powders with lower Cu concentration in the product material. Under current experimental conditions the Cu and Zn content in the bulk of Cu_2ZnSnS_4

monograins could be changed only up to 1.4 at% and Sn content 0.3 at%. The Cu, Zn and Sn content in $Cu_2ZnSn(S_{0.7}Se_{0.3})_4$ monograins could be changed by 1.7, 2.0 and 0.5 at%, respectively. The composition of $Cu_2ZnSnSe_4$ monograins was changeable in the widest range: Cu, Zn and Sn content in the monograins was changed by 2.1, 2.5 and 0.9 at%, respectively. The single phase composition region for kesterite type monograin powders is narrow. In the powders synthesized outside the single phase area, secondary phases were found, identified as Sn_2S_3, SnS_2, $Cu_{2-x}S$ and ZnS in the case of Cu_2ZnSnS_4, ZnSe, $SnSe_2$ or Cu_xSe in the case of $Cu_2ZnSnSe_4$ and ZnS(Se), Sn(Se) and CuS(Se) solid solutions in the case of $Cu_2ZnSn(S_{0.7}Se_{0.3})_4$. All monograins exhibited p-type conductivity and the grain resistance of all the monograins increased with the decreasing concentration ratio of Cu/(Zn+Sn) and the increasing ratio of Zn/Sn. The shape of powder crystals depends on the volume ratio of flux to material, but the shape is not influenced by the initial material composition.

The characteristics of MGL solar cells depend on the bulk composition of synthesized monograins and can be improved by post-growth annealing in various gas atmospheres by applying additional sulfur, selenium, SnS_2, or $SnSe_2$ source into the annealing atmosphere in an isothermal or a two-temperature zone annealing arrangement. The best conversion efficiencies were achieved with copper-poor and zinc-rich monograins using the two-temperature zone setup with an additional tin chalcogenide source. $Cu_2ZnSnSe_4$ MGL solar cells based on powders treated in the $SnSe_2$ atmosphere resulted in an efficiency of 4.4%. MGL solar cells based on Cu_2ZnSnS_4 monograins treated in the SnS_2 atmosphere resulted in an efficiency of 7.4%.

KOKKUVÕTE

Päikesepatareides kasutatavate monoterapulbriliste nelikühendite koostise ja termotöötluste uurimine

Tänu optimaalsele otsese keelutsooni laiusele, kõrgele neeldumiskoefitsiendile ja laialdaselt levinud mittetoksilistele koostisosadele on kesteriidid (Cu_2ZnSnS_4 (CZTS), $Cu_2ZnSnSe_4$ (CZTSe) ja $Cu_2ZnSn(S_{0,7}Se_{0,3})_4$ (CZTSSe)) ühed lootust-andvamad päikesepatarei absorbermaterjalid. Seni on kesteriitide baasil valmistatud päikesepatarei suurimaks efektiivsuseks mõõdetud 11,1%. Käesolevas doktoritöös käsitletakse kesteriitsete monoterapulbriliste materjalide omadusi sõltuvalt nende algkoostisest ja erinevate termiliste järelkäsitluste tehnoloogilistest parameetritest. Täpsemalt on antud töös uuritud monoterapulbrite süsteesimiseks valitud lähte-ainete koguste suhete ja erinevates gaasikeskkondades läbi viidud termotöötluste mõju süsteesitud pulbri omadustele ja faasikoostisele, sest loodavate päikese-elementide väljundparameetrid on suurel määral nende protsesside poolt määratud.

Töös kasvatati $Cu_2ZnSn(S_{1-x}Se_x)_4$ (x = 0; 0,3; 1) monoterapulbrid KI-sulandaja juuresolekul, kasutades erinevaid Cu/(Zn+Sn) ja Zn/Sn kontsentratsioonide suhteid. Süsteesitud monoterasid töödeldi väävli, seleeni, SnS_2 või $SnSe_2$ atmosfääris, kasutades kas isotermilist (koos või ilma täiendava aururõhuallikata) või kahetsoonilist süsteemi. Termotöödeldud monoterasid kasutati monoterakihiliste päikeseelementide valmistamiseks. Järeltöödeldud ja töötlemata monoterade elementkoostise, faasikoostise ja elektriliste ning morfoloogiliste uuringute teostamiseks kasutati vastavalt järgnevaid mõõtmismeetodeid: EDX, XRD, Raman-spektroskoopia, kahe sondi meetod ning SEM. Päikeseelementide opto-elektriliste omaduste iseloomustamiseks kasutati spektraaltundlikkuse (*QE*) ja volt-amper kõverate mõõtmisi.

Töö käigus leiti, et monoterade koostist on võimalik kontrollida prekursorite segu algkoostise muutmisega. Esmakordselt leiti, et vask ja tsink on mingil määral omavahel vahetatavad: suurem vasesisaldus annab võimaluse süsteesida madalama tsingi kontsentratsiooniga monoterapulbreid ning vastupidi – suurem tsingi kontsentratsioon prekursorite segus tagab madalama vasesisalduse süsteesitud materjalides. Antud eksperimentaalsete tingimuste puhul on võimalik muuta vase- ja tsingisisaldust süsteesitud ühefaasilistes Cu_2ZnSnS_4 monoterapulbrites kuni 1,4 at% ja tinasisaldust 0,3 at%. Vase-, tsingi- ja tinasisaldus ühefaasilistes $Cu_2ZnSn(S_{0,7}Se_{0,3})_4$ monoterapulbrites oli muudetav vastavalt 1,7; 2,0 ja 0,5 at%. Kõige rohkem oli võimalik varieerida $Cu_2ZnSnSe_4$ ühefaasiliste monoterapulbrite koostist, kus vase-, tsingi- ja tinasisaldus võivad muutuda vastavalt 2,1; 2,5 ja 0,9 at%. Ühefaasiline koostise piirkond kesteriit-tüüpi monoterapulbrites on kitsas. Väljaspool ühefaasilist piirkonda kasvatatud Cu_2ZnSnS_4 monoterad sisaldasid Sn_2S_3, SnS_2, $Cu_{2-x}S$ ja ZnS lisafaase, $Cu_2ZnSnSe_4$ monoterad sisaldasid ZnSe, $SnSe_2$ või Cu_xSe lisafaase ning väljaspool ühefaasilist piirkonda süsteesitud

$Cu_2ZnSn(S_{0,7}Se_{0,3})_4$ monoteradest leiti ZnS(Se), Sn(Se) ja CuS(Se) lisafaase. Kõik monoterad olid *p*-tüüpi juhtivusega ning nende takistus suurenes [Cu]/([Zn]+[Sn]) ja [Zn]/[Sn] suhete alandamisel. Monoterade kuju on määratud materjali ja sulandaja mahtude suhtega, kuid ei sõltu prekursorite koostisest (erinevate komponentide koguste suhtest vastavates prekursorites).

Valmistatud päikesepatareide väljundparameetrid sõltuvad sünteesitud mono-terapulbrite koostisest ning neid on võimalik parandada töös uuritud monoterade täiendava väävli, seleeni, SnS_2 või $SnSe_2$ aururõhutöötlusega kas isotermses või kahetsoonilises süsteemis. Kõrgeimad päikeseelemendi kasutegurid saavutati, kasutades vasevaese ja tsingirikka koostisega monoterasid, mida oli täiendavalt töödeldud kahetsoonilises süsteemis $SnSe_2$ või SnS_2 aururõhus. Suurimad $Cu_2ZnSnSe_4$ päikesepatareide väljundparameetrid saavutati monoteradega, mida oli täiendavalt töödeldud $SnSe_2$ aururõhus, andes maksimaalseks päikesepatarei kasuteguriks 4,4%. Parima kasuteguri 7,4% andis SnS_2 aururõhus töödeldud Cu_2ZnSnS_4 monoterade baasil valmistatud monoterakiht-päikesepatarei.

APPENDIX A

ELSEVIER

European Materials Research Society Conference
Symp. Advanced Inorganic Materials and Concepts for Photovoltaics

Synthesis of Cu_2ZnSnS_4 monograin powders with different compositions

K. Muska[*], M. Kauk, M. Altosaar, M. Pilvet, M. Grossberg, O. Volobujeva

Tallinn University of Techology, Ehitajate tee 5,Tallinn 19086, Estonia

Abstract

The effect of changes in the composition ratios of Cu/(Zn+Sn) and Zn/Sn in initial precursor mixtures on the final composition and properties of Cu_2ZnSnS_4 (CZTS) monograin powders has been investigated. EDX studies revealed that Cu/(Zn+Sn) concentration ratios in the single phase powders can be changed only from 0.92 to 0.95 and Zn/Sn ratios only from 1.0 to 1.03. Raman spectra of all powders showed main peaks around 287, 338, and 375 cm^{-1} characteristic for CZTS materials. Larger deviations from stoichiometry results in CZTS powder crystals with secondary phases, identified as Sn_2S_3, SnS_2, $Cu_{2-x}S$ and ZnS. All CZTS monograins have *p*-type conductivity with an electrical resistance in the range of 1.3×10^3 to 1.6×10^4 Ω, depending on the initial composition of the precursor mixture.

© 2011 Published by Elsevier Ltd. Selection and/or peer-review under responsibility of Organizers of European Materials Research Society (EMRS) Conference: Symposium on Advanced Inorganic Materials and Concepts for Photovoltaics.

Keywords: Cu_2ZnSnS_4; CZTS; composition; Raman

1. Introduction

Cu_2ZnSnS_4 (CZTS) is a semiconductor with a direct band gap of about 1.5 eV and an absorption coefficient of 10^4 cm^{-1}, and for this reason it is a potential material for solar cell application. Demonstrated efficiencies of up to 6.8% as well as it`s use of only cheap and abundant elements make

─────────
[*] Corresponding author. Tel.: +3-72-620-3362; fax: +3-72-620-3367.
E-mail address: muska@staff.ttu.ee

CZTS a promising alternative to current photovoltaic materias [1]. It is found that Cu-poor and Zn-rich composition of material improve the efficiency of CZTS solar cells because Cu vacancies forming shallow acceptor levels in CZTS lead to p-doping, while Zn-rich conditions prevent the substitution of Cu on Zn sites, which gives rise to relatively deep acceptor levels [2]. Therefore, a tight control of the composition and the structure of CZTS are important for achieving high efficiency solar cells. However, there have been only few studies determining the compositional limits in CZTS. A comprehensive analysis of the Cu_2S-ZnS-SnS_2 pseudo-ternary system, carried out by Olekseyuk *et al*, showed that single phase Cu_2ZnSnS_4 is present only within a rather narrow range of compositions. Theoretically even a 2-3% compositional variation could lead to phase separation [3].

The aim of this study was to determine the exact compostional limits to obtain single phase CZTS in our monograin powder synthesis. The work includes a systematic comparison of the influence of the initial composition of the precursor mixture on the CZTS powder composition formed. For this purpose powders with various initial compositions were synthesised focusing mainly on the "Cu-poor" and "Zn-rich" composition region (compare Fig. 6).

2. Experimental

In this study Cu_2ZnSnS_4 powder materials with different compositions were synthesized in molten potassium iodide as a flux material sealed in evacuated quartz ampoules. Starting materials were high-purity powders of CuZnSn-alloy and elemental S. In order to adjust the CuZnSn-alloy composition self-synthesized CuS and SnS and commercial ZnS of high purity were added. The precursors were mixed in desired molar ratios and milled in ball mill, degassed under dynamic vacuum, sealed into evacuated quartz ampoules and annealed isothermally at 1013 K for 90 hours. After the synthesis the flux material was removed by deionised water.

The shape and surface morphology of the crystals were examined by high resolution scanning electron microscopy (SEM). The chemical composition of the monograin powders was determined from the bulk of polished crystals using energy dispersive x-ray spectroscopy (EDX). Room temperature (RT) Raman spectra were recorded using a Horiba's LabRam HR high resolution spectrometer equipped with a multichannel CCD detection system in backscattering configuration. The electrical resistances of the grains were measured by contacting single grains with two indium contacts. An ohmic behaviour of the contacts was assumed based on the linearity of the *I-V* dependence. The conductivity type of materials was determined using the hot-probe method.

3. Results and discussion

Figure 1 gives the values of the Cu/(Zn+Sn) and the Zn/Sn ratios in the synthesized CZTS powders calculated from the EDX analysis as a function of these ratios used in the precursor composition. It can be seen that even though the Cu/(Zn+Sn) ratio in the precursors mixture was changed from 0.82 to 1.1, the compositional ratio Cu/(Zn+Sn) in the grown powders varied only from 0.93 to 1.03. At the same time the Zn/Sn ratio in the synthesized materials decreased with increasing Cu content in the precursor mixture from 1.03 to 0.92. This leads to the assumption that both Zn and Cu are forming also separate phases in the material. The SEM and EDX investigations showed that all powders with initial compositional ratio of Cu/(Zn+Sn) below 0.95 contain extra phase of ZnS. The Raman analysis confirmed the presence of this ZnS phase by it's Raman peak at 351 - 353 cm^{-1} [4]. All Raman spectra of CZTS powders independent of the Cu-content showed the characteristic Raman frequencies of CZTS at 286, 338, and 375 cm^{-1} (Fig.2) [4]. In the case of the lowest Cu content in the precursors (Cu/(Zn+Sn) = 0.82) also further additional phases like SnS and SnS_2 were detected at 166, 189, 220 and 313 cm^{-1}, respectively [5].

SEM images of polished CZTS crystals are shown in Figure 3a. According to these SEM results, some CZTS crystals contained areas of secondary phases. In Cu-rich conditions (Cu/(Zn+Sn) ≥ 1.0), extra phases of $Cu_{2-x}S$ were detected also by EDX analysis (see Fig. 3b). The presence of this compound was also confirmed by it's Raman peak at 473 cm^{-1} [4]. The formation of $Cu_{2-x}S$ on the Cu-rich side of compositions is in agreement with the phase diagram assembled by Olekseyuk et al [3]. On the Cu-deficient side, the border of the CZTS phase lies in the region where the ratio of Cu/(Zn+Sn) = 0.92 - 0.95 if Zn/Sn = 1.03, also in agreement with our results.
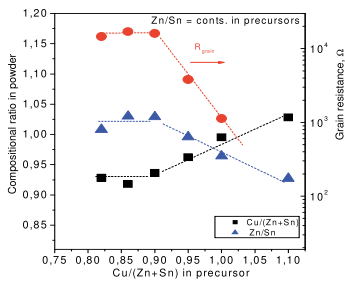
Fig. 1. The compositional ratios of CZTS powders and grain resistance in dependence of Cu/(Zn+Sn) in precursors
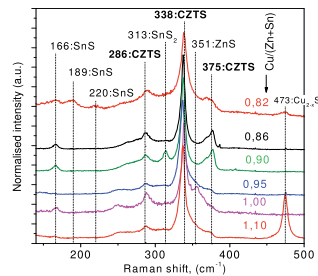
Fig. 2 RT Raman spectra of CZTS powders with different ratio of Cu/(Zn+Sn) in precursors (Zn/Sn = conts.)
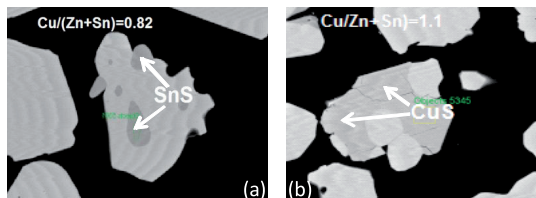
Fig. 3 SEM images of polished CZTS crystals.

All the CZTS monograins in the first series exhibit p-type conductivity regardless of the Cu/(Zn+Sn) and the Zn/Sn ratios. The dependence of the grain resistance on the initial Cu/(Zn+Sn) ratio is given in Fig. 1. (right axis). The measured resistance of the grains decreases from 1.4×10^{4} to 1.4×10^{3} Ω with increasing Cu content in the precursor mixture. Cu-rich and Sn-rich powders have the lowest grain resistance. This could be attributed to the formation of the highly conductive Cu_xS phase on the surface of the grains probably deposited when cooling down the synthesis mixture. Due to this these materials may be not suitable for fabricating solar cells [6].

Next, we investigated similar compositional dependences by varying the Zn-content in the initial precursor mixtures while keeping the Cu/Sn ratio constant. Figure 4 shows Cu/(Zn+Sn) and Zn/Sn values as determined in the final powders as a function of the initial Zn/Sn ratio for Cu/Sn = const. The powder composition can only be varied in the range of Zn/Sn between 0.9 and 1.03. Increasing the Zn content in precursor mixture to more than 1.03 does not change the composition of product powders. The ratio of Cu/(Zn+Sn) remains almost constant (around 0.93- 0.95) in Zn-rich powders (Zn/Sn > 1.03). Raman spectra (Fig. 5) exhibit CZTS peaks at 286, 338, and 375 cm^{-1}. For the Sn-rich powders the Raman spectra reveal the presence of additional Sn_2S_3 and SnS_2 phases with characteristic modes at 304 and 313 cm^{-1}, respectively [4]. The additional peak at 363 cm^{-1} and the broadening of the peak at 338 cm^{-1} can be

assigned to some separate ternary Cu-Sn-S phases [7] among the powder crystals. Powders with compositional ratios of Zn/Sn > 1.03 contain an additional ZnS phase present as separate crystals as it was confirmed by SEM and EDX. Therefore, increasing the Zn-content in the precursor does not widen the range of single-phase CZTS.

When varying the Zn content in the initial material composition also the grain resistance of larger grains was measured and values from $1,3 \times 10^3$ to $1,6 \times 10^4$ Ω were determined. The grain resistance decreases with decreasing the Zn content as seen in fig. 4 (right axis).
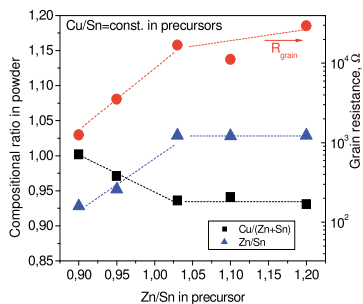
Fig.4 Compositional Zn to Sn ratios in powder and CZTS monograin resistance in dependence of Zn/Sn concentration ratio used in precursors
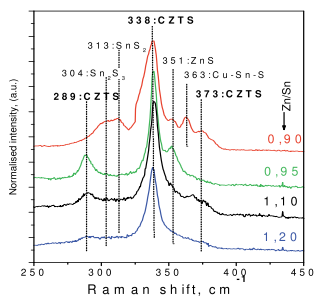
Fig. 5 RT Raman spectra of CZTS with different ratio of Zn/Sn in precursors (Cu/Sn = conts.)

On the basis of these studies, a pseudo-ternary composition diagram was deduced. In fig. 6 the stoichiometric composition of Cu_2ZnSnS_4 is shown by red dot. The black dots represent the initial compositions for the first series of materials investigated in this study and the blue dots mark the initial composition of precursors for the second series of materials reported here. The black and blue hollow circles represent compositions of the synthesised powders. In our study we focused mainly on the "Cu-poor" and "Zn-rich" regions, indicated by red triangle. Also, some powders were synthesized outside of this region in order to clarify the compositional limits of the system. Our results indicate that only two initial compositions are in the "Sn-poor" region. Even a 2 mol% Sn-deficiency in the initial mixture of components results in a "Sn-rich" composition of the powders.
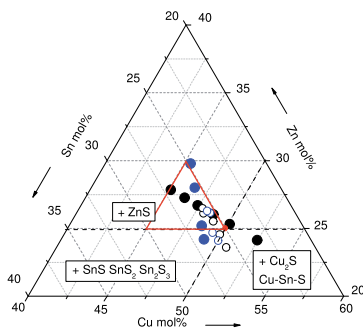
Fig.6. Pseudo-ternary composition diagram showing the position of stoichiometric CZTS (red dot), initial (black and blue dots) and final compositions (hollow circles) for CZTS monograins powder used in this study.

The results indicate that the final composition of the monograin powders can be adjusted only in the following regions: Cu content between 47.8 - 50.8 mol%, Zn content between 23.6 - 26.5 mol% and Sn content between 25.4 - 26.0 mol%. CZTS powders without any secondary phases were synthesised only from precursor compositions with a Cu content of 48.7 to 49.0 mol%, a Zn content of 25.5 to 26.0 mol%, and a Sn content of 25.3 to 25.5 mol%.

In conclusion, the single phase composition region for CZTS monograin powder synthesis is very narrow. Already a few percent deviation from the stoichiometric composition leads to the formation of extra phases in addition to the CZTS material. In the case of excess Zn (Zn/Sn > 1.03), ZnS forms as a secondary phase. In the opposite case, under Zn-poor conditions, separate Sn-S phases are present in addition to the ZnS phase. A Cu-rich composition results in an additional $Cu_{2-x}S$ phase on the powder crystal surfaces. So, single phase CZTS monograin powders can be synthesised only from a precursor mixture comprising metal ratios of Cu/(Zn+Sn) = 0.92 - 0.95 and Zn/Sn = 1.0 - 1.03.

4. Conclusions

The compositional analysis of Cu_2ZnSnS_4 monograin powders synthesised from different initial precursor compositions was used to determine the single phase region in the phase diagram of this material. The results show that the initial composition of the precursor mixture has a major impact on the final powder composition and it`s electrical behaviour. Already a slight deviation from the stochiometric composition leads to the formation of extra phases in addition to the formed crystals. Single phase CZTS monograin powders can be grown in molten KI with precursor metal ratios of Cu/(Zn+Sn) = 0,92 - 0.95 and Zn/Sn =1.0 - 1.03. All the as-grown monograin powders exhibited p-type conductivity. The grain resistance increases with decreasing ratio of Cu/(Zn+Sn) and increasing ratio of Zn/Sn.

Acknowledgements

References

[1] Wang K, Gunawan O, Todorov T, Shin B, Chey SJ, Bojarczuk NA, Mitzi DB, Guha S. Thermally evaporated Cu_2ZnSnS_4 solar cells. Applied Physics Letters 2010; **97**: 143508

[2] Chen S, Gong XG, Walsh A, Wei SH. Defect physics of the kesterite thin-film solar cell absorber Cu_2ZnSnS_4. Appl. Phys. Lett. 2010; **96**: 021902

[3] Olekseyuk ID, Dudchak IV, Piskach LV. Phase equilibria in the Cu_2S-ZnS-SnS_2 system, Journal of Alloys and Compounds 2004; **368**, pp.135-143

[4] Wang K, Shin B, Reuter KB, Todorov T, Mitzi DB, Guha S. Structural and elemental characterization of high efficiency Cu_2ZnSnS_4 solar cells. Applied Physics Letters 2011; **98**: 01912

[5] Price LS, Parkin IP, Hardy AME, Clark RJH. Atmospheric Pressure Chemical Vapor Deposition of Tin Sulfides (SnS, Sn_2S_3, and SnS_2) on Glass. Chem. Mater. 1999; **11**, 1792-1799

[6] Tanaka T, Yoshida A, Saiki D, Saito K, Guo Q, Nishio M, Yamaguchi T. Influence of composition ratio on properties of Cu_2ZnSnS_4 thin films fabricated by co-evaporation. Thin Solid Films 2010; **518**, S29-S33

[7] Fernandes PA, Salome PMP, da Cunha AF. Cu_xSnS_{x+1} (x = 2, 3) thin films grown by sulfurization of metallic precursors deposited by dc magnetron sputtering. Phys. Status Solidi C **7**, 2010; No. 3-4, 901-904

ELSEVIER

European Materials Research Society Conference
Symp. Advanced Inorganic Materials and Concepts for Photovoltaics

Influence of compositional deviations on the properties of Cu$_2$ZnSnSe$_4$ monograin powders

K. Muska[*], M. Kauk, M. Grossberg, M. Altosaar, J. Raudoja, O. Volobujeva

Tallinn University of Technology, Ehitajate tee 5, Tallinn 19086, Estonia

Abstract

We have investigated the influence of compositional deviations on the properties of Cu$_2$ZnSnSe$_4$ (CZTSe) monograin powders in order to determine the optimal preparation conditions for CZTSe based photovoltaic solar cells. EDX results indicate that to obtain a single phase CZTSe powder the initial composition of precursors should be in the range of $0.83 <$ Cu/(Zn+Sn) < 1.0. If Cu/(Zn+Sn) ≥ 1.0 secondary phases were found by Raman investigations and identified as SnSe$_2$ and Cu$_x$Se. The CZTSe grain resistance increased with decreasing the ratio of Cu/(Zn+Sn) and increasing the ratio of Zn/Sn. The shape of as-grown CZTSe powder crystals depends mostly on the mass ratio of flux/CZTSe. All Cu$_2$ZnSnSe$_4$ (CZTSe) monograins exhibited *p*-type conductivity.

© 2011 Published by Elsevier Ltd. Selection and/or peer-review under responsibility of Organizers of European Materials Research Society (EMRS) Conference: Symposium on Advanced Inorganic Materials and Concepts for Photovoltaics.

Keywords: Cu$_2$ZnSnSe$_4$; CZTSe; composition; Raman; morphology

1. Introduction

Cu$_2$ZnSnSe$_4$ (CZTSe) is a promising solar cell material due to it's direct bandgap around 1.04 eV, it's large absorption coefficient ($> 10^4$ cm^{-1}), and the cheap technology of it's production as all elemental components are abundant in the earth's crust [1].

In this study quaternary CZTSe is grown in monograin form. Powder technologies are one of the cheapest technologies for materials production and it is shown that the synthesis of CZTSe from initial binary compounds in the isothermal re-crystallization in different molten fluxes appears to be a relatively simple, inexpensive and convenient method to produce powder materials with very good crystal structure, homogeneity, and reduced concentration of inherent defects. The advantages of the developed powder

* Corresponding author. Tel.: +3-72-620-3362; fax: +3-72-620-3367.
E-mail address: muska@staff.ttu.ee

materials are: (1) single-crystalline structure of every grain; (2) uniform distribution of doping impurities; (3) narrow granulometric composition [2, 3].

A prerequisite for high efficiency solar cells is the use of single phase materials, which according to the theoretical calculations is very demanding. The chemical potential region for stable single phases is very small [4]. It is important to note that up to now only few studies have been published on the phase diagram of Cu_2Se-$ZnSe$-$SnSe_2$ [5, 6].

Results of a previous study of the dependence of physical properties of $CuInSe_2$ monograin materials on the ratio of Cu/In [7] suggest that there is a need to also investigate the effect of different Cu/(Zn+Sn) and Zn/Sn ratios on the properties of CZTSe materials. These studies allow to determine the limits of compositional ratios for the growth of single phase CZTSe, and also to optimize the synthesis conditions for producing CZTSe materials with the desired properties. With this objective, we have carried out the current investigations. The present paper reports the effects of different compositional ratios on the properties of CZTSe monograin powders and identifies the optimum conditions to obtain high quality powders.

2. Experimental

In this study CZTSe powder materials with different compositions were synthesized from high- purity compounds (CuZnSn alloy, Cu-Se, ZnSe and SnSe) and elemental Se in the liquid phase of a flux material in evacuated quartz ampoules. The CuZnSn metal alloy and ZnSe binary compound precursors used for the CZTSe monograin synthesis were commercial compounds. CuSe and SnSe binary compounds were self-synthesized from high purity elements in evacuated quartz ampoules at temperatures of 773 and 1013 K, respectively. The latter precursors were grinded in an agate mortar before use in the powder growth process. As a flux material, water-soluble potassium iodide (KI) was used. The precursors were mixed in desired amounts and ratios, milled in a ball mill, degassed under dynamic vacuum, sealed into evacuated quartz ampoules and heated isothermally at 1013 K for 90 hours.

The formation of CZTSe monograin powders takes place during the heating process in the liquid phase of the flux. The latter must be used in an amount exceeding the limit for sintering of the initial precursor particles. The amount of the components for the CZTSe synthesis and the amount of flux were taken nearly equal to provide enough volume of the liquid phase for filling the free volume between the solid particles, which is one prerequisite for monograin growth. The formation of primary CZTSe particles begins after the melting of the flux material [8]. After the formation of the primary CZTSe particles the recrystallization starts. This thermodynamically-driven spontaneous process occurs because larger particles are energetically more favoured than smaller particles. The growth is stopped by quenching the synthesis ampoules to room temperature. The flux material is removed by leaching with deionized water and solid particles are washed by decantation. The released monograin powder is dried in a hot-air thermostat and sieved to narrow fractions from 20 µm to 112 µm.

The shape and surface morphology of the crystals were determined by high resolution scanning electron microscope (SEM). The chemical composition of the monograin powders was analyzed by energy dispersive x-ray spectroscopy (EDX). Room temperature (RT) Raman spectra were recorded by using a Horiba`s LabRam HR high resolution spectrometer equipped with a multichannel CCD detection system in backscattering configuration. The electrical resistance of the grains was determined by pressing the grain between two indium contacts. The ohmic behaviour of the contacts was proven by the linearity of the *I-V* curves. The conductivity type was determined by the hot-probe method.

3. Results and discussion

3.1. Analysis of elemental and phase composition

For the study of the influence of the Cu content in CZTSe, four powders were grown with different Cu content in precursors (21.6 mol% - 26.2 mol%) while the molar ratios of Zn/Sn = 1.03 and Se/Metal = 1.0 were kept constant. The composition of the monograin powders as molar ratios of Cu/(Zn+Sn) and Zn/Sn

are presented in Figure 1. It is seen that the molar ratio Cu/(Zn+Sn) of the product powders increases from 0.86 to 0.96 in the range of initial Cu/(Zn+Sn) values of 0.9 - 1.0. However, the ratio of Zn/Sn in the powders even decreases from 1.03 in to 0.98.
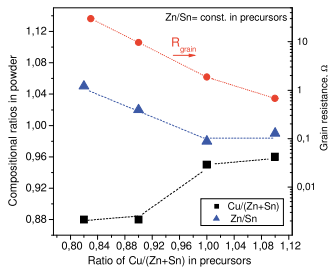
Fig. 1. Cu/(Zn+Sn) and Zn/Sn concentration ratios in powders and grain resistance as a function of Cu/(Zn+Sn) in precursors.
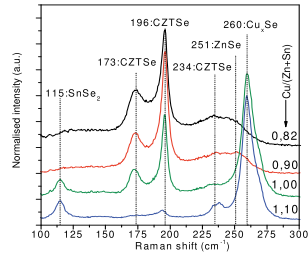
Fig. 2. RT Raman spectra of CZTSe with different Cu/(Zn+Sn) ratios in powders (Zn/Sn=1,03 and Se/Met=1).

RT Raman spectra of powder crystals (Fig. 2) revealed three main peaks at 196, 173 and 234 cm^{-1} which are characteristic for CZTSe [9]. In Cu-poor conditions (Cu/(Zn+Sn)) < 1.0), the presence of ZnSe at 251 cm^{-1} [10] as separate phase was detected. In the synthesis process part of the precursors and the formed material at growth temperature remains dissolved in the flux. During the cooling period the dissolved components precipitate from the flux and deposit on the surface of powder crystals. We suppose that very weak Raman modes of ZnSe originate from these deposits. In Cu-rich conditions (Cu/Zn+Sn) $\geq$ 1,0), Cu_xSe and $SnSe_2$ phases were detected at 260 cm^{-1} and 115 cm^{-1}, respectively [11, 12].

The results show that for single phase CZTSe powder growth starting with Zn/Sn = 1.03 the precursors ratio of Cu to other metals must be kept in the range of 0.83 < Cu/(Zn+Sn) < 1.0. Already in the case of Cu/(Zn+Sn) = 1.0, other phases become clearly detectable by Raman analysis.

The dependence of the CZTSe grain resistance on the Cu/(Zn+Sn) initial ratio is also shown in Fig.1 (right axis). The grain resistance decreases from 50 Ω to 0.4 Ω with increasing Cu/(Zn+Sn) ratio. All monograin powders exhibited *p*-type conductivity regardless of the Cu/(Zn+Sn) ratio. It can be concluded from these results that from Cu-rich precursors a semi-metallic Cu_xSe secondary phase is formed having a very low resistance and thereby preventing the use of the monograins for solar cells.

We also investigated a similar compositional dependence changing the Zn/Sn ratio in the precursors between 0.9 and 1.2, while the ratio of Cu/Sn = 1.85 was kept constant (Figure 3). However, Cu/(Zn+Sn) was changing from 0.83 to 0.96 in the previously found region of the single phase CZTSe. The results indicate that increasing the Zn content in the initial composition (Zn/Sn > 1.03) causes the decrease of the Cu content in the powders.

RT Raman spectra (Fig. 4) of powder crystals reveal three main peaks of CZTSe at 196, 173 and 234 cm^{-1}. Raman spectra of materials synthesized in Zn-rich conditions (Zn/Sn) $\geq$ 1.1), show existence of ZnSe as a secondary phase. In Zn-poor conditions (Zn/Sn) < 1.0 $SnSe_2$ phase emerges in addition to the ZnSe phase.

The results of this series using a constant ratio of Cu/Sn = 1.85 in the initial materials show that by adding excess of Zn (Zn/Sn = 1.03 - 1.1) the single phase region expands to the Cu-deficiency side. The resistances of CZTSe monograins with different Zn/Sn ratios are shown in Fig.3 on the right axis. All monograin powders in this series exhibited *p*-type conductivity regardless of Zn/Sn ratio. The grain resistance increased from 2 Ω to 234 Ω with increasing Zn/Sn ratio.
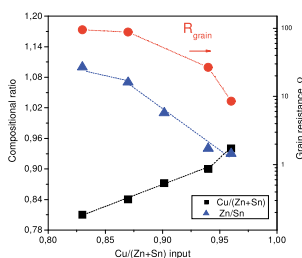
Fig. 3. Cu/(Zn+Sn) and Zn/Sn concentration ratios in powders and grain resistance as a function of Cu/(Zn+Sn) in precursors.
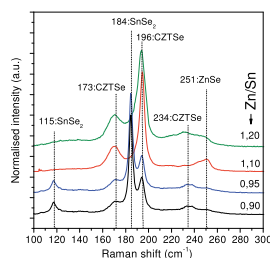
Fig. 4. RT Raman spectra of CZTSe with different Zn/Sn ratio in powders (Cu/Sn) = 1.85 and Se/Met = 1.03)

Summarising the results of both series of experiments we have shown that the composition of the powders can be tailored by changing both - the initial Cu and the Zn content taking into account that an increase of one of the component causes the decrease of the other at the same time.

Subsequently, we investigated monograin compositions when varying the ratio of Se/(Cu+Zn+Sn) in the precursors between 0.96 and 1.09 while the molar ratios of Cu/(Zn+Sn) and Zn/Sn were kept constant at 0.9 and 1.03 respectively. It can be concluded from the EDX and Raman studies that the bulk composition of the monograins did not change. However, a lack of chalcogen (Se/Met = 0.96) leads to the presence of additional Cu_xSe phases, which were not present in the case of excess of chalcogen (Se/Met = 1.03). At even higher Se/Met ratios (1.09) ZnSe and $SnSe_2$ phases were detected.

3.2. Morphology

In addition to the spectroscopic and electrical investigations also a morphological analysis of the referred set of materials was performed. SEM micrographs showed that the grown powder crystals had tetragonal shape with either sharp or rounded edges. It was found that there is no clear dependence of the shape of the crystals on the Cu/(Zn+Sn) or Zn/Sn ratio. However, the shape of the CZTSe powder crystals depends strongly on the volume ratio of flux to CZTSe (cm^3/cm^3), as can be seen in Figure 5. In the case of excess of flux (Flux/CZTSe > 1.6), the powder crystals had a tetragonal shape with very well formed crystal planes compared to powders grown in a lack of flux material (CZTSe/Flux < 0.54) which had rounded edges. In the case of a very low Flux/CZTSe value, there is not enough KI in the initial mix for monograins to grow undisturbed, thus the neighbouring monocrystals start to implicate each other hindering the formation of individual crystals. Also CuSe and Se from the initial precursors might start to act like flux material and the resulting material has more rounded edges due to much higher solubility of the material in CuSe-Se than in KI [8]. In the case of surplus KI, the monograins have more space to grow and therefore can obtain more regular-shaped planes and form tetragonal crystals. First results of a detailed EDX analysis of the powders grown after adding different amounts of Flux material indicate that in of the case of KI deficiency (CZTSe/KI = 0.4) powders with increased Cu/(Zn+Sn) and decreased Zn/Sn ratios are obtained. All the other CZTSe/KI ratios showed no significant changes in their compositional ratios.
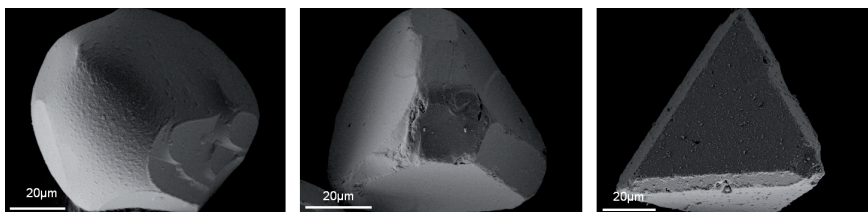
Fig. 5 SEM images of crystals grown with different ratio (cm^3/cm^3) of flux to CZTSe (a) 0.4, (b) 1.6 and (c) 4.9

4. Conclusions

Cu$_2$ZnSnSe$_4$ powders with various compositions were synthesised by isothermal crystallization method and the influence of the initial compositional ratios on the structural, morphological and electrical properties of CZTSe powders were investigated. The shape of CZTSe powder crystals depends mostly on the volume ratio of flux/CZTSe. Single-phase CZTSe monograins can be obtained in the range of 0,83 < Cu/(Zn+Sn) < 1.0 and Zn/Sn from 1.03 to 1.1. All other precursor compositions leads to the appearance of secondary phases, which are identified as ZnSe, SnSe$_2$ or Cu$_x$Se. All monograin powders exhibited *p*-type conductivity with resistance increasing from 0,4 Ω to 230 Ω with decreasing the ratio of Cu/(Zn+Sn) and increasing ratio of Zn/Sn.

Acknowledgements

References

[1] Ito K, Nakazawa T, Jpn. J. Electrical and Optical Properties of Stannite-Type Quaternary Semiconductor Thin Films. Appl. Phys. 1988; **27**, 2094-2097

[2] Mellikov E , Hiie J, Altosaar M. Producibility of II-VI. Materials and Devices. SPIE Proceedings 1994; **222**, 177-185

[3] Altosaar M, Jagomägi A, Kauk M, Krunks M, Krustok J, Mellikov E et al. Monograin layer solar cells. Thin Solid Films. 2003; **431 –432**, 466–469

[4] Chen S, Gong X G, Walsh A, Wei S-H. Defect physics of the kesterite thin-film solar cell absorber Cu2ZnSnS4. Appl. Phys. Lett. 2010; **96**, 021902

[5] Dudchak I V, Piskach L V. Phase equilibria in the Cu2SnSe3–SnSe2–ZnSe system. J. Alloys Comp. 2003; **351**, 145-150

[6] Олексеюк I Д, Дудчак I В, Піскач Л В. Фазові рівноваги в квазіпотрійній системі Cu2Se-ZnSe-Cu2SnSe3. Physics and Chemistry of Solid State 2001; №**1** , 195-200

[7] Kauk M, Altosaar M, Raudoja J, Timmo K et al.. Growth of CuInSe2 monograin powders with different compositions. Thin-Film Compound Semiconductor Photovoltaics. Res. Soc. Symp. Proc. Vol. **865**, 2005.

[8] Klavina I, Kaljuvee T, Timmo K, Raudoja J, Traksmaa R, Altosaar M, Meissner D. Study of Cu2ZnSnSe4 monograin formation in molten KI starting from binary chalcogenides. Thin Solid Films. 2011; in press

[9] Grossberg M, Krustok J, Timmo K, Altosaar M. Radiative recombination in Cu2ZnSnSe4 monograins studied by photoluminescence spectroscopy. Thin Solid Films. 2009; **517**, 2489–2492

[10] Perna G, Lastella M, Ambrico M, Capozzi V. Temperature dependance of the Optical Properties of ZnSe Fims Deposited on Quartz Substrate.Appl. Phys. 2006; A **83**, 127-130

[11] Morell G, Katiyar R S, Weisz S Z, Walter T, Schock H W, Balberg I. Crystalline phases at the p- to n-type transition in Cu-ternary semiconducting films. Appl. Phys. Lett. 1996; **69**, 987-989

[12] Lucovsky G, Mikkelsen J C, Liang W Y, White R M, Martin R M. Optical phonon anisotropies in the layer crystals SnS$_2$ and SnSe$_2$. Phys. Rev. 1976; B **14**, 1663-1669

K. Muska, M. Kauk, M. Grossberg, M. Altosaar, M. Pilvet, T. Varema, K. Timmo, O. Volobujeva, A. Mere. Impact of $Cu_2ZnSn(Se_xS_{1-x})_4$ (x = 0.3) compositional ratios on the monograin powder properties and solar cells. *Thin Solid Films* (provisionally accepted).

Impact of $Cu_2ZnSn(Se_xS_{1-x})_4$ (x=0.3) compositional ratios on the monograin powder properties and solar cells

K. Muska*, M. Kauk, M. Grossberg, M. Altosaar, M. Pilvet, T. Varema, K. Timmo, O. Volobujeva. A. Mere

Tallinn University of Technology, Ehitajate tee 5, Tallinn 19086, Estonia

*Corresponding author. Tel.: +372 55695688

E-mail address: Katri.Muska@ttu.ee

Abstract

We have investigated synthesis conditions and different properties of the quaternary $Cu_2ZnSn(Se_xS_{1-x})_4$ (x= 0.3) (CZTSSe) monograin powders in order to determine the best preparation conditions for the realization of CZTSSe powder as absorber material in monograin layer solar cells. CZTSSe powders with different initial compositions were synthesized in the liquid phase of potassium iodide flux in evacuated quartz ampoules. Energy dispersive x-ray spectroscopy studies revealed that Cu/(Zn+Sn) ratio of final powder can be changed from 0.91 to 1 and Zn/Sn ratio from 0.9 to 1.04. Raman spectra of the CZTSSe monograin powders showed peaks of some secondary (mostly binary) phases. To improve the properties of synthesized powders as-grown monograins were heat-treated in sealed quartz ampoules in controlled Se, S and SnS_2 atmospheres using a two–temperature zone arrangement. It was found that the effect of heat-treatments on the output parameters of CZTSSe monograin layer solar cells depends strongly on the initial powder composition.

Keywords: CZTSSe; Composition; Thermal treatment; Solar cell

1. Introduction

$Cu_2ZnSn(S_xSe_{1-x})_4$ (CZTSSe) is a promising absorber material for solar cell as it contains abundant and cheap elements, which could help to lower the cost of solar electricity. The other desirable properties of CZTSSe as solar cell absorbers include also *p*-type conductivity, high absorption coefficient and direct band gap of about 1.02 - 1.5 eV, depending on the S to Se ratio [1]. The highest reported solar cell efficiency achieved with CZTSSe based absorbers has been so far 10.1% [2].

Chen et al. found that Cu-poor and Zn-rich conditions improved the efficiency of Cu_2ZnSnS_4 (CZTS) solar cells because Cu-poor conditions enhance the formation of Cu vacancies, which enhance shallow acceptors in CZTS, while Zn-rich conditions suppress the substitution of Cu at Zn sites, which give rise to relatively deep acceptors. Therefore, it is critical to control the chemical composition of the CZTS absorber layer to produce high-efficiency CZTS solar cells [3]. Previously [4, 5] we showed that powder technology can be used to synthesize Cu_2ZnSnS_4 and $Cu_2ZnSnSe_4$ (CZTSe) single phase monograin powders. In the present work, we studied whether and how the composition of $Cu_2ZnSn(S_{0.7}Se_{0.3})_4$ solid solution in monograin powder form can be controlled by varying the initial precursor composition. We also investigated the influence of CZTSSe powder composition on the performance of CZTSSe monograin layer (MGL) solar cells. Furthermore, we annealed the synthesized powders in different gas atmospheres (S, Se and SnS_2) and studied the influence of annealing process to MGL solar cell parameters.

2. Experimental details

CZTSSe monograin powders with different Cu/(Zn+Sn) and Zn/Sn ratios were synthesized from Cu-Zn-Sn metal alloy powder with composition $Cu_{1.67}Zn_{1.03}Sn_{1.0}$ and elemental S and Se in evacuated quartz ampoules in the liquid phase of KI as flux. The composition was modified by addition of high-purity Cu_2S, SnSe and ZnSe powders. More detailed description about monograin growth and formation process can be found in [5]. The ratios of the initial elemental components are shown in Table 1.

After the synthesis, as-grown powders were annealed in a two-temperature-zone quartz tubular vacuum reactor where the temperature of the selenium, sulfur or SnS_2 source and the temperature of CZTSSe zone were controlled and regulated independently. CZTSSe powders were heated at 740°C (higher temperature zone) while the inexhaustible source of selenium and sulfur for producing controlled vapor atmosphere was heated at 650°C and 465°C, respectively. In such arrangement the vapor pressure of Se (S) in ampoules was determined by the temperature of an inexhaustible Se (S) source. The temperature of SnS_2 determining the vapor pressure of SnS_2 was chosen 740°C in order to avoid Sn loss by evaporation and/or to provide Sn for self-reorganization of CZTSSe composition. After annealing, the ampoules were taken out of the furnace and cooled down on a ceramic plate at room temperature. According to the results of previous study dealing with two-zone heat-

treatments of Cu_2ZnSnS_4 and $Cu_2ZnSnSe_4$ [6], the duration of heating for 30 minutes was chosen for all treatments.

Table 1 Elemental composition and ratios of initial precursors of CZTSSe monograin powders.

Sample	Precursors	Elemental compositions and ratios of input precursors								
		Cu at%	Zn at%	Sn at%	S at%	Se at%	Cu/(Zn+Sn)	Zn/ Sn	Cu/Sn	S/(S+Se)
1	CuZnSn +Se + S	22.57	13.92	13.51	35.00	15.00	0.82	1.03	1.67	0.70
2	CuZnSn + Se + S+ Cu$_2$S	23.15	13.62	13.23	35.00	15.00	0.86	1.03	1.75	0.70
3	CuZnSn + Se + S+ Cu$_2$S	23.70	13.34	12.95	35.00	15.00	0.90	1.03	1.83	0.70
4	CuZnSn + Se + S+ Cu$_2$S	24.37	13.01	12.63	35.00	15.00	0.95	1.03	1.93	0.70
5	CuZnSn + Se + S + Cu$_2$S	25.00	12.68	12.32	35.00	15.00	1.00	1.03	2.03	0.70
6	CuZnSn + Se + S + Cu$_2$S + SnSe	24.53	12.09	13.38	36.05	15.00	0.96	0.90	1.83	0.71
7	CuZnSn + Se + S + Cu$_2$S + SnSe	24.21	12.59	13.20	36.05	15.00	0.94	0.95	1.83	0.71
8	CuZnSn +Se + S+ Cu$_2$S + ZnSe	23.28	13.99	12.72	36.05	15.00	0.87	1.10	1.83	0.71
9	CuZnSn + Se + S + Cu$_2$S + ZnSe	22.70	14.89	12.41	36.05	15.00	0.83	1.20	1.83	0.71
10	CuZnSn + Se + S + Cu$_2$S + ZnSe	21.63	16.55	11.82	36.05	15.00	0.76	1.40	1.83	0.71

The chemical composition of the monograin powders was analyzed by energy dispersive x-ray spectroscopy (EDX) on ZEISS HR SEM ULTRA 55 with accelerating voltage 7 kV and a beam current 3 nA. Phase composition of the monograins was determined by room temperature (RT) micro-Raman spectroscopy using Horiba`s LabRam HR high resolution spectrometer in backscattering configuration with wavelength 532 nm. Crystalline structure was studied by X-Ray diffraction (XRD), the measurements were performed on a Rigaku ULTIMA IV diffractometer with Cu Kα radiation (λ=1.54056 Å, 40 kV, 40 mA) using the silicon strip detector D/teX Ultra. The electrical resistance of the grains was determined by pressing individual grains (around 150-200 μm in diameter) between indium contacts and the type of conductivity was determined by hot probe measurements using Potentiometer and Brymen BM 338 Multimeter. All post-treated monograin powders were used as absorber materials in MGL solar cells. The MGL solar cells had superstrate structure: graphite/MGL/CdS/ZnO/glass, where the MGL consists of a monolayer of powder grains embedded into an organic resin. The monograins were embedded into polymer so that the upper part of the grains remained uncovered. CdS was deposited on the top of MGL by chemical bath deposition, followed by radio frequency sputtering of i-ZnO and conductive ZnO:Al. Finally In-grid contacts were evaporated on top of ZnO window layer and the structure was glued on a glass. For back conducting, the bottom part of MGL was etched with concentrated H_2SO_4 to remove some polymer from the crystal surfaces, the exposed monograins were polished and graphite contacts were applied. The active area of the MGL solar cells was ~ 75% of the total area. The solar cells were evaluated by measuring the current density versus voltage (J-V) characteristics by Keithley 2400 electrometer under standard test conditions (AM 1.5, 100 mW/cm^2).

3. Results and discussion

3.1 Analysis of elemental and phase composition of as-grown monograin powders

Figure 1 presents the pseudo-ternary composition diagram for CZTSSe. The star in the figure represents the stoichiometric composition of $Cu_2ZnSn(Se_x,S_{1-x})_4$, the filled dots represent the initial CZTSSe compositions and the hollow dots represent the composition of synthesized monograin powders.

Unfortunately, there are published phase diagrams only for pure selenide [7] and pure sulfide systems [8]. For solid solutions the borders of single phase CZTSSe are unknown. Considering both systems the monograin powder with the lowest Cu content was synthesized in the region, where LT-ZnS(Se), SnS(Se)$_2$ and CZTSSe exist together. EDX analysis confirmed, that the powder contained also different binaries (Sn$_2$Se$_3$, ZnSe, ZnS, SnSe$_2$) and ternary compounds (Cu$_3$SnS$_4$, Cu$_2$SnS$_3$). It can be seen from the Figure 1 that even though the initial Cu content in precursors was changed from 21.6 at% to 25.0 at%, the Cu content in the final CZTSSe monograins changed between 23.3 and 25.0 at%. We assume that this is the Cu deviation range of single phase $Cu_2ZnSn(Se_{0.3}S_{0.7})_4$ compound.
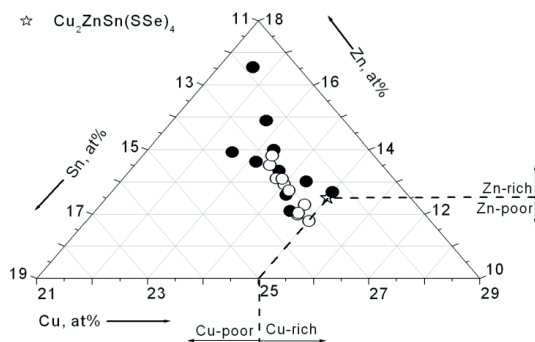
Figure 1 Pseudo-ternary composition diagram of atomic percentages of metals in CZTSSe monograins. The position of stoichiometric CZTSSe (star), initial (filled dots) and final compositions (hollow circles) are shown.

The initial Zn content in precursors was varied from 12.1 at% to 16.5 at%. The Zn content in final powders changed between 11.8 at% and 13.8 at%, which is less than 2 at%. Sn concentration in initial precursor mixtures was changed from 11.8 to 13.5 at%. The Sn content in the final products deviates only 0.5 at% (12.8-13.3 at%), which is only third of the initial variation. Cu-and Sn-rich compositions (Zn/Sn<0.95) led to the formation of $Cu_xS(Se)$ and SnS(Se) secondary phases in the grains. Similar behavior was also seen in our previous work dealing with pure sulfide and selenide materials, where the ranges of single phase existence of quaternary compounds were found to be rather narrow [4, 5].

Raman spectroscopy is useful to analyze the phase composition in pure CZTS and CZTSe samples. But Raman spectra of the CZTSSe solid solutions are complicated to read due to the bimodal behavior of the spectra [9]. The RT Raman spectra of CZTSSe monograins are shown in Figure 2. The dominating CZTSSe Raman peaks were detected at 163, 195, 226, 234, 285 and 336 cm^{-1}. In the case of initially Zn-rich materials (Sample 9 on Figure 2, Zn/Sn=1.04 calculated from EDX), the presence of ZnS(Se) secondary phases were detected from Raman peaks at 205, 251 and 350 cm^{-1}. In general, the Raman peaks of secondary phases have quite low intensities in comparison with the intensities of CZTSSe peaks. SnS(Se)$_2$ phase with characteristic mode at 299 cm^{-1}, and Cu_xSe phase with Raman peak at 259 cm^{-1} are present in Cu-rich (Sample 4, Cu/(Zn+Sn)=1.0 by EDX) and Sn-rich (Sample 6, Zn/Sn=0.9 by EDX) materials. However, the intensity of Cu_xSe peak is very low.
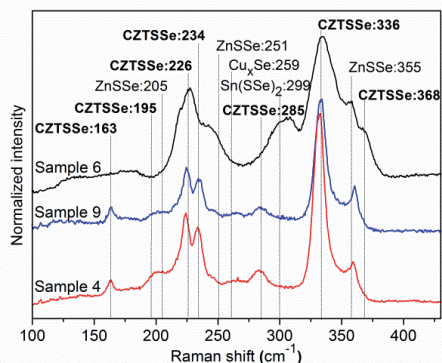
Figure 2 RT Raman spectra of CZTSSe monograin powders with different compositions.

There is a slight change in the Raman peak positions indicating a variation in the S/Se ratio in the materials. This is in correlation with EDX results, where it was noticeable that in most of the materials the S/(S+Se) ratio in final material was slightly increased if compared to the initial ratio. The increase of S/(S+Se) ratio is the highest in Sn-rich material thus the spectra are slightly shifted to the right side towards to the peak positions of the pure Cu_2ZnSnS_4. The quite broad Raman peaks of $Cu_2ZnSn(Se_xS_{1-x})_4$ solid solutions are correlated with the increasing

structural disorder due to the random distribution of S and Se atoms in the lattice that leads to fluctuations in the masses and force constants in the neighborhood [9].

Figure 3 presents the XRD patterns of CZTSSe monograin powders, which resulted in solar cells with the highest efficiencies. Most of the diffraction peaks correspond to kesterite structure (112), (240/220), (312/116), (008) and (332). The other, less dominant peaks are also mostly attributed to the kesterite Cu_2ZnSnS_4 (ICDD: 01-075-4122) [10], but Rietveld analysis also suggested the presence of ZnS (peaks at around 29.3°, 42°, 55° and 63°(ICDD: 01-074-4981), Cu_2Se_x (ICDD: 00-047-1448) and Cu_4Se_3 (ICDD: 00-042-0925) at $2\Theta = 27°$ and 71°. However, ZnS phase is not well distinguishable from kesterite phase, because their diffraction peaks overlap [11].
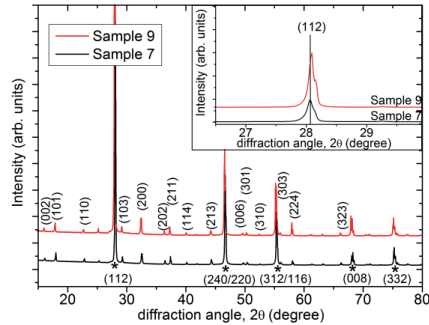
Figure 3 The X-ray diffraction pattern of $Cu_2ZnSn(S_{0.7}Se_{0.3})_4$ monograin powders with different initial metal ratios.

Similarly to Raman spectroscopy, XRD shows a shift of the peaks. This is due to the change of S/Se ratio in the final monograin materials. While both of the materials were synthesized with initial S/(S+Se) ratio of 0.71 and differ only by the metal ratios, the final materials became more S-rich having the S/(S+Se) ratio 0.74 in the case of Sample 9 (Cu/(Zn+Sn)=0.88 and Zn/Sn= 1.04 in powder) and 0.73 in the case of Sample 7 (Cu/(Zn+Sn)=0.98 and Zn/Sn= 0.91 in powder).

3.2 Heat treatments in different gas atmospheres and solar cell device characterization
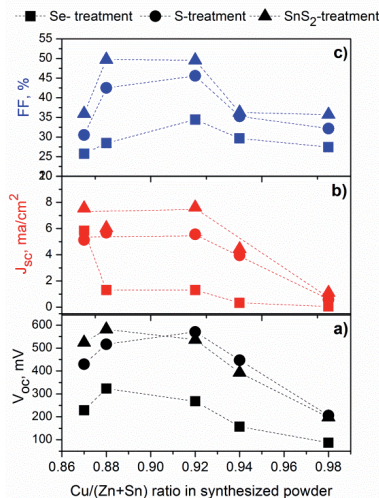
Figure 4 a) Open circuit voltage (V_{oc}), b) Current density (j_{sc}) and c) Fill factor (FF) in dependence of different Cu/(Zn+Sn) ratios in synthesized material after Se_2 (squares), S_2 (dots) and SnS_2 (triangles) treatment.

CZTSSe monograin powders with various compositions were annealed in different atmospheres and subsequently MGL solar cells were prepared. Figure 4 shows the influence of Se, S and SnS_2 treatments on the solar cell properties based on absorber material with different Cu to Zn+Sn ratios. It is seen from the Figure 4a, that the highest open circuit voltages (570-580mV) were achieved for solar cells based on CZTSSe absorbers with Cu/(Zn+Sn) ratios between 0.88 and 0.92 and Zn/Sn between 1.01-1.04. When material composition is Cu- and Sn-rich (Cu/(Zn+Sn)≤0.94) or very Zn-rich and Cu-poor, the output parameters show rather poor performance. This is most likely due to the secondary phases formed on the monograin surface which could also be seen from the values of resistances of these materials. In the case of copper rich materials, the surface of the grains contains $Cu_xS(Se)$ secondary phases, which results in their high conductivity. The measured grain resistance confirmed low resistance of these materials (around 100 Ω) opposite to slightly Cu-poor and Zn-rich materials, which had resistance over 4000 Ω. Selenization of absorber resulted in the lowest open circuit voltages regardless of the Cu/(Zn+Sn) ratios. Compared to sulfurization, the open circuit voltage of solar cells was up to 300 mV lower.

EDX analysis of CZTSSe crystals showed that ratio of S/(S+Se) = 0.71 in bulk did not change after treatments, but the surface of the monograins became more Se-rich (S/(S+Se) = 0.5) after selenization and more S-rich after S and SnS_2 treatments (S/(S+Se) = 0.77).

4. Conclusions

The Cu content in the bulk of $Cu_2ZnSn(Se_xS_{1-x})_4$ (x= 0.3) monograins can be changed only from 23.3-25.0 at%, Zn content can be changed from 11.8 to 13.8 at% and Sn content from 12.8-13.3 at%. Most of the monograins contained ZnS(Se) secondary phases in the bulk of the grains, but materials with Cu- and Sn-rich compositions also contained secondary phases of Sn(Se) and CuS(Se). It was found, that by changing the initial metal ratios in precursors, the S/Se ratio in the synthesized powders increases up to 5%, which leads to slight peak shifts in XRD and Raman spectra towards the peak positions of the pure Cu_2ZnSnS_4.

The S and SnS_2 vapor-treatments improve the parameters of MGL solar cells, increasing the open circuit voltage up to 300 mV compared to selenization. The best solar cell characteristics were achieved with Cu/(Zn+Sn) ratio of 0.88-0.92 and Zn/Sn ratio of 1-1.04. The S/(S+Se) ratio in the monograins surface increases slightly during S and SnS_2 treatments, but decreases significaly during Se treatment.

References

[1] K. Timmo, M. Altosaar, J. Raudoja, K. Muska, K. Kauk, M. Pilvet, T. Varema, M. Danilson. O. Volobujeva, E. Mellikov, Sol. Energy Mater. Sol. Cells 94 (2010) 1889
[2] D. Aaron R. Barkhouse, O. Gunawan, T. Gokmen, T. K. Todorov, D. B. Mitzi, Prog. Photovolt. Res. Appl. 20 (2012) 6
[3] K. Tanaka, Y. Fukui, N. Moritake, H. Uchiki, Sol. Energy Mater. Sol. Cells 95 (2011) 838
[4] K. Muska, M. Kauk, M. Grossberg, J. Raudoja, O. Volobujeva, Energy Procedia 10 (2011) 323
[5] K. Muska, M. Kauk, M. Altosaar, M. Pilvet, M. Grossberg, O. Volobujeva, Energy Procedia 10 (2011) 203
[6] M. Kauk, K. Muska, M. Altosaar, J. Raudoja, M. Pilvet, T. Varema, K. Timmo, O. Volobujeva. Energy Procedia 10 (2011) 197
[7] I.V. Dudchak, L.V. Piskach, J. Alloys Compd. 351 (2003) 145
[8] I.D. Olekseyuk, I.V. Dudchak, L.V. Piskach. J. Alloys Cmpd 368 (2004) 135
[9] M. Grossberg, J. Krustok, J. Raudoja, K. Timmo, M. Altosaar, T. Raadik, Thin Solid Films 519 (2011) 7403
[10] J. He, L. Sun, S. Chen, P. Yang, J. Chu. J. Alloys Cmpd 511 (2012) 129
[11] A. Redinger, D. M. Berg, P. J. Dale, S. Siebentritt, J. Am. Chem. Soc. 133 (2011) 3320

European Materials Research Society Conference
Symp. Advanced Inorganic Materials and Concepts for Photovoltaics

Effects of sulphur and tin disulphide vapour treatments of Cu$_2$ZnSnS(Se)$_4$ absorber materials for monograin solar cells

M. Kauk [*], K. Muska, M. Altosaar, J. Raudoja, M. Pilvet, T. Varema, K.Timmo, O. Volobujeva

Tallinn University of Technology, Ehitajate tee 5, Tallinn, 19086 Estonia

Abstract

The aim of this study was to find a heat-treatment procedure for monograin powders using a controllable reactive gas phase to improve the CZTS(Se) crystal surface for effectively working *p-n* junctions. The influence of an isothermal treatment in S and SnS$_2$ vapour on the parameters of monograin layer solar cells is depending on the CZTS(Se) initial composition. The efficiencies of solar cells improve continuously with increasing temperatures of the absorber materials' post-annealing from 823 to 973K under constant sulphur vapour pressure of 100 Torr. The highest values of J_{sc}= 18.4 mA/cm^2 and V_{oc}= 720 mV were obtained for a device made from CZTS powder annealed at 1013K in SnS$_2$ vapour.

Keywords: Cu$_2$ZnSnS(Se)$_4$; solar cells; annealing

1. Introduction

Cu$_2$ZnSn(S$_x$Se$_{1-x}$)$_4$ is theoretically derived from CuIn(S$_x$Se$_{1-x}$)$_2$ by substitution of 50% of the In atoms by Zn and the other half by Sn atoms. This isoelectronic substitution produces a material with many properties being similar to the ternary compound. However, it is crucial that it no longer contains any rare or expensive elements. The desirable properties include *p*-type conductivity, a high absorption coefficient (larger than 10^4 cm^{-1}) and a direct bandgap of about 1.04-1.5 eV (depending on the ratio of S/Se) [1]. In

---

[*] Corresponding author. Tel.: +372-620-3362; fax: +372-620-3367.
E-mail address: kmarit@staff.ttu.ee

our previous reports [2, 3] we showed that monograin powders of $Cu_2ZnSnSe_4$ and $Cu_2ZnSn(Se,S)_4$ solid solutions can be prepared by isothermal crystallization from binary compound precursors in molten potassium iodide. A high temperature (970–1000 K) synthesis and the homogenization in the molten phase of flux material results in an uniform composition of powder crystals of these complex multicomponent compounds. Therefore, the monograin powder technology enables to grow $Cu_2ZnSn(S,Se)_4$ materials with homogeneous composition usable for monograin layer solar cells.

In order to achieve high-efficiency solar cells, often post-treatments of the absorber layers are required. For example, a successful method to prepare CZTS with a good solar cell efficiency is a solution-based method to deposit a precursor followed by a short annealing in sulphur at 813 K. Also evaporated thin films are often annealed in a H_2S or S atmosphere in order to improve their photovoltaic performance [4]. There are many papers [5-7] concerning the Sn loss during these annealing processes. The vapour pressure of liquid Sn is far too low to see direct evaporation of the element, but tin sulphides are volatile and decompose as following: $2SnS_2(s) \rightarrow Sn_2S_3(s) + \frac{1}{2}S_2(g) \rightarrow 2SnS(g) + \frac{1}{2}S_2(g)$. Weber *et. al* [5] studied the loss of Sn from CZTS films and proposes that above 823 K CZTS decomposition occurs: $Cu_2ZnSnS_4(s) \rightarrow Cu_2S(s) + ZnS(s) + SnS(g) + \frac{1}{2}S_2(g)$. So, for keeping the reactions on the left side and to avoid the decomposition of quaternary compounds it is crucial to keep the sulfur pressure high especially at the high temperatures used in annealing processes. Redinger *et. al* [6] also showed that controlling the Sn losses in the annealing environment improves the solar cell efficiency significantly and reproducibly.

In our previous studies [8], it was shown that due to the distribution of material between the liquid flux and the solid CZTS(Se) crystals during the synthesis process, some part of material is dissolved in flux material at growth temperature. In the cooling period, these dissolve species precipitate on the solid crystal surfaces. Therefore, as-grown monograins need some chemical etching and annealing before the formation of *p-n* junction. In previous studies an isothermal annealing at 1013 K was used, where the atmosphere in the ampoules was determined by the equilibrium vapour pressure formed inside closed CZTS(Se) ampoules. By varying the cooling regimes, Sn-S(Se) crystals with different compositions were deposited on the walls of the ampoules. Therefore, the isothermal arrangement was replaced by a two-temperature zone arrangement, where the atmosphere in the ampoules is controlled by the temperature of an inexhaustible S or SnS_2 source in the lower temperature zone of the post annealing system.

In this paper, the effect of annealing treatments on the structural and compositional properties and also on the parameters of the CZTS(Se) monograin layer solar cells are discussed.

2. Experimental details

$Cu_2ZnSnS(Se)_4$ powder materials with different compositions were synthesized from high-purity metal sulfides (selenides) and elemental S (Se) in the liquid phase of a flux material in evacuated quartz ampoules. The details about monograin growth process can be found in [2, 3].

The post-treatments were carried out in closed ampoules additional S or SnS_2 as sulfur and/or SnS_2 sources using a two-temperature zone arrangement. The powder and the sources were in different temperature zones. For comparison, isothermal arrangement with and without additional SnS_2 were used. In a first setup, sealed ampoules were placed into a two-zone tube furnace, where the temperature of both zones were controlled and regulated precisely. In such an arrangement, the vapour pressure of the S or SnS_2 sources was determined and controlled by the lowest temperature in the system. In isothermal arrangements, CZTS powder and component (SnS_2) were in two separated chambers at the same temperature.

The bulk chemical composition of the monograin powders were analyzed by energy dispersive x-ray spectroscopy (EDS). The phase composition of the asgrown and post-treated powders was studied by room temperature (RT) Raman spectroscopy. All post-treated monograin powders were used as absorber materials in monograin layer solar cells (MGL). The MGL solar cell combines the features of a monocrystalline solar cell and a thin film solar cell. The photoactive layer is formed by the semiconductor

CZTS(Se) material with single-crystalline grains embedded into an epoxy resin called a monograin membrane. The monograin membranes are covered with CdS by chemical bath deposition followed by sputtering i-ZnO/ ZnO:Al layers. The active area of the MGL solar cells is ~ 75% of the total area. The solar cells were examined by measuring the current density versus voltage (*J-V*) characteristics and by spectral response measurements.

3. Results and discussion

In a first experiment the CZTSe monograin powders with different compositional ratios were annealed in an atmosphere of excess SnS_2 at 1013 K for 30 minutes. Figures 1a and 1b show the SEM images of a CZTSe single grain and its surface, respectively. The heat-treatment in SnS_2 atmosphere leads to a rough surface of the monograins.
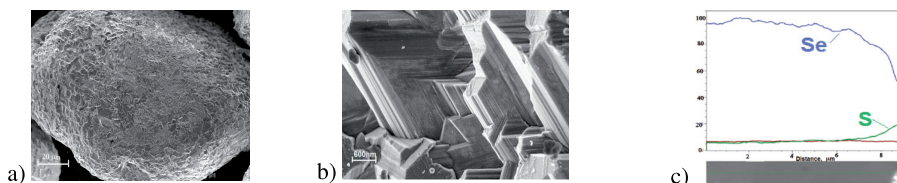
Fig. 1. SEM images of a) CZTSe monograin and b) its surface and c) EDX profile after isothermal SnS_2-treatment at 1013K

In order to clarify the depth of the sulphur diffusion at different annealing temperatures (823 - 1013K), pure CZTSe monograin powders were analyzed in cross section SEM images. Figure 1c shows the EDX compositional profile of a CZTSe monograin after annealing in SnS_2 vapour for 15 minutes at 1013K. The depth of the S diffusion increases from 0.2 to 2 µm with increasing the annealing temperature from 823 K to 1013 K. The sulphur content increases up to 10 mole % in the CZTSe powder surface according to this EDX analysis. According to EDX results, the annealing in SnS_2 vapour leads to different compositions than found for the as-grown powders. From this behaviour, we can conclude that the incorporation of Sn via SnS_2 vapour does not proceed in a random way but is determined by the phase diagram border on the SnS_2 side or by the solubility of SnS_2 in CZTS. In as-grown powders with compositional ratios of Cu/(Zn+Sn)=0.98 and Zn/Sn=1.0 secondary phases of ZnS(Se) and Cu_2S(Se) were found in Raman measurements. As long as enough Cu_2S and ZnS is present, SnS_2 from the gas phase can be incorporated into the powder to form CZTS.

Table 1. Solar cell parameters for different sulphur vapour pressures and temperatures of the CZTS zone used.

T_{mat} [K]	p_S [Torr]	V_{oc} [mV]	J_{sc}, [mA/cm^2]	FF, [%]	η_{max}, [%]
untreated		184	1.8	27	0.1
823	100	645	15.8	56	5.6
873	100	661	17.4	61	6.2
923	100	627	13.5	55	6.1
973	100	665	18.0	62	6.6
973	30	542	10.9	47	2.6
973	300	637	14.6	56	4.6
973	1000	644	16.0	57	5.8
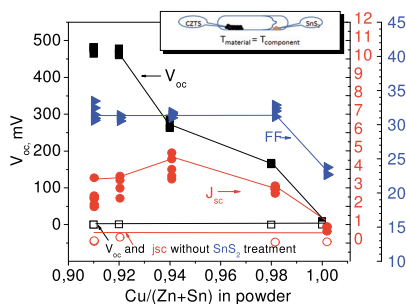
Fig. 2. Influence of an isothermal treatment in SnS_2 vapour on the parameters of MGL solar cells in dependence of the CZTS(Se) initial composition.

In order to determine the influence of the isothermal treatment in SnS_2 vapour on the solar cell parameters, several powders with different Cu/(Zn+Sn) ratios were used to prepare MGL solar cells. Figure 2 shows that the influence of the isothermal treatment in SnS_2 vapour is depending on the composition of the CZTS(Se). An improvement in solar cell parameters is remarkable if the ratio of Cu/(Zn+Sn) is in the range of 0.91-0.94 and the Zn/Sn ratio is equal or higher than one (Zn-rich samples). If the initial composition of the material is more Cu- and Sn-rich (Zn/Sn <1), the output parameters of these MGL solar cells are extremely poor. This could be due to the very low grain resistance (~100 Ω) of the Cu-rich and Sn-rich materials compared with the resistances of Cu-poor and Zn-rich materials (~1000Ω). Raman studies reveal that these low resistant materials contain CuS(Se) and SnS(Se) phases. CuS(Se) is well known as having semi-metallic nature and have a tendency to degrade the open circuit voltage [9]. Another reason for the poor performance of Zn-poor powders can be very likely be due to the presence of Cu-Sn-S phases. Cu_2SnS_3 with a band gap of about 0.95eV can result in a lowering of the open circuit voltage [10]. Therefore, these materials are not suitable for manufacturing solar cells.

With the aim to prevent the decomposition of CZTS and the Sn loss, we also investigated the influence of sulphur vapour pressure treatment of the absorber materials on their solar cell parameters. A series of powders were annealed at temperatures between 823 and 1013K. The sulphurisation time and the sulphur vapour pressures were varied from 10 to 60 minutes and from 30 to 1000 Torr, respectively. For these sulphurisation studies powders with compositional ratios of Cu/(Zn+Sn) = 0.89 and Zn/Sn=1.1 were used. Raman spectra of the sulphurised powders exhibit main peaks of CZTS at 287, 338 and 373 cm^{-1} [11]. Also, the ZnS secondary phases were found at 353 cm^{-1} [11]. Due to the high band gap value (3.54 eV) and the high resistivity we believe that ZnS is acting as insulator. This means that the presence of ZnS reduces the active area and the current density of MGL solar cells. Table 1 gives the maximum parameters of CZTS solar cells prepared from sulphurised materials. These MGL solar cells show V_{oc} values of up to 665 mV and *FF* of up to 62 %. The efficiencies of CZTS MGL solar cells improve continuously after annealing in S vapour pressures of 100 Torr at 823 to 973 K. The annealing of the absorber powders under higher S vapour pressures does not lead to a further improvements of the solar cell parameters. If the vapour pressure of S was lower than 100 Torr, the precipitation of SnS_2 on the walls of the ampoules was visible. Relatively low S vapour pressure ($P_S \leq 30$ Torr) did not prevent the tin loss from CZTS, which led to a Sn-poor surface region. The electronic structure of a Sn-depleted surface is not favourable for the formation of well working *p-n* junction, as indicated by the poor solar cell efficiencies.

Table 2. Electrical characteristics of devices annealed at various temperatures of the SnS_2 zone (T_{mat}= 1013K).

$T_{comp.}$ [K]	V_{oc} [mV]	J_{sc} [mA/cm^2]	FF [%]	η_{max} [%]
603	473	3.1	29	0.4
833	442	1.5	38	0.1
873	440	2.7	43	0.4
898	553	2.0	56	0.4
923	645	16.	56	5.2
973	680	11.7	60	4.7
1013	720	18.4	60	7.4
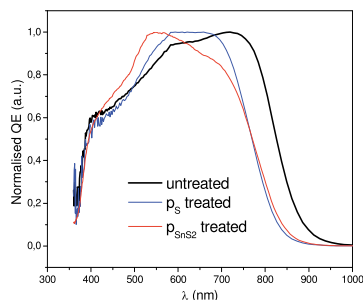
Fig. 3. QE of MGL solar cells using the a) untreated, b) sulphurised and c) annealed under SnS_2 vapor.

In order to find the optimum annealing temperature in SnS_2 atmosphere the CZTS powders were annealed at temperatures between 603 K and 1013 K for a constant time (10 min). The temperature of the CZTS zone was kept constant (T_{mat}=1013 K). For this study powders with an initial compositional ratios of Cu/(Zn+Sn)=0.89 and Zn/Sn=1.1 were used. EDX results revealed that the compositional ratios did not change after annealing in SnS_2 vapour. This confirms also that the annealing in SnS_2 vapour is a self

limiting process and does not have any influence on the CZTS composition if this is equal to the composition at a border in the phase diagram. We can assume that the values of the compositional ratios correlate to the border of the homogeneous phase composition. Table 2. shows the results of the best output parameters achieved from these MGL solar cells. The results show that different annealing temperatures significantly affect the photovoltaic behaviour. The highest J_{sc}=18.4 mA/cm^2 and V_{oc}=720 mV values were obtained from the devices with the CZTS powder being annealed at 1013 K in SnS$_2$ vapour. The main improvements in V_{oc} and J_{sc} values were obtained for materials annealed at temperatures higher than 923 K. The best V_{oc} is close to the highest as yet reported value for CZTS [12]. A major drawback is the low J_{sc} values obtained for the solar cell structures, which may be due to recombination losses at the active interface, i.e. between CZTS and CdS.

Fig. 3 shows the relative quantum efficiencies of the CZTS MGL devices based on untreated, S-annealed and SnS$_2$- annealed samples. As the result, the absorption edge of annealed CZTS shifts to shorter wavelengths. The derivatives of the QE with respect to wavelength gives rough estimation of the effective band gap of the absorber material. The estimated band gap for annealed CZTS is around 1.5 eV. and for asgrown CZTS material is around 0.1 eV lower than after annealing. Although we used Cu-poor and Zn-rich powders, it is possible that some secondary phases precipitate from the flux on the grain surface in the powder quenching processes. So, we assume that chemical pre-treatment and heat-treatment under SnS$_2$ vapour remove the secondary phases from the CZTS monograin surface.

4. Conclusions

It has been shown that MGL solar cell parameters improved remarkable after sulphur or SnS$_2$ heat-treatments of CZTSSe absorber materials. The influence of an isothermal treatment of SnS$_2$ vapour on the parameters of monograin layer solar cells is depending on the CZTS(Se) initial composition. Relatively low S vapour pressure ($P_S \leq 30$ Torr) and temperature of SnS$_2$ zone ($T_{comp} < 560^oC$) in two-temperature zone arranement, did not prevent the tin loss from Cu$_2$ZnSnS$_4$, which led to a Sn-poor surface region. The electronic structure of a Sn-depleted surface is not favourable for the formation of well working *p-n* junction, as indicated by the poor solar cell efficiencies.

Acknowledgements

References

[1] Chen S, Walsh A. *et al*. Compositional dependence of structural and electronic properties of Cu$_2$ZnSn(S,Se)$_4$ alloys for thin film solar cells. *Physical Review B* 2011; **83**:125201

[2] Timmo K, Altosaar M, Raudoja J, Muska K, Kauk M, *et al*. Sulfur-containing Cu$_2$ZnSnSe$_4$ monograin powders for solar cells. *Sol. Energy Mat. and Solar Cells* 2010; **94-11**:1889-1892

[3] Altosaar M, Raudoja J, Timmo K, Danilson M, Grossberg M *et al*. Cu$_2$ZnSnSe$_4$ monograin powders for solar cell application. *Proceeding of WCPEC* 2006:468-470

[4] Katagiri H, Saitoh K, Washio T *et al*. Development of thin film solar cell based on Cu$_2$ZnSnS$_4$ thin films. *Sol. Energy Mat. and Solar Cells* 2001;**65**:141-148

[5] Weber A, Mainz R, and Schock HW. On the Sn loss from thin films of the material system Cu–Zn–Sn–S in high vacuum. *J.Appl. Phys.* 2010;**107**:013516

[6] Redinger A, Berg DM, Dale PJ, and Siebentritt S. The consequences of kesterite equilibria for efficient solar cells. *J. Am. Chem. Soc.* 2011;**133**(10):3320–332

[7] Redinger A, Siebentritt S. Coevaporation of Cu$_2$ZnSnSe$_4$ thin films. *Appl. Phys. Lett.* 2010;**97**:092111

[8] Timmo K., Altosaar M., Raudoja J. *et al.* Chemical etching of Cu$_2$ZnSn(S,Se)$_4$ monograin powder *Proc. of 35th IEEE Photovoltaic Specialists Conference* 2010;1982-1985

[9] Katagiri H, Jimbo K, Tahara M, Araki H, Oishi K. The influence of the composition ratio on CZTS-based thin film solar cells. *Mater. Res. Soc. Symp. Proc.* 2009;**1165**

[10] Wang K, Shin B, Reuter KB, Todorov T, Mitzi DB, Guha S. Structural and elemental characterization of high efficiency Cu$_2$ZnSnS$_4$ solar cells. *Appl. Phys. Lett.* 2011;**98**:051912

[11] Wang K, Gunawan O, Todorov T, Shin B, Chey SJ, Bojarczuk NA *et al.* Thermally evaporated Cu$_2$ZnSnS$_4$ solar cells. *Appl. Phys. Lett.* 2010;**97**:143508

[12] Katagiri H, Ishigaki N, Ishida T, Saito K. Characterization of Cu$_2$ZnSnS$_4$ thin films prepared by vapor phase sulfurization *Jpn. J. Appl. Phys.* 2001;**40**:500-504

PAPER V

M. Kauk, M. Altosaar, **K. Muska**, M. Pilvet, J. Raudoja, K. Timmo, T. Varema, M. Grossberg, E. Mellikov, O.Volobujeva. Post-growth annealing effect on the performance of $Cu_2ZnSnSe_4$ monograin layer solar cells. *Thin Solid Films* (provisionally accepted).

Post-growth annealing effect on the performance of $Cu_2ZnSnSe_4$ monograin layer solar cells

M. Kauk-Kuusik*, M. Altosaar, K. Muska, M. Pilvet, J. Raudoja, K. Timmo, T. Varema, M. Grossberg, E.Mellikov, O.Volobujeva

Tallinn University of Technology, Ehitajate tee 5, Tallinn 19086, Estonia

*marit.kauk@ttu.ee

Abstract

In this work, we investigated the effect of annealing of absorber powder on the conversion efficiency of $Cu_2ZnSnSe_4$ (CZTSe) monograin layer solar cells. CZTSe powders were synthesized from binary compounds and elemental Se in the liquid phase of KI in evacuated quartz ampoules at 740^oC. In order to study the effect of post-treatments of the absorber material different annealing parameters such as Se and/or $SnSe_2$ vapor pressure, annealing time and temperature were varied with the aim to gain uniform, good quality absorber materials for monograin layer solar cells. The annealing temperature was found to be crucial for the performance of CZTSe monograin layer solar cells. The conversion efficiency of solar cells improved significantly after the heat treatment. The effect can be attributed to the change of the absorber material composition and the crystals surface properties suitable for the effective *p-n* junction formation. The best solar cell showed the value of V_{oc} 350 mV, j_{sc}=23.8 mA/cm^2, FF =57 % and the efficiency of 4.4%.

1. Introduction.

The $Cu_2ZnSnSe_4$ (CZTSe) compound has attracted a considerable attention as an alternative absorber in thin film solar cells because CZTSe is a *p*-type semiconductor with a band gap of 1.0 eV and has an absorption coefficient that is larger than $10^4 cm^{-1}$, which match the prerequisites for a solar absorber material [1].

Recently, the record efficiency of liquid-processed CZTSe solar cell yielded 10.1% [2]. However, although device performance was greatly improved, basic researches on CZTSe material itself are insufficient. For example, fabrication of compositionally uniform CZTSe film is still hard task due to Sn-loss during annealing process. Usually, a high temperature annealing in chalcogen atmosphere is essential to form a well-crystallized and single phase CZTSe. It is well known that CZTSe quickly decomposes at temperatures higher than 400°C [3- 5]. The decomposition rate, however, depends drastically on the experimental conditions such as temperature, total pressure inside the annealing container and partial pressures of all involved volatile species. As monograin powder synthesis is an isothermal process, the Sn loss in the synthesis process is not a problem. The problem rises in the post-treatment step. In our previous studies [6], it was shown that due to the distribution of material between the liquid flux and the solid CZTSe crystals during the synthesis process, some part of material is dissolved in molten flux at growth temperature. In the cooling period, the dissolved part precipitates on the solid crystal surfaces. Therefore, as-grown monograins need some chemical etching and annealing before the formation of *p-n* junction. It has been found that Br_2–methanol treatment followed by immersion in an aqueous solution of KCN [7] and annealing in $SnSe_2$ or Se vapors heals crystals' surfaces to the device quality. Considering that high efficiency CZTSe solar cell can be realized just with Cu-poor and Zn-rich CZTSe [8], the proper adjustment of chemical composition of CZTSe is a prerequisite for well working solar cells. Hence, systematic annealing experiments under controlled temperature and atmosphere come to be significant.

Here, we report the effect of post-growth annealing and sequential etching of CZTSe monograin absorbers with different compositions on the performance of CZTSe monograin layer (MGL) solar cells.

2. Experimental details

The CZTSe absorber materials, used for MGL solar cells in this study were synthesized by isothermal recrystallization method in molten flux. The details about monograin growth process could be found in [9].

After the removal of flux, the post-treatments were carried out in closed quartz ampoules using two-temperature zone arrangement. Elemental Se or $SnSe_2$ pellets were placed into the lower temperature zone of the ampoules. CZTSe powder was heated in the higher temperature zone. The temperatures of both zones were regulated and controlled independently. The lowest temperature in the ampoule determined the vapor pressure of Se or $SnSe_2$. After annealing, the ampoules were taken out of the furnace and cooled down on a ceramic plate at room temperature.

Prior to CdS deposition, the post-treated monograin powders were sequentially etched with fresh-made 1% bromine in methanol and in the 10% aqueous solution of KCN at room temperature in order to remove

secondary phases. Bromine etching is an oxidative and leaves elemental Se on the crystals' surface [7] that was removed by following cyanide etching. After etching, the crystals were washed in deionized water.

The bulk chemical compositions of the monograin powders were analyzed by energy dispersive x-ray spectroscopy (EDX) on ZEISS HR SEM ULTRA 55 with accelerating voltage 7 kV and a beam current 3 nA. The phase composition of the asgrown and post-treated powders was studied by room-temperature (RT) micro-Raman spectroscopy using Horiba`s LabRam HR spectrometer with incident laser light with wavelength 532 nm. The narrow granulometric fraction of the post-treated monograin powders was used as absorber materials in MGL solar cells. The MGL solar cell combines the features of a single crystalline solar cell and a thin film solar cell. Embedding the CZTSe grains into a layer of epoxy resin formed the photoactive layer called a monograin membrane. The monograin membranes were covered with CdS by chemical bath deposition followed by sputtering of i-ZnO/ ZnO:Al layers. Solar cell structures were completed by vacuum evaporation of 1-2mm thick indium grid contacts onto the ZnO window layer. The active area of the MGL solar cells was ~ 75% of the total area. The solar cells were characterized by measuring the current density versus voltage (I-V) characteristics by Keithley 2400 electrometer under standard test conditions (AM 1.5, 100 mW/cm^2).

3. Results and discussion

As reported earlier by different authors [3-5], CZTSe decomposes at temperatures higher than 400 °C. According to Redinger et al. [4] the loss of Sn cannot be compensated by any significant SnSe partial pressure. Scragg et al. [3] showed by two different kinetic models that ambient vapor phase with both components- chalcogen and Sn-compound- is a prerequisite for stability of Cu_2ZnSnS_4 (CZTS) surface. Both proposed models predicted that if the product of the sulfur and SnS vapor pressures exceeds a certain value, the CZTS surface would be completely stabilized. It is therefore important to determine this critical value, in order to produce CZTSe with good surface quality that is vital for solar cell performance. In the present study, $SnSe_2$ or Se sources to produce and regulate the gas phase composition were used.

Following reactions describe the decomposition of CZTSe (1) and formation of gas phase above CZTSe by heating. $SnSe_2$ as a separate source decomposes at high temperatures according to the reactions (2) and (3) providing SnSe and Se into gas phase. It is known that Se in saturated gas phase consists of oligomers Se_n (g), where n = 2, 3, 5, 6, 7, 8, and the proportions of them are depending on temperature [10].

$$Cu_2ZnSnSe_4 \text{ (s)} \Leftrightarrow Cu_2Se(s) + ZnSe(s) + SnSe_2(s) \tag{1}$$

$$SnSe_2 \text{ (s)} \Leftrightarrow SnSe(s) + 1/n \ Se_n(g) \qquad Kp = P_{Sen}^{1/n} \tag{2}$$

$$SnSe(s) \Leftrightarrow SnSe(g) \qquad Kp_{SnSe} = P_{SnSe} \tag{3}$$

$$Cu_2ZnSnSe_4 \text{ (s)} \Leftrightarrow Cu_2Se(s) + ZnSe(s) + SnSe(g) + 1/n \ Se_n \text{ (g)} \qquad Kp_{CZTSe} = P_{SnSe} \ P_{Sen}^{1/n} \tag{4}$$
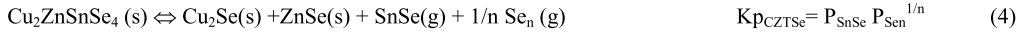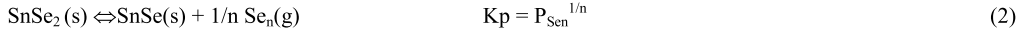
Kp - equilibrium constant and P- partial pressure of components.

As analyzed by mass-spectrometry [11] vapor phase above solid SnSe(s) (melting point 861°C) consists mainly from SnSe atoms described by the equilibrium (3). The equilibrium vapor pressure of pure SnSe is more than 4 orders of magnitude lower than the vapor pressure on pure $SnSe_2$ or pure Se as can be seen in Fig. 1 (constructed on the base of data published in [10]). From the equation of equilibrium (4) it can be derived that the reaction (4) is shifted to the left side if $lgP_{Sen} > 1/n$ ($lgK_{CZTSe} - lgP_{SnSe}$) and the incorporation of Sn from the gas phase of $SnSe_2$ into the crystal of CZTSe could occur. If applied vapor pressure of Se is lower than determined by the equilibrium of reaction (4) in a closed ampoule with CZTSe, the composition of CZTSe changes due to the decomposition process by an extent determined by the applied Se pressure.
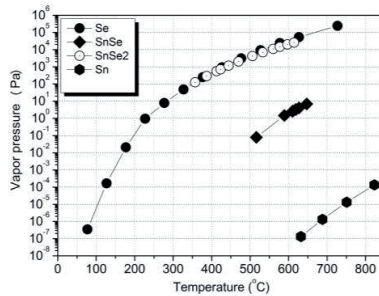
Figure 1. Vapor pressure on pure Sn, Se, $SnSe_2$, SnSe (constructed on the base of data published in [10])

Figure 2 displays typical Raman spectra of asgrown and annealed CZTSe monograin powder with compositional ratios of [Cu]/([Zn]+[Sn])=0.81 and [Zn]/[Sn] =1.13. Annealing was done in $SnSe_2$ vapor at 740^oC. RT Raman spectra of both CZTSe powder crystals revealed four main peaks at 196, 173, 222 and 234 cm^{-1} which are characteristic for CZTSe [12]. Raman analysis showed that a secondary phase with the Raman peak at 186 cm^{-1} [13] was formed on the surface of CZTSe monograins after annealing. It can be attributed to $SnSe_2$ or to some Cu-Sn-Se ternary compound. EDX analysis from mechanically polished crystals showed that Cu-content decreased 0.5 at% from 23.2 to 22.7 at%, Zn content decreased from 15.3at% to 14.9at% and Sn content increased from 13.5at% to 13.8at% after annealing in $SnSe_2$ vapor. In order to remove the formed secondary phase, the sequential etching with bromine in methanol and with cyanide solution on the annealed CZTSe monograins was performed.
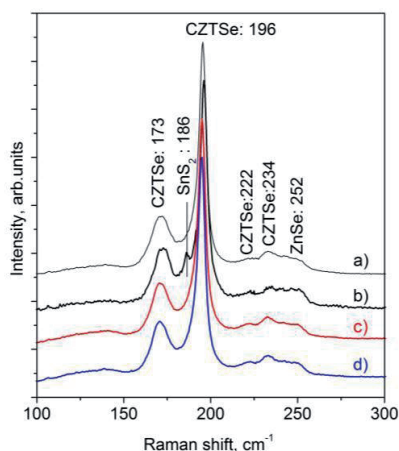
Figure 2. Raman spectra of CZTSe monograin powders: a) asgrown, b) $SnSe_2$-annealed, c) annealed and bromine-in-methanol etched and d) annealed and bromine-in-methanol etched followed by KCN etching.

Figure 3 illustrates a typical etch pattern observed on the monograin surface after the sequential etching. The bromine etchant produced well-defined triangular pits on some faces of crystals and crystal columns on the other type of faces. After bromine etching, the dark red liquid is usually visible on the surface of monograins. This liquid could be either Br_2Se_3 or Br_4Se_2 [14]. Before the second etching, the powder was washed in water. Se excess from the surface was etched off in a cyanide solution. The Raman scattering peak at 186cm^{-1} (Fig. 2) completely disappeared after the sequential chemical etching while no change was observed in the main peaks of CZTSe at 173, 196, 222 and 234 cm^{-1}. Also ZnSe peak at 252 cm^{-1} remained [12].
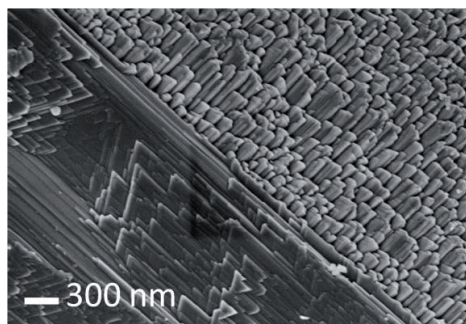
Figure 3. SEM image of a monograin surface after etching with bromine in methanol solution.

Figure 4 shows the I-V characteristics of a) asgrown, b) $SnSe_2$-annealed c) $SnSe_2$-annealed and etched with bromine in methanol and d) annealed and etched with two etchants CZTSe-based MGL solar cells. After the $SnSe_2$-annealing and sequential etching before CdS deposition, the open circuit voltage, current density and FF

improved remarkably. Therefore, sequential etching was used in all following annealing experiments before CdS deposition.
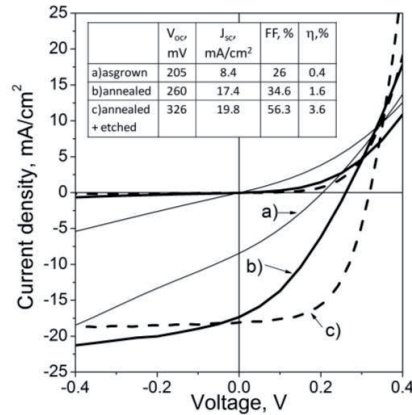
Figure 4. Current-voltage characteristics of CZTSe solar cells under illumination: a) asgrown, b) annealed in SnSe$_2$ vapor and b) annealed and etched before CdS deposition.

In order to elucidate the optimal conditions of post-annealing of absorber powders for CZTSe MGL solar cells, different Se or SnSe$_2$ vapor pressures were applied for several periods starting from 10 minutes up to 16 hours. The optimal annealing time was found to be 30 minutes. The temperature of material zone was varied from 550 °C to 740°C. The ratios of metal concentration in the used un-treated CZTSe powder were [Cu]/([Zn]+[Sn])= 0.81 and [Zn]/[Sn] = 1.13. After annealing in SnSe$_2$ vapor, both compositional ratios decreased to 0.80 and 1.10, respectively. Se-vapor treatment of CZTSe absorber in the temperature range 550- 650°C was beneficial for V$_{oc}$ and FF values as shown in Figure 5. The values of V$_{oc}$ and FF of solar cells based on SnSe$_2$-treated absorbers were lower than those of MGL solar cells based on Se-treated CZTSe absorbers. CZTSe annealing in both atmospheres over 650°C, decreased the solar cell parameters continuously with increasing the temperature of material zone.
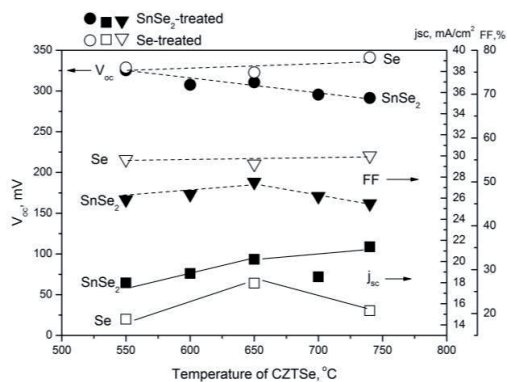
Figure 5. The values of V$_{oc}$, FF and j$_{sc}$ of CZTSe MGL solar cells in dependence of annealing temperature in material zone.

The composition of CZTSe absorber has strong influence on the performance of solar cells. Therefore, to confirm clearly the effect of absorber composition to CZTSe MGL device performance, we annealed powders of a large deviation of compositional ratios: 0.79<[Cu]/([Zn]+[Sn])<0.95 and 0.93< [Zn]/[Sn] <1.2. The annealing temperature in material zone was 650°C and in component zone 600°C.
Figure 6 shows the dependence of powder composition on the device performance after annealing in Se or SnSe$_2$ atmospheres. The values of V$_{oc}$ were depending on the [Cu]/([Zn]+[Sn]) and [Zn]/[Sn] ratios in powder. The highest V$_{oc}$=350mV was gained with Cu-poor ([Cu]/([Zn]+[Sn])=0.81-0.83) and Zn-rich ([Zn]/[Sn] =1.1)

powders. The values of j_{sc}=23.8 mA/cm^2 were also the highest in these regions. The performance of solar cells is very poor if the powder's compositional ratio [Cu]/([Zn]+[Sn])> 0.85. In our previous study [9], it was found that by increasing the Cu content in powders, the [Zn]/[Sn] ratio decreased and the CZTSe materials were Sn-rich ([Zn]/[Sn] <1). There is a high probability that Cu- and Sn-rich materials contain secondary phases and due to this the solar cells showed very low performance.
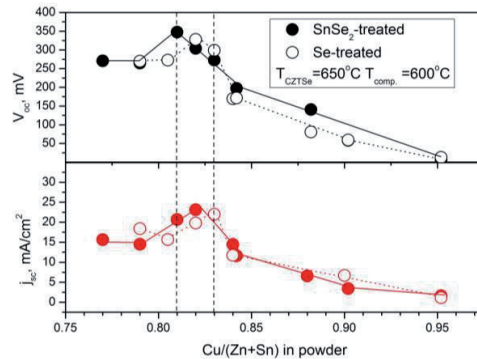
Figure 6. V_{oc} and j_{sc} of CZTSe MGL solar cells based on SnSe$_2$- and Se-treated absorbers as functions of the compositional ratio [Cu]/([Zn]+[Sn]) in absorber material.

By using the optimized SnSe$_2$-annealing conditions, such as temperature in material zone of 650°C and temperature of SnSe$_2$ zone of 600°C, powder compositional ratios of [Cu]/([Zn]+[Sn])= 0.81 and [Zn]/[Sn] = 1.12, the CZTSe MGL solar cell with 4.4% efficiency were obtained.

4. Conclusion.

The results of this study suggest that the composition of absorber material can be tuned and the quality of MGL solar cells can be improved by post-treatment of CZTSe powders in Se and/or SnSe$_2$ vapors. The annealing temperature was found to be crucial for the final performance of CZTSe MGL solar cells. The conversion efficiency of solar cells improved significantly due to heat treatment procedure in SnSe$_2$ atmosphere and the sequential chemical etching before CdS deposition. The highest efficiencies of MGL solar cells were gained with Cu-poor ([Cu]/([Zn]+[Sn])=0.81-0.83) and Zn-rich ([Zn]/[Sn] =1.1) powders.

References

[1] R. A.Wibowo, W. H. Jung, K. H. Kim J. Phys. Chem. Solids 71 (2010) 1702.
[2] S. Bag, O. Gunawan, T. Gokmen, Y. Zhu, T. Todorov, D. Mitzi, Energy Environ. Sci**.** 5, (2012) 7060
[3] J. J. Scragg, T. Ericson, T. Kubart, M. Edoff, C. Platzer-Björkman, *Chem. Mater.* 23(20) (2011) 4625.
[4] A. Redinger, D. M. Berg, P. J. Dale, R. Djemour, L.Gütay, T.Eisenbarth, N. Valle, S. Siebentritt, IEEE J. Photovoltaics, 1 (2) (2011) 200.
[5] A. Weber, R. Mainz, and H. W. Schock, J. Appl. Phys. 107 (2010) 013516.
[6] M. Kauk, K. Muska, M. Altosaar, J. Raudoja, M. Pilvet, T. Varema, K.Timmo, O. Volobujeva, Energy Procedia 10 (2011)197.
[7] K. Timmo, M. Altosaar, J. Raudoja, M. Grossberg, M. Danilson, O. Volobujeva, E. Mellikov, in Proceedings of the 35th IEEE Photovoltaic Specialists Conference, 20-25 June (2010), Honolulu (HI), USA (IEEE, New York, 2010), pp. 1982.
 [8] D.B. Mitzi, O.I. Gunawan, T.K. Todorov, K. Wang, S. Guha, Sol. Energy Mater. Sol. Cells, 95 (2011) 1421.

[9] K. Muska, M. Kauk, M. Grossberg, J. Raudoja, O. Volobujeva, Energy Procedia 10 (2011) 323.

[10] J. I. Gerasimov, A. N. Krestovnikov, S. I. Gorbov, Khimicheskaya termodinamika v tsvetnoi metallurgii. T. VI. Termodinamika selena i selenidov, tellura i telluridov: Spravochnik. M.: Metallurgiya (1974) 312

[11] R. F. Brebrick, A. J. Strauss, J. Chem. Phys., 40 (1964) 3230.

[12] M. Altosaar, J. Raudoja, K. Timmo, M. Danilson, M. Grossberg, J. Krustok, and E. Mellikov Phys. Stat. Sol. (a) 205, No. 1, (2008) 167–170

[13] G. Lucovsky, J. C. Mikkelsen, W. Y. Liang, R. M. White, R. M. Martin, Phys. Rev. B 4, 14 (1976)1663.

[14] S. Gezci, J. Woods, J. Mater. Sci. 7 (1972) 603

ELULOOKIRJELDUS

Isikuandmed

Ees- ja perekonnanimi   Katri Muska
Sünniaeg ja -koht   28.01.1982, Tallinn, Eesti
Kodakondsus   eestlane
E-posti aadress   Katri.Muska@gmail.com

Hariduskäik

Õppeasutus	Lõpetamise aeg	Haridus (eriala/kraad)
Tallinna Tehnikaülikool	2007	Loodusteaduste magistrikraad (MSc)
Tallinna Tehnikaülikool	2005	Loodusteaduste bakalaureusekraad (BSc)
Tallinna Tehnikagümnaasium	2000	Keskharidus

Keelteoskus (alg-, kesk- või kõrgtase)

Keel	Tase
Eesti keel	kõrgtase
Inglise keel	kõrgtase
Vene keel	algtase
Soome keel	algtase

Täiendusõpe

Õppimise aeg	Täiendusõppe korraldaja nimetus
03.03.2011-04.03.2011	FMTDK teaduskonverents. Nordic Forum konverentsikeskus, Tallinn, Eesti.
28.06.2010-30.06.2010	FMTDK suvekool "Functional materials and applications". Pühajärve puhkekeskus, Eesti.
16.10.2009-20.10.2009	"Nordic seminar on modelling of CIGS devices". Ångström Laboratory, Uppsala University, Uppsala, Rootsi.
26.05.2008-30.05.08	Course no 51 "Thin Film Deposition at the Nanoscale: Mechanisms and Applications". Ångström Laboratory, Uppsala University, Uppsala, Rootsi.
19.02.2008-20.02.2008	MMTDK Teaduskonverents. Kääriku, Eesti.
27.08.2006-31.08.2006	The 8th International Conference-School. Advanced materials and technologies. Palanga, Leedu.
21.08.2006-25.08.2006	Noorteadlaste suvekool, Pärnu, Eesti.

Teenistuskäik

Aeg	Asutus	Amet
2009-	Crystalsol OÜ	Arendusinsener
2008-2009	Tallinna Tehnikaülikool	Teadur
2007-2008	Tallinna Tehnikaülikool	Erakorraline teadur
2005-2007	Tallinna Tehnikaülikool	Insener

Tunnustused

2006, Archimedese sihtasutuse üliõpilastööde konkursil II koht bakalaureusetöö „Keemiliselt sadestatud CdS kilede morfoloogia ja lõõmutamise uurimine" eest

2006, Tallinna Tehnikaülikooli Arengufondi magistriõppe stipendium

Kaitstud lõputööd

„Keemilise vanni koostise ja termotöötluse mõju kloriidsest lahusest sadestatud CdS kilede omadustele". Magistritöö, juhendaja vanemteadur Jaan Hiie

„Keemiliselt sadestatud CdS kilede morfoloogia ja lõõmutamise uurimine". Bakalaureusetöö, juhendaja Julia Kois (MSc) ja vanemteadur Jaan Hiie

Teadustöö põhisuunad

Loodus- ja tehnikateadused

Protsessitehnoloogia ja materjaliteadus

Muud uurimisprojektid

Protsesside ja mehhanismide uurimine, mis limiteerivad $Cu_2ZnSn(S,Se)_4$ kui päikesepatarei absorbermaterjali saagist sünteesil sulade soolade keskkonnas

Uued materjalid ja tehnoloogiad tuleviku päikeseenergeetikale

Mittetoksilistest ja maapõues laialt levinud materjalidest valmistatud monoterakiht-päikesepatareide arendamine

CURRICULUM VITAE

Personal data

Name	Katri Muska
Date and place of Birth	28.01.1982, Tallinn, Estonia
Citizenship	Estonian
E-mail	Katri.Muska@gmail.com

Education

Educational institution	Graduation year	Education (field of study/degree)
Tallinn University of Technology	2007	Master's Degree in Natural Sciences (MSc)
Tallinn University of Technology	2005	Bachelor's Degree in Natural Sciences (BSc)
Tallinn Technical Secondary School	2000	Secondary education

Language competence/skills (fluent; average; basic skills)

Language	Level
Estionian	fluent
English	fluent
Russian	basic
Finnish	basic

Special courses

Period	Educational or other organization
03.03.2011-04.03.2011	FMTDK Research Conference. Nordic Forum Conference Centre, Tallinn, Estonia.
28.06.2010-30.06.2010	FMTDK Summer School "Functional materials and applications", Pühajärve, Estonia.
16.10.2009-20.10.2009	"Nordic seminar on modelling of CIGS devices". Ångström Laboratory, Uppsala University, Uppsala, Sweden.
26.05.2008-30.05.08	Course no 51 "Thin Film Deposition at the Nanoscale: Mechanisms and Applications". Ångström Laboratory, Uppsala University, Uppsala, Sweden.
19.02.2008-20.02.2008	MMTDK Conference. Kääriku, Estonia.
27.08.2006-31.08.2006	The 8th International Conference-School. Advanced materials and technologies. Palanga, Lithuania.
21.08.2006-25.08.2006	Summer School of Young Scientists. Valgeranna, Pärnu, Estonia

Professional Employment

Period	Organization	Position
2009-	Crystalsol OÜ	Development engineer
2008-2009	Tallinn University of Technology	Researcher
2007-2008	Tallinn University of Technology	Extraordinary Researcher
2005-2007	Tallinn University of Technology	Other staff

Awards

2006, Archimedes Foundation, Students' research prize, II place

2009, Scholarship of the Development Foundation of Tallinn University of Technology

Defended thesis

"Influence of bath composition and annealing on the properties of CdS films deposited from chloride solution". Master thesis, supervisor Senior Researcher Jaan Hiie

"Investigation of the morfology and annealing process of chemically deposited CdS thin films". Bachelor thesis, supervisor Julia Kois (MSc) and Senior Researcher Jaan Hiie.

Main areas of scientific work/ Current research topics

Natural Sciences and Engineering

Process Technology and Materials Science

Other research projects

Development of CZTS monograin powders towards abundant and non-toxic materials for solar cells

Processes and factors limiting the yield of $Cu_2ZnSn(S,Se)_4$ monograin powders in synthesis of solar cell absorber materials in molten salts

New materials and technologies for solar energetics

List of publications

1. K. Muska, M. Kauk, M. Grossberg, M. Altosaar, M. Pilvet, T. Varema, K. Timmo, O. Volobujeva, A. Mere. Impact of $Cu_2ZnSn(Se_xS_{1-x})_4$ (x=0.3) compositional ratios on the monograin powder properties and solar cells. Thin Solid Films (provisionally accepted).

2. M. Kauk, M. Altosaar, K. Muska, M. Pilvet, J. Raudoja, K. Timmo, T. Varema, M. Grossberg, E. Mellikov, O.Volobujeva. Post-growth annealing effect on the performance of CZTSe monograin layer solar cells. Thin Solid Films (provisionally accepted).

3. K. Muska, M. Kauk, M. Grossberg, J. Raudoja, O. Volobujeva. Influence of compositional deviations on the properties of $Cu_2ZnSnSe_4$ monograin powders. Energy Procedia 10 (2011) 323 - 327.

4. K. Muska, M. Kauk, M. Altosaar, M. Pilvet, M, Grossberg, O. Volobujeva. Synthesis of Cu_2ZnSnS_4 Monograin Powders with Different Compositions. Energy Procedia 10 (2011) 203 - 207.

5. M. Kauk, K. Muska, M. Altosaar, J. Raudoja, M. Pilvet, T. Varema, K.Timmo, O. Volobujeva. Effects of sulphur and tin disulphide vapour treatments of $Cu_2ZnSnS(Se)_4$ absorber materials for monograin solar cells. Energy Procedia 10 (2011) 197 - 202.

6. E. Mellikov, D. Meissner, M. Altosaar, M. Kauk, J. Krustok, A. Öpik, O. Volobujeva, J. Iljina, K. Timmo, I. Klavina, J.Raudoja, M. Grossberg, T. Varema, K. Muska, M. Ganchev, S. Bereznev, M. Danilson. Solar Energy Materials Research at Tallinn University of Technology. Advanced Materials Research, 2011, xx - xx (in press).

7. K. Timmo, M. Altosaar, J. Raudoja, K. Muska, M. Pilvet, M. Kauk, T. Varema, M. Danilson, O. Volobujeva, E. Mellikov. Sulfur-containing $Cu_2ZnSnSe_4$ monograin powders for solar cells. Solar Energy Materials&Solar cells 94 (2010) 1889-1892.

8. M. Kauk, K. Muska, M. Altosaar, M. Danilson, O. Volobujeva, T. Varema. ZnO Grown by Chemical Solution Deposition. In Proceedings of the 35th IEEE Photovoltaics Specialists: 35th Photovoltaic Specialist Conference, Hawaii Convention Center Honolulu, Hawaii, June 20-25, 2010. IEEE, 2010, 002452 - 002456.

9. E. Mellikov, M. Altosaar, J. Raudoja, K.Timmo, O. Volobujeva, M. Kauk, J. Krustok, T. Varema, M. Grossberg, M. Danilson, K. Muska, K. Ernits, F. Lehner, D.Meissner. $Cu_2(ZnxSn_{2-x})(SySe_{1-y})4$ monograin materials for photovoltaics. George G. Wicks, Jack Simon, Ragaiy Zidan, Edgar Lara-Curzio, Thad Adams, Jose Zayas, Abhi Karkamkar (Eds.). Materials

Challenges in Alternative and Renewable Energy (137 - 142) The American Ceramic Society, Wiley-Blackwell (2010).

10. K. Ernits, K. Muska, M. Danilson, J. Raudoja, T. Varema, O. Volobujeva, M. Altosaar. Anion effect of zinc source to chemically deposited ZnS(O,OH) films. Advances in Material Science and Engineering, 2009, 372708.

11. K. Ernits, M. Danilson, K. Muska, O. Volobujeva, M. Altosaar, Chemical Bath Deposited ZnS Thin Films for CuIn(S,Se)$_2$ Solar Cells. In: Proceedings of 3rd Nordic PV Conference: Proceedings of 3rd Nordic PV Conference, Tallinn, Estonia, 18-19 May 2009.

12. O. Volobujeva, J. Kois, R. Traksmaa, K. Muska, S. Bereznev, M. Grossberg, E. Mellikov. Influence of annealing conditions on the structural quality of CuInSe$_2$ thin films. Thin Solid Films 516 (2008) 7105 - 7109.

13. J. Hiie, K. Muska, V. Valdna, V. Mikli, A. A. Taklaja, A. Gavrilov. Thermal annealing effect on structural and electrical properties of chemical bath deposited CdS films. Thin Solid Films 516 (2008) 7008 - 7012.

14. J. Hiie, T. Dedova, V. Valdna, K. Muska. Comparative study of nanostructured CdS thin films prepared by CBD and spray pyrolysis: Annealing effect. Thin Solid Films 511-512 (2006) 443 - 447.

DISSERTATIONS DEFENDED AT
TALLINN UNIVERSITY OF TECHNOLOGY ON
NATURAL AND EXACT SCIENCES

1. **Olav Kongas**. Nonlinear Dynamics in Modeling Cardiac Arrhytmias. 1998.
2. **Kalju Vanatalu**. Optimization of Processes of Microbial Biosynthesis of Isotopically Labeled Biomolecules and Their Complexes. 1999.
3. **Ahto Buldas**. An Algebraic Approach to the Structure of Graphs. 1999.
4. **Monika Drews**. A Metabolic Study of Insect Cells in Batch and Continuous Culture: Application of Chemostat and Turbidostat to the Production of Recombinant Proteins. 1999.
5. **Eola Valdre**. Endothelial-Specific Regulation of Vessel Formation: Role of Receptor Tyrosine Kinases. 2000.
6. **Kalju Lott**. Doping and Defect Thermodynamic Equilibrium in ZnS. 2000.
7. **Reet Koljak**. Novel Fatty Acid Dioxygenases from the Corals *Plexaura homomalla* and *Gersemia fruticosa.* 2001.
8. **Anne Paju**. Asymmetric oxidation of Prochiral and Racemic Ketones by Using Sharpless Catalyst. 2001.
9. **Marko Vendelin**. Cardiac Mechanoenergetics *in silico*. 2001.
10. **Pearu Peterson**. Multi-Soliton Interactions and the Inverse Problem of Wave Crest. 2001.
11. **Anne Menert**. Microcalorimetry of Anaerobic Digestion. 2001.
12. **Toomas Tiivel**. The Role of the Mitochondrial Outer Membrane in *in vivo* Regulation of Respiration in Normal Heart and Skeletal Muscle Cell. 2002.
13. **Olle Hints**. Ordovician Scolecodonts of Estonia and Neighbouring Areas: Taxonomy, Distribution, Palaeoecology, and Application. 2002.
14. **Jaak Nõlvak**. Chitinozoan Biostratigrapy in the Ordovician of Baltoscandia. 2002.
15. **Liivi Kluge**. On Algebraic Structure of Pre-Operad. 2002.
16. **Jaanus Lass**. Biosignal Interpretation: Study of Cardiac Arrhytmias and Electromagnetic Field Effects on Human Nervous System. 2002.
17. **Janek Peterson**. Synthesis, Structural Characterization and Modification of PAMAM Dendrimers. 2002.
18. **Merike Vaher**. Room Temperature Ionic Liquids as Background Electrolyte Additives in Capillary Electrophoresis. 2002.
19. **Valdek Mikli**. Electron Microscopy and Image Analysis Study of Powdered Hardmetal Materials and Optoelectronic Thin Films. 2003.
20. **Mart Viljus**. The Microstructure and Properties of Fine-Grained Cermets. 2003.
21. **Signe Kask**. Identification and Characterization of Dairy-Related *Lactobacillus*. 2003
22. **Tiiu-Mai Laht**. Influence of Microstructure of the Curd on Enzymatic and Microbiological Processes in Swiss-Type Cheese. 2003.
23. **Anne Kuusksalu**. 2–5A Synthetase in the Marine Sponge *Geodia cydonium*. 2003.
24. **Sergei Bereznev**. Solar Cells Based on Polycristalline Copper-Indium Chalcogenides and Conductive Polymers. 2003.

25. **Kadri Kriis**. Asymmetric Synthesis of C_2-Symmetric Bimorpholines and Their Application as Chiral Ligands in the Transfer Hydrogenation of Aromatic Ketones. 2004.

26. **Jekaterina Reut**. Polypyrrole Coatings on Conducting and Insulating Substracts. 2004.

27. **Sven Nõmm**. Realization and Identification of Discrete-Time Nonlinear Systems. 2004.

28. **Olga Kijatkina**. Deposition of Copper Indium Disulphide Films by Chemical Spray Pyrolysis. 2004.

29. **Gert Tamberg**. On Sampling Operators Defined by Rogosinski, Hann and Blackman Windows. 2004.

30. **Monika Übner**. Interaction of Humic Substances with Metal Cations. 2004.

31. **Kaarel Adamberg**. Growth Characteristics of Non-Starter Lactic Acid Bacteria from Cheese. 2004.

32. **Imre Vallikivi**. Lipase-Catalysed Reactions of Prostaglandins. 2004.

33. **Merike Peld**. Substituted Apatites as Sorbents for Heavy Metals. 2005.

34. **Vitali Syritski**. Study of Synthesis and Redox Switching of Polypyrrole and Poly(3,4-ethylenedioxythiophene) by Using *in-situ* Techniques. 2004.

35. **Lee Põllumaa**. Evaluation of Ecotoxicological Effects Related to Oil Shale Industry. 2004.

36. **Riina Aav**. Synthesis of 9,11-Secosterols Intermediates. 2005.

37. **Andres Braunbrück**. Wave Interaction in Weakly Inhomogeneous Materials. 2005.

38. **Robert Kitt**. Generalised Scale-Invariance in Financial Time Series. 2005.

39. **Juss Pavelson**. Mesoscale Physical Processes and the Related Impact on the Summer Nutrient Fields and Phytoplankton Blooms in the Western Gulf of Finland. 2005.

40. **Olari Ilison**. Solitons and Solitary Waves in Media with Higher Order Dispersive and Nonlinear Effects. 2005.

41. **Maksim Säkki**. Intermittency and Long-Range Structurization of Heart Rate. 2005.

42. **Enli Kiipli**. Modelling Seawater Chemistry of the East Baltic Basin in the Late Ordovician–Early Silurian. 2005.

43. **Igor Golovtsov**. Modification of Conductive Properties and Processability of Polyparaphenylene, Polypyrrole and polyaniline. 2005.

44. **Katrin Laos**. Interaction Between Furcellaran and the Globular Proteins (Bovine Serum Albumin β-Lactoglobulin). 2005.

45. **Arvo Mere**. Structural and Electrical Properties of Spray Deposited Copper Indium Disulphide Films for Solar Cells. 2006.

46. **Sille Ehala**. Development and Application of Various On- and Off-Line Analytical Methods for the Analysis of Bioactive Compounds. 2006.

47. **Maria Kulp**. Capillary Electrophoretic Monitoring of Biochemical Reaction Kinetics. 2006.

48. **Anu Aaspõllu.** Proteinases from *Vipera lebetina* Snake Venom Affecting Hemostasis. 2006.

49. **Lyudmila Chekulayeva**. Photosensitized Inactivation of Tumor Cells by Porphyrins and Chlorins. 2006.

50. **Merle Uudsemaa**. Quantum-Chemical Modeling of Solvated First Row Transition Metal Ions. 2006.

51. **Tagli Pitsi**. Nutrition Situation of Pre-School Children in Estonia from 1995 to 2004. 2006.

52. **Angela Ivask**. Luminescent Recombinant Sensor Bacteria for the Analysis of Bioavailable Heavy Metals. 2006.

53. **Tiina Lõugas**. Study on Physico-Chemical Properties and Some Bioactive Compounds of Sea Buckthorn (*Hippophae rhamnoides* L.). 2006.

54. **Kaja Kasemets**. Effect of Changing Environmental Conditions on the Fermentative Growth of *Saccharomyces cerevisae* S288C: Auxo-accelerostat Study. 2006.

55. **Ildar Nisamedtinov**. Application of ^{13}C and Fluorescence Labeling in Metabolic Studies of *Saccharomyces* spp. 2006.

56. **Alar Leibak**. On Additive Generalisation of Voronoï's Theory of Perfect Forms over Algebraic Number Fields. 2006.

57. **Andri Jagomägi**. Photoluminescence of Chalcopyrite Tellurides. 2006.

58. **Tõnu Martma**. Application of Carbon Isotopes to the Study of the Ordovician and Silurian of the Baltic. 2006.

59. **Marit Kauk**. Chemical Composition of $CuInSe_2$ Monograin Powders for Solar Cell Application. 2006.

60. **Julia Kois**. Electrochemical Deposition of $CuInSe_2$ Thin Films for Photovoltaic Applications. 2006.

61. **Ilona Oja Açik**. Sol-Gel Deposition of Titanium Dioxide Films. 2007.

62. **Tiia Anmann**. Integrated and Organized Cellular Bioenergetic Systems in Heart and Brain. 2007.

63. **Katrin Trummal**. Purification, Characterization and Specificity Studies of Metalloproteinases from *Vipera lebetina* Snake Venom. 2007.

64. **Gennadi Lessin**. Biochemical Definition of Coastal Zone Using Numerical Modeling and Measurement Data. 2007.

65. **Enno Pais**. Inverse problems to determine non-homogeneous degenerate memory kernels in heat flow. 2007.

66. **Maria Borissova**. Capillary Electrophoresis on Alkylimidazolium Salts. 2007.

67. **Karin Valmsen**. Prostaglandin Synthesis in the Coral *Plexaura homomalla*: Control of Prostaglandin Stereochemistry at Carbon 15 by Cyclooxygenases. 2007.

68. **Kristjan Piirimäe**. Long-Term Changes of Nutrient Fluxes in the Drainage Basin of the Gulf of Finland – Application of the PolFlow Model. 2007.

69. **Tatjana Dedova**. Chemical Spray Pyrolysis Deposition of Zinc Sulfide Thin Films and Zinc Oxide Nanostructured Layers. 2007.

70. **Katrin Tomson**. Production of Labelled Recombinant Proteins in Fed-Batch Systems in *Escherichia coli*. 2007.

71. **Cecilia Sarmiento**. Suppressors of RNA Silencing in Plants. 2008.

72. **Vilja Mardla**. Inhibition of Platelet Aggregation with Combination of Antiplatelet Agents. 2008.

73. **Maie Bachmann**. Effect of Modulated Microwave Radiation on Human Resting Electroencephalographic Signal. 2008.

74. **Dan Hüvonen**. Terahertz Spectroscopy of Low-Dimensional Spin Systems. 2008.

75. **Ly Villo**. Stereoselective Chemoenzymatic Synthesis of Deoxy Sugar Esters Involving *Candida antarctica* Lipase B. 2008.

76. **Johan Anton**. Technology of Integrated Photoelasticity for Residual Stress Measurement in Glass Articles of Axisymmetric Shape. 2008.

77. **Olga Volobujeva**. SEM Study of Selenization of Different Thin Metallic Films. 2008.

78. **Artur Jõgi**. Synthesis of 4'-Substituted 2,3'-dideoxynucleoside Analogues. 2008.

79. **Mario Kadastik**. Doubly Charged Higgs Boson Decays and Implications on Neutrino Physics. 2008.

80. **Fernando Pérez-Caballero**. Carbon Aerogels from 5-Methylresorcinol-Formaldehyde Gels. 2008.

81. **Sirje Vaask**. The Comparability, Reproducibility and Validity of Estonian Food Consumption Surveys. 2008.

82. **Anna Menaker**. Electrosynthesized Conducting Polymers, Polypyrrole and Poly(3,4-ethylenedioxythiophene), for Molecular Imprinting. 2009.

83. **Lauri Ilison**. Solitons and Solitary Waves in Hierarchical Korteweg-de Vries Type Systems. 2009.

84. **Kaia Ernits**. Study of In_2S_3 and ZnS Thin Films Deposited by Ultrasonic Spray Pyrolysis and Chemical Deposition. 2009.

85. **Veljo Sinivee**. Portable Spectrometer for Ionizing Radiation "Gammamapper". 2009.

86. **Jüri Virkepu**. On Lagrange Formalism for Lie Theory and Operadic Harmonic Oscillator in Low Dimensions. 2009.

87. **Marko Piirsoo**. Deciphering Molecular Basis of Schwann Cell Development. 2009.

88. **Kati Helmja**. Determination of Phenolic Compounds and Their Antioxidative Capability in Plant Extracts. 2010.

89. **Merike Sõmera**. Sobemoviruses: Genomic Organization, Potential for Recombination and Necessity of P1 in Systemic Infection. 2010.

90. **Kristjan Laes**. Preparation and Impedance Spectroscopy of Hybrid Structures Based on $CuIn_3Se_5$ Photoabsorber. 2010.

91. **Kristin Lippur**. Asymmetric Synthesis of 2,2'-Bimorpholine and its 5,5'-Substituted Derivatives. 2010.

92. **Merike Luman**. Dialysis Dose and Nutrition Assessment by an Optical Method. 2010.

93. **Mihhail Berezovski**. Numerical Simulation of Wave Propagation in Heterogeneous and Microstructured Materials. 2010.

94. **Tamara Aid-Pavlidis**. Structure and Regulation of BDNF Gene. 2010.

95. **Olga Bragina**. The Role of Sonic Hedgehog Pathway in Neuro- and Tumorigenesis. 2010.

96. **Merle Randrüüt**. Wave Propagation in Microstructured Solids: Solitary and Periodic Waves. 2010.

97. **Marju Laars**. Asymmetric Organocatalytic Michael and Aldol Reactions Mediated by Cyclic Amines. 2010.

98. **Maarja Grossberg**. Optical Properties of Multinary Semiconductor Compounds for Photovoltaic Applications. 2010.

99. **Alla Maloverjan**. Vertebrate Homologues of Drosophila Fused Kinase and Their Role in Sonic Hedgehog Signalling Pathway. 2010.

100. **Priit Pruunsild**. Neuronal Activity-Dependent Transcription Factors and Regulation of Human *BDNF* Gene. 2010.

101. **Tatjana Knjazeva**. New Approaches in Capillary Electrophoresis for Separation and Study of Proteins. 2011.

102. **Atanas Katerski**. Chemical Composition of Sprayed Copper Indium Disulfide Films for Nanostructured Solar Cells. 2011.

103. **Kristi Timmo.** Formation of Properties of $CuInSe_2$ and $Cu_2ZnSn(S,Se)_4$ Monograin Powders Synthesized in Molten KI. 2011.

104. **Kert Tamm**. Wave Propagation and Interaction in Mindlin-Type Microstructured Solids: Numerical Simulation. 2011.

105. **Adrian Popp**. Ordovician Proetid Trilobites in Baltoscandia and Germany. 2011.

106. **Ove Pärn**. Sea Ice Deformation Events in the Gulf of Finland and This Impact on Shipping. 2011.

107. **Germo Väli**. Numerical Experiments on Matter Transport in the Baltic Sea. 2011.

108. **Andrus Seiman**. Point-of-Care Analyser Based on Capillary Electrophoresis. 2011.

109. **Olga Katargina**. Tick-Borne Pathogens Circulating in Estonia (Tick-Borne Encephalitis Virus, *Anaplasma phagocytophilum*, *Babesia* Species): Their Prevalence and Genetic Characterization. 2011.

110. **Ingrid Sumeri**. The Study of Probiotic Bacteria in Human Gastrointestinal Tract Simulator. 2011.

111. **Kairit Zovo**. Functional Characterization of Cellular Copper Proteome. 2011.

112. **Natalja Makarytsheva**. Analysis of Organic Species in Sediments and Soil by High Performance Separation Methods. 2011.

113. **Monika Mortimer**. Evaluation of the Biological Effects of Engineered Nanoparticles on Unicellular Pro- and Eukaryotic Organisms. 2011.

114. **Kersti Tepp**. Molecular System Bioenergetics of Cardiac Cells: Quantitative Analysis of Structure-Function Relationship. 2011.

115. **Anna-Liisa Peikolainen**. Organic Aerogels Based on 5-Methylresorcinol. 2011.

116. **Leeli Amon**. Palaeoecological Reconstruction of Late-Glacial Vegetation Dynamics in Eastern Baltic Area: A View Based on Plant Macrofossil Analysis. 2011.

117. **Tanel Peets**. Dispersion Analysis of Wave Motion in Microstructured Solids. 2011.

118. **Liina Kaupmees**. Selenization of Molybdenum as Contact Material in Solar Cells. 2011.

119. **Allan Olspert**. Properties of VPg and Coat Protein of Sobemoviruses. 2011.

120. **Kadri Koppel**. Food Category Appraisal Using Sensory Methods. 2011.

121. **Jelena Gorbatšova**. Development of Methods for CE Analysis of Plant Phenolics and Vitamins. 2011.

122. **Karin Viipsi**. Impact of EDTA and Humic Substances on the Removal of Cd and Zn from Aqueous Solutions by Apatite. 2012.

123. **David Schryer**. Metabolic Flux Analysis of Compartmentalized Systems Using Dynamic Isotopologue Modeling. 2012.

124. **Ardo Illaste**. Analysis of Molecular Movements in Cardiac Myocytes. 2012.

125. **Indrek Reile**. 3-Alkylcyclopentane-1,2-Diones in Asymmetric Oxidation and Alkylation Reactions. 2012.

126. **Tatjana Tamberg**. Some Classes of Finite 2-Groups and Their Endomorphism Semigroups. 2012.

127. **Taavi Liblik**. Variability of Thermohaline Structure in the Gulf of Finland in Summer. 2012.

128. **Priidik Lagemaa**. Operational Forecasting in Estonian Marine Waters. 2012.

129. **Andrei Errapart**. Photoelastic Tomography in Linear and Non-linear Approximation. 2012.

130. **Külliki Krabbi**. Biochemical Diagnosis of Classical Galactosemia and Mucopolysaccharidoses in Estonia. 2012.

131. **Kristel Kaseleht**. Identification of Aroma Compounds in Food using SPME-GC/MS and GC-Olfactometry. 2012.

132. **Kristel Kodar**. Immunoglobulin G Glycosylation Profiling in Patients with Gastric Cancer. 2012.

133. **Kai Rosin**. Solar Radiation and Wind as Agents of the Formation of the Radiation Regime in Water Bodies. 2012.

134. **Ann Tiiman**. Interactions of Alzheimer`s Amyloid-Beta Peptides with Zn(II) and Cu(II) Ions. 2012.

135. **Olga Gavrilova**. Application and Elaboration of Accounting Approaches for Sustainable Development. 2012.

136. **Olesja Bondarenko**. Development of Bacterial Biosensors and Human Stem Cell-Based *In Vitro* Assays for the Toxicological Profiling of Synthetic Nanoparticles. 2012.